

# MÁSTER UNIVERSITARIO EN Ingeniería Industrial

## TRABAJO FIN DE MÁSTER

***DESIGN OF A 2+1 PARALLEL  
CONTINUUM ROBOT FOR PICK AND  
PLACE***

<b>Student</b>	Baños Paz, Ricardo
<b>Director</b>	Altuzarra Maestre, Oscar
<b>Department</b>	<i>Mechanical Engineering Department</i>
<b>Academic year</b>	2017-2018

Bilbao, 13 febrero 2018

## BASIC INFORMATION OF THE PROJECT

- Title: Design of a 2+1 parallel continuum robot for pick and place.
- Abstract: The ongoing research on nonlinear flexure analysis of mechanism required a prototype that would allow the testing of the models and algorithms developed. By the end of the project the robot was successfully built and connected to the controllers that allowed testing it. The key factors during its design were taking advantage of all the resources already available at the university to keep the costs down and meeting the initial requirements so that the comparisons against the models would remain relevant. By comparing the initial test results to the static simulations some discrepancies were found, and the trajectory testing rose concern about some of the compromises made during the design and assembly phases. To be able to develop the idea further the limitations of the prototype should be addressed. However, the potential benefits of compliant mechanisms themselves justify that effort.
- Keywords: Compliant mechanism; Continuum robot; pick and place; parallel manipulator; rod;
- Título: Diseño de un robot paralelo continuo de 2+1 grados de libertad para tareas de pick and place .
- Resumen: La investigación actualmente en curso sobre el análisis de flexión no lineal de mecanismos requería la construcción de un prototipo que permitiese probar los modelos y algoritmos desarrollados. Al final del presente proyecto se llevó a cabo con éxito la construcción robot y se conectó a los sistemas de control pertinentes. Los factores más importantes durante su diseño fueron aprovechar todo lo posible los recursos de los que ya disponía la universidad para reducir los costes del proyecto y además respetar los requerimientos del prototipo para mantener relevantes las comparaciones con los modelos. Tras comparar los resultados de los ensayos iniciales con simulaciones estáticas se encontraron ciertas discrepancias, y la ejecución de trayectorias en el prototipo quedó patente

los sacrificios realizados durante las fases de diseño y montaje. Para poder desarrollar el concepto en mayor profundidad deberían subsanarse dichas limitaciones. No obstante, los beneficios potenciales de los mecanismos compliant en sí mismos ya justificarían el esfuerzo.

- Palabras clave: Mecanismos compliant ; robot continuo; recoger y colocar; manipulador paralelo; barra.
- Titulua: Jaso eta utzi operaziorako pentsatutako 2+1 continuum robot paralelo baten diseña.
- Laburpena: Flexio ez-lineala aztertzen duen ikerketa honetarako, garatutako modelo eta algoritmoak entsaiatzea ahalbideratzen duen prototipo bat beharrezkoa da. Proiektu amaierarako, robota arrakastaz eraiki zen, berau kontrolatzea ahalbideratzen duten kontroladoreei konektaturik. Robotaren diseñuari dagokionez, funtsezko faktoreak hurrengoak dira: unibertsitatearen baliabide guztiak aprobetxatzea proiektuaren kostua ahalik eta txikiena izateko eta hasierako eskakizunak betetzea modeloen konparazio egoki bat ahalbideratzeko. Lehenengo entseguak modelo estatikoarekin konparatzean, desadostasun batzuk aurkitu ziren. Izan ere, ibilbide entseguak diseiñu eta muntaketa fasean egindako konpromiso batzuekin erlazionatutako kezka erakutsi zuen. Proiektu honen ideia gehiago garatzeko, prototipoaren limitazioak kontuan hartu eta gainditu beharko liratezke. Hala ere, mekanismo konpatibleek dituzten onura potentzialak ahalegina justifikatzen dute.
- Hitzgakoak: Compliant mekanismoa; Continuum robot; Jaso eta utzi; Manipuladore paraleloa; barra.



## Contents

1.	Introduction.....	1
2.	Context .....	4
3.	Goals and Scope of the project.....	6
4.	Benefits contributed by the thesis.....	7
5.	Requirements for the prototype.....	9
6.	State of the art.....	15
6.1.	Relevant theory on the topic .....	16
6.2.	Alternatives in the market already .....	20
6.3.	Patents and relevant research.....	22
7.	Risk Analysis .....	27
8.	Design of the prototype.....	29
8.1.	Part description.....	29
8.1.1.	Subassembly 1:.....	30
8.1.2.	Subassembly 2:.....	37
8.1.3.	Subassembly 3:.....	43
8.2.	Assembly process.....	47
8.3.	Possible future implementations.....	52
9.	Prototype Testing.....	55
9.1.	Equipment used.....	55
9.2.	Tests performed.....	60
9.2.1.	Test 1: Quasi-static Torque Test.....	60
9.2.2.	Test 2: EPOS Studio Setup .....	65



9.2.3. Tests with the PXI .....	69
10. Task description and project phases .....	74
11. Planning: Gantt diagram .....	78
12. Overall Project Expenses .....	79
13. Conclusions and Future Outlines: .....	80
14. References.....	84
15. Appendix.....	86
15.1. FeiyuTech WG specsheet:.....	86
15.2. Blueprints: .....	87
15.3. Motor:.....	101
15.4. Gearhead:.....	102
15.5. Results test 1: steps of 100 qc.....	103
15.6. EPOS Studio System Parameters: .....	105

## FIGURE INDEX

Figure 1: Example of a continuum robot for on-wing inspection/repair of gas turbine engines (3).....	1
Figure 2: Example of Compliant Mechanism Using Flexure Hinges (4) .....	5
Figure 3: Sketch of the initial concept for the prototype. ....	9
Figure 4: Dimensional requirements for the prototype.....	10
Figure 5: Example of Matlab code of where to change material properties and dimensions. ....	11
Figure 6: Simulated trajectory for the model in Matlab.....	11
Figure 7: Buckling test on the lathe.....	13
Figure 8: Comparison between the full working space of the mechanism with different values of $k$ and a comparable ABB Flexpicker. ....	13
Figure 9: Traction test on 10-mm nylon bars.....	14
Figure 10: Traction test results for 10-mm nylon bars.....	14
Figure 11: Traction test for the material used in the 3-D printer.....	15
Figure 12: Rod portion of length $ds$ subjected to distributed external forces and moments, also showing internal forces and moments.....	16
Figure 13: ABB IRB360 FlexPicker.....	21
Figure 14: US4765795 drawing of full manipulator.....	23
Figure 15: Example of continuum structure using strips. ....	23
Figure 16: Continuum robot with pre-curved rods. ....	24
Figure 17: Hexapod example for third device claimed.....	24
Figure 18: Flexible parallel manipulator. ....	25
Figure 19: Planar parallel robot mechanism on a sliding platform.....	25



Figure 20: Robotic case packing system. .... 26

Figure 21: Rigid-flexible coupling type flexible mechanical arm. .... 26

Figure 22: Different positions for the manipulator made of ground coffee..... 27

Figure 23: Subassemblies of the prototype..... 30

Figure 24: Shaft-bar coupling. .... 30

Figure 25: Case 1 Stress..... 32

Figure 26: Case 1 Deformation. .... 32

Figure 27: Case 2 Stress..... 33

Figure 28: Case 2 Deformation. .... 33

Figure 29: Case 3 Stress..... 34

Figure 30: Case 3 Deformation. .... 34

Figure 31: Elbow. .... 35

Figure 32: Parts forming the R joint..... 35

Figure 33: Bars forming the mechanism. .... 36

Figure 34: Detail of how the length of the bars was determined. .... 37

Figure 35: Detail of the parts on the drivetrain. .... 37

Figure 36: The support plate..... 38

Figure 37: Motor flange adapter..... 39

Figure 38: Motor flange..... 39

Figure 39: Bearing in its housing..... 40

Figure 40: Detail for the axis height and affected dimensions..... 40

Figure 41: Beam coupling..... 41

Figure 42: Shaft. .... 41

Figure 43: Critical shaft distance detail.....	42
Figure 44: Motor and gearhead mounted on a previous prototype.....	42
Figure 45: FeiyuTech WG 3-axis gimbal.....	43
Figure 46: Testing for permanent deformations on the rubber band.....	44
Figure 47: Testing the system with the belts and pulleys.....	45
Figure 48: Clamps for the rubber and the belt.....	45
Figure 49: Detail of how the clamps work.....	46
Figure 50: The two different styles of pulleys.....	46
Figure 51: Parts to house the pulleys.....	47
Figure 52: The two end effector options.....	47
Figure 53: All the parts.....	48
Figure 54: Glue bars 1.....	48
Figure 55: Glue bars 2.....	49
Figure 56: Powertrain assembly.....	49
Figure 57: Powertrain assembly, alignment.....	50
Figure 58: Preliminary Assembly.....	50
Figure 59: Mounting of the prototype to the structure.....	51
Figure 60: Prototype finally assembled and mounted on its structure.....	51
Figure 61: Example for the working space of the prototype in space.....	52
Figure 62: Omron X-Delta 2+1 variant sketch.....	53
Figure 63: Festo semi-rotary drives DVRS.....	54
Figure 64: EPOS2 Controllers.....	55
Figure 65: Control Center.....	56





Figure 66: EPOS Studio. Motor actuation tab.....	57
Figure 67: EPOS Studio. Data recorder.....	58
Figure 68: EPOS Studio. Object Dictionary.....	58
Figure 69: The PXI.....	59
Figure 70: LabVIEW program UI.....	60
Figure 71: Torque measuring test.....	61
Figure 72: Digital level used.....	61
Figure 73: Use of laser level to ensure a vertical trajectory.....	62
Figure 74: Example of differences in current and angle between M1 and M2.....	63
Figure 75: EPOS Software Set Up example.....	63
Figure 76: Combined results from the tests and simulations for different values of Young's modulus on the flexible bars.....	65
Figure 77: Data from EPOS Studio. Plots for Position Actual Value and Position Demand Value.....	66
Figure 78: Example of how test 2 developed.....	67
Figure 79: Position Control Parameters.....	68
Figure 80: P-gains on the LabVIEW program.....	70
Figure 81: Example of the motors becoming unstable during a trajectory.....	71
Figure 82: Changing the cycle period inside the LabVIEW program.....	72
Figure 83: Trajectory with unwanted steps.....	72
Figure 84: Component critical failure.....	73
Figure 85: Showing the correct alignment of the mechanism.....	80



## TABLE INDEX

Table 1: Collection of commercial pick and place Delta robots.....	21
Table 2: Cycle times for ABB IRB 360 FlexPicker.....	22
Table 3: Risk exposure matrix.....	28
Table 4: FEM Analysis results.....	32
Table 5 : Results from tuning the position PID on the EPOS Studio.....	69
Table 6: Task 1.....	74
Table 7: Task 2.....	75
Table 8: Task 3.....	75
Table 9: Task 4.....	76
Table 10: Task 5.....	76
Table 11: Task 6.....	77
Table 12: Task 7.....	77
Table 13: Labour costs.....	79
Table 14: Amortizations costs.....	79
Table 15: Cost of the expenses.....	79
Table 16: Overall expenses.....	80

## 1. Introduction

Any device that achieves its goal through the bending or deformation of some or one of its elements can be considered a compliant mechanism (1). In recent history, when the need for a machine or device to perform a certain task arose, designers would normally resort to a design comprised of rigid parts linked using some hinges or joints. This is still mostly the case, but thanks especially to the advances on computing and the complexity that some tasks might require, the use of solutions consisting of compliant elements is becoming more mainstream. This is the case for the so-called continuum robots. Continuum robots are a kind of manipulator that is able to assume continuous curved shapes by continuously bending, as if it had an infinite number of degrees of freedom (2). The inspiration for this kind of devices comes naturally from nature, one of the clearest examples for such a device being an elephant trunk.



Figure 1: Example of a continuum robot for on-wing inspection/repair of gas turbine engines (3)

More details about compliant mechanisms are presented later, as a complement to the project itself and to better understand the motivations behind it and its importance. However, the remainder of this section presents an overview of what is to come in the rest of this document.

This thesis gathers all the details and information regarding the process, concepts and outcome of all the work carried out as part of the Master Thesis of the Master in Industrial Engineering, with a Major in Mechanical Engineering. The thesis focuses primarily on the design and assembly of the first prototype that develops the original idea about a parallel continuum robot, and the initial experiments carried out to test it. In addition, the conclusions of the thesis are also an important part of the document, as they state not only the discoveries made along the process but also the future outlines to develop this first concept further and possible modifications and improvements to the already existing prototype.

On the following section of the document, the basic ideas concerning compliant mechanisms and continuum robots are explained and how the project itself ties in to the project currently being developed inside the Compmech research group, also including a brief introduction about the group itself. Next, the goals and scope of the project are discussed, followed by the benefits contributed by the thesis.

After laying out everything that the project strives to achieve, and also a brief introduction about the subject matter and where it fits in inside the current activities of the group, the following sections start to focus more on the details. Firstly, the initial concept for the prototype is explained, along with its dimensional requirements and a rough estimation of the mechanical requirements.

The description of the prototype is followed by a section on the state of the art that focuses on three different topics. The first one covers the fundamental theories on compliant mechanisms and continuum mechanics on which the mathematical models for the prototype are based. Secondly, the different current solutions already on the market for pick and place operations are presented, along with some of their relevant specifications, those that the prototype should try to rival at some point in the future. Finally, as a way to look at possible future commercial solutions, seven patents on both pick and place robots and continuum robots are introduced.

Then the risk analysis that was carried out for this project is presented, including a matrix that ranks the various factors according to their probability of occurring and their possible impact on the project.

The document continues by describing in detail the how the prototype evolved from the initial design stages to becoming an actual physical device that is now in the lab. This description includes a detailed description of the prototype itself, the various parts that form it and the assembly process that took place.

After the thorough description of the mechanism, some possible additions or modifications are presented. These additions have to do both with improving its functionality and also with increasing its mobility. Afterwards, the text continues with a description of the tests that were carried out on the prototype and the conclusions that could be drawn from their results.

As for the aspects of the project having to do with its management, the timeline of the project is broken down into the different tasks and milestones that compose it and they are also presented with the use of a Gantt diagram. The organizational aspects then lead to the economic aspects of the project, which include an overview of the costs of the project with all the expenses incurred during its unfolding.

Lastly, the project is revisited in the conclusions, highlighting the most relevant outcomes and implications. Then, some possible future outlines are suggested, which could signal a possible direction to follow for the further development of the prototype.

## 2. Context

This master thesis, Design of a 2+1 parallel continuum robot for pick and place , has been developed within the CompMech Research Group, inside the project called Ultra Flexible Parallel Kinematic Machines (MEDUSA) (reference: DPI2015-64450-R). CompMech is a research group belonging to the Department of Mechanical Engineering at the Faculty of Engineering in Bilbao. Its research focuses mainly on the design and analysis of parallel manipulators (4). Various members of the group take part in the project. The main researchers are professors Oscar Altuzarra and Fran Campa, other participating researchers are professors Mikel Diez, Charles Pinto and Javier Corral. Additionally, there are two PhD students developing their respective thesis under this project: Diego Caballero and Daniel Diaz-Caneja.

More precisely, this thesis is based on part of the work on Diego s PhD thesis. On the initial stages of his PhD, he started by developing a Matlab algorithm that solves the static problem of a rod. In order to test how well that model translates to real life, amongst many other goals that are stated later, the mechanism that is brought to life along these pages was conceived. Therefore, this master thesis builds upon the knowledge already provided by other researchers. Throughout the completion of the thesis more content based on the mechanism was created, such as a Simulink model for the control of the motors on the prototype by professor Campa. This model is later used for the testing phase of the prototype, and it should be noted that developing that model would have been beyond the scope of the thesis itself. Not only the director s guidance but also the contributions by the other researchers have greatly helped improve the development and the overall outcome of the thesis.

So far, only a brief definition about compliant mechanisms has been provided. It is now time to provide a more detailed introduction. One of the main reasons why compliant mechanisms have not widely caught on is because how complicated it can be to design them. In a conventional mechanism, generally speaking, each element has a single function. When it comes to compliant mechanisms though, more than one function might

be fulfilled by a single element. Therefore, making their design process much more challenging. It is the leaps forward in material engineering (the wide array of polymeric and composite materials now commercially available), raw computational power and design technics that are enabling the design of new compliant mechanisms.

There are different advantages that make compliant mechanisms attractive for designers. Integrating different functions into a single element can lead to a reduction in costs due to simplifying the assembly process (fewer components to assemble, store and manufacture). Using the deformations of the elements that comprise the mechanism instead of adding joints to it can also increase its performance by reducing the wear and the backlash, and this also eliminates the need of lubrication. Additionally, there is de advantage of being able to miniaturize compliant mechanisms (1). Compliant mechanisms in general also tend to be fairly light weight, adding to the above listed benefits.



Figure 2: Example of Compliant Mechanism Using Flexure Hinges (4)

As well as advantages, those inherent characteristics that compliant mechanisms have also increase the difficulty of their design. The integration of different functions into fewer elements forces the need of designing simultaneously for force and motion. This difficulty is further increased when nonlinearities have to be considered, which usually

happens when working with large deformations. Another aspect that should be considered is fatigue on the flexible elements. Since the motion of the mechanism is generated from the bending of flexible parts, stresses are generated there, which if repetitive they could lead to fatigue loads. Therefore, the fatigue life of the sensible elements should exceed the expected life for the mechanism. Two other important aspects concerning the stresses on a mechanism remain: stored strain energy and stresses applied over long periods of time. The strain energy stored on the flexible elements due to its loading state could greatly change the position of the mechanism if a sudden load variation occurred. Lastly, loads applied over long periods of time could lead to permanent deformations on the mechanism, effect that should be avoided with a careful design and choice of material.

As we can see, the technological advances, new materials and the new models being developed by researchers are greatly increasing the relevance of compliant mechanisms, both commercially and for further research. As such, this Master thesis aims to humbly contribute to that research by building a prototype for a compliant mechanism (the 2+1 parallel continuum robot) and attempting to get it ready to test the design as a pick and place manipulator in the future. It is of the utmost importance that the design of the mechanism is relatively modular, so that its design can be tweaked with ease so that further testing can be performed and the compromises that the actual design might have can be addressed, should the researchers team decide that the concept ought to be developed further.

### 3. Goals and Scope of the project

Up until now, the underlying concepts of the thesis have been discussed, while only briefly mentioning what the thesis itself set out for. It is now time to clearly state the scope of this master thesis as an engineering project and dive deeper into what it wants to achieve.

As for the scope of the project, it comprises the working prototype, and the document containing the thesis itself. The written document is of the utmost importance, as it



gathers all the necessary information for its further development: all the design details and assembly process, important when making any modifications to the prototype, and the results and procedures for the initial tests, which should provide a solid basis for the time when further testing is required.

Throughout the completion of the master thesis, various goals have been kept in mind, some of them having to do more with the prototype and some others with the memoir itself. It is the conjunction of both that is required for achieving the goals of the project, which are now stated:

- Optimizing the resources already available, build a prototype that can be compared to a similarly sized commercial parallel manipulator, for example: (6).
- The prototype s design should take into consideration future modifications and additions to the prototype.
- Provide insight about Diego s theoretical research by comparing the result from the Matlab simulations against test results.
- Write a comprehensive document, trying to make it easy to understand and build upon.

## 4. Benefits contributed by the thesis

Up until this point, only the advantages of compliant mechanisms in general have been discussed. In this section, the focus changes to consider the benefits contributed by this thesis in particular, which may have an impact on a wide variety of fields.

Academically, the most obvious contribution for this prototype is to allow testing the algorithms and theories developed under Diego s PhD thesis. Even if up until now only the static models were tested, having the working prototype makes that testing the dynamic models developed for the mechanism much easier to test. However, there are some other benefits as well. Having a prototype with known limitations and aspects that need improving or further development provides a source for more projects in which more students could work. This would greatly benefit both parties of the agreement, as

the research group would have the prototype evolve and move forward and the students would have the perfect framework to develop a successful bachelor or master thesis.

If this concept is developed further after the completion of this master thesis and the flaws that the mechanism might have in the present are solved the resulting prototype could positively contribute in continuum robots becoming more widely used. Go-to solution when you need to perform pick and place operations and due to some factor, the mass of the robot becomes a critical factor. The use of new materials (composites and polymers) could allow for the use of the robot in corrosive or generally adverse environments where a more conventional manipulator could not be used. Moreover, that could also result in the production of more environmentally friendly robots.

Also connected to previous point, this could yield designs for robots that are safer to work around them and that might prevent severe accidents from happening if workers needed to work side by side with those manipulators.

A design like this could be cheaper to manufacture, so that might encourage some companies using this kind of robots instead of workers to perform such monotonous tasks, getting rid of low quality jobs that no one wants to perform, and encouraging better ones. It also has a simpler design. So its maintenance might be easier and cheaper, making factories less dependent on manufacturers for the maintenance of the robots.

## 5. Requirements for the prototype

As part of testing out the Matlab models Diego made about rods bending, and one of the main things of the research group being parallel manipulators on its various forms, the design proposed to develop for this project exploited those two things.

First and foremost, the prototype should be able to cover at least the same working space as the robots that it is going to be compared against, hence, the theoretical dimensions provided for the initial concept would yield a similar, if not smaller footprint than one of those delta parallel manipulators.

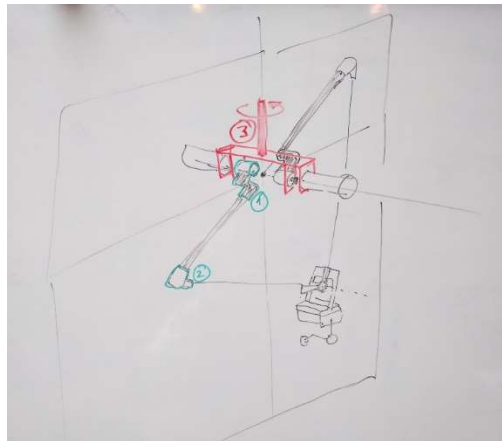


*Figure 3: Sketch of the initial concept for the prototype.*

Of course, in order to fully compare it to one of those delta robots it should be able to cover a three-dimensional space. However, before making the jump to 3D we had to make sure that the idea for the planar mechanism worked. So, that is why for this project the design and testing process only covers the planar mechanism. The planar mechanism itself would consist of four bars, two flexible bars and two rigid. The bars should be connected in pairs of a flexible and a rigid bar, glued together at a fixed  $115^\circ$  angle. Then the flexible bars would meet at an R joint, where the end effector would be located, and each rigid bar would be connected to one motor. In Figure 4, the black lines represent

the rigid bars, and the red lines the flexible bars, and the dimensions shown are the theoretical ones. The design phase of the project consists of giving physical form to that concept that has just been explained.

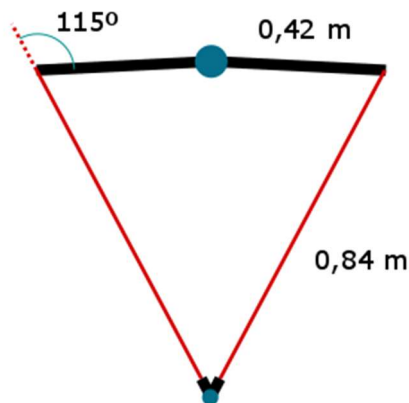


*Figure 4: Dimensional requirements for the prototype.*

The other main issue concerning requirements for the prototype are its mechanical requirements. The main parameter here is the torque at the motors. Even if the motors to be used were known already, as they were available from previous prototypes, the concern was knowing how well those motors would be able to cope with the forces generated on the prototype.

This information is presented again later in the design phase. Nevertheless, the motor and gearhead combination that was at our disposal was an RE 40 (part number 148867) DC motor and a GP 32 A (part number 166158) planetary gearhead. The limiting factor for this combination would be the continuous torque that it can provide, which can be calculated by multiplying the continuous torque that the motor can provide by the reduction the gearhead has:

$$0.177 \text{ Nm} * 14 = 2.478 \text{ Nm}$$

After obtaining the torque on the shaft of the gearhead the next step is to run the Matlab simulations to obtain some values to compare them both. The inputs for the program are the properties of the flexible bars, in this case 10 mm thick nylon bars and the

dimensions of the mechanism (Figure 5). The tests that were carried out to obtain the mechanical properties of the nylon bars are presented later in the section.

```

##### GEOMETRIC AND MECHANICAL PROPERTIES #####
d = 10.47e-3 ;      % Diameter of the section [m]
r = 0.5*d ;
I = 0.25*pi*r^4 ;  % Intertial of the cross-section [m^4]
A = pi*r^2 ;      % Cross section area [m^2]

E = 1.01717e9 ;    % Young's modulus [Pa]

ro = 1133 ;        % Densitiy of the flexible bar [kg/m^3]

% Geometric parameters of the assembled mechanism
h = 0.0 ;          % [m]
Lrigid = 0.42 ;    % [m]
Lflex = 0.768 ;   % [m] 0.84-0.05 ;
d1 = 0.05 ;       % [m]
d2 = 0.05 ;       % [m]
alpha = 115/180*pi ; % [rad]
  
```

*Figure 5: Example of Matlab code of where to change material properties and dimensions.*

It should be noted that at these early stages of the project the Matlab programs consisted on solving the Inverse kinematic problem of the mechanism statically. That meant that as accurate as the model might be, in a real motion the loads are bound to reach higher values due to the inertia of the elements of the mechanism, even more so if a weight is added on the end effector.

The simulation shown covers the perimeter of the working space, starting at the origin position for the mechanism, at (0, 0), and no load at the end effector is considered, just the mechanism s own weight.

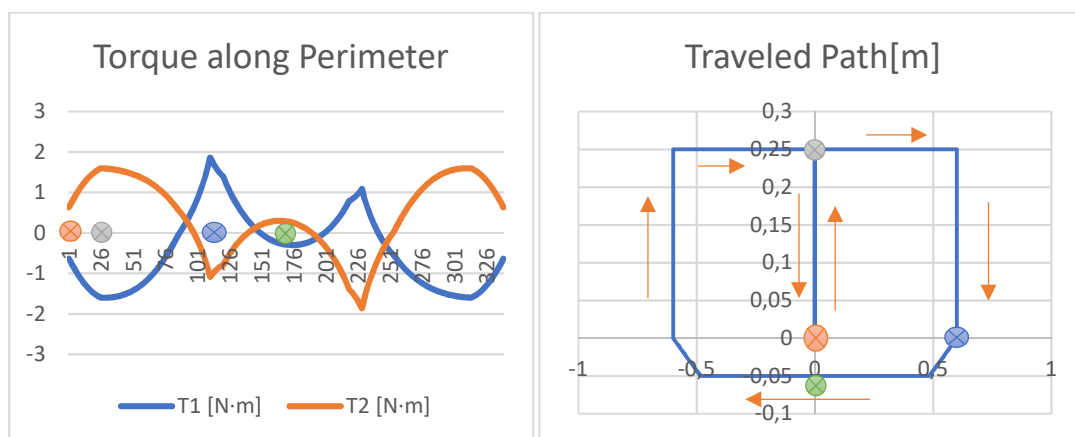


*Figure 6: Simulated trajectory for the model in Matlab.*

Looking at the results, it can be seen that values of almost 2 Nm are reached at two different points along the trajectory, the ones represented with a grey and a blue dot in Figure 6. This being the case for static loading and no external load on the mechanism it can be expected that the motors will struggle to generate the desired motions on the prototype. However, that value did not deter the project from moving forward with those motors, as they would just get the work done to start testing some slow motions and see how the design turned out.

Another two aspects to take into account were the materials that would be used. First regarding the flexible bars, for whose selection some preliminary testing was carried out between rods of different materials that were available already from experiments carried out in the past. After much consideration the 10-mm nylon bar was deemed to be the most appropriate for the application. Therefore, the testing described in the following paragraphs only shows the factors that make those nylon bars adequate for our application, without mentioning the other materials that were included in the tests. Secondly, it is widely known that estimating the properties of a 3D printed material is quite difficult, due to the various factors that influence them, such as the direction when printing the parts and the solidity of the final printed part, even if it was solid on the CAD model.

The testing of the flexible rods began by performing a test to obtain the buckling load of the rod. The test consisted on clamping both ends of a rod in the lathe, with a force measuring sensor on one end and compressing it as much as possible Figure 7, obtaining a buckling load of 60 N. From that load the flexion modulus for the bar was obtained:  $EI = 0.6206Nm^2$ , and considering the diameter of the bar the equivalent flexion Young's modulus was calculated:  $E_{flex} = 1.22GPa$ .

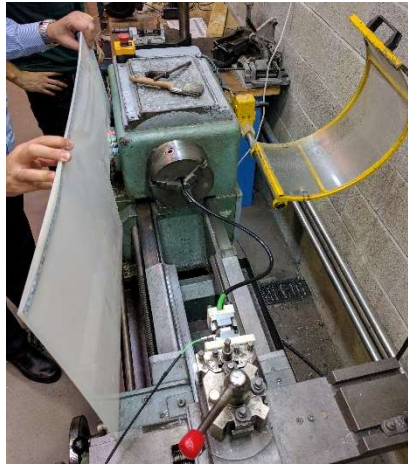


*Figure 7: Buckling test on the lathe.*

After obtaining  $E_{flex}$ , various simulations were run on the Matlab programs, for different values of the curvature ( $k$ ) that those rods could have. Figure 8 shows that bars with a curvature of at least 3 m<sup>-1</sup> can cover the desired working space. Combining the curvature with the equivalent flexion Young's modulus concluded that the bars should at least have a yield strength of at least 18 MPa.

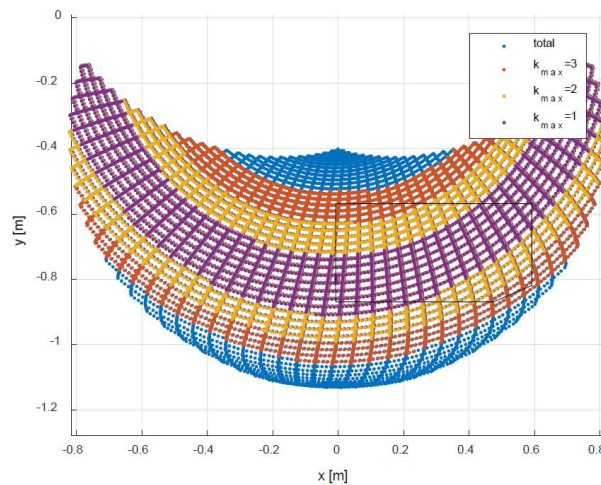


*Figure 8: Comparison between the full working space of the mechanism with different values of  $k$  and a comparable ABB Flexpicker.*

The final test that validated the use of those rods was a traction test Figure 9. The main takeaway from this test was that the resulting yield strength was above 40 MPa, more

than doubling our previous requirement of 18 MPa. Therefore, making the 10-mm nylon rods fit for the mechanism.



*Figure 9: Traction test on 10-mm nylon bars.*

Additionally, we also obtained the traction Young's modulus for the bars, should it be of use in the future, which had an approximate value of  $E = 918.3\text{MPa}$ . The results of those tests can be seen in Figure 10.

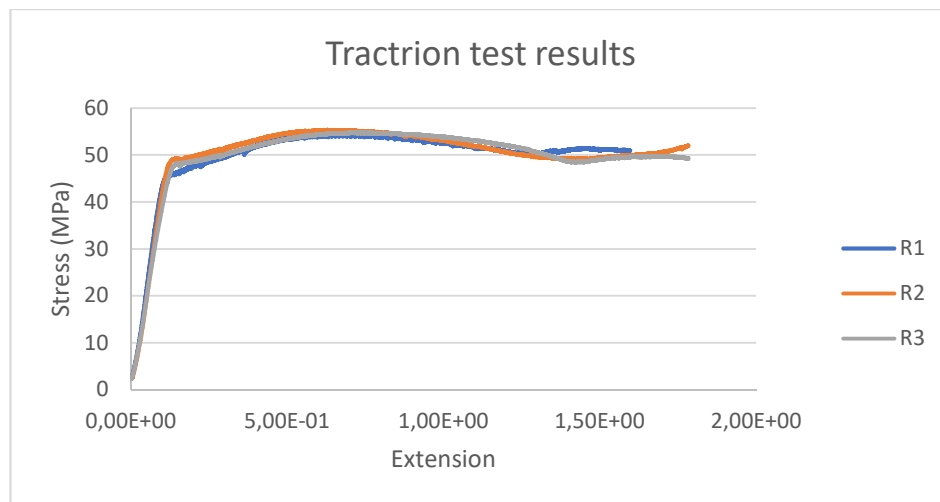


*Figure 10: Traction test results for 10-mm nylon bars.*

As for the ABS plastic used on the 3D-printer, a few (three) test specimens were printed, with a 150 mm length and a  $11.9 \times 7.3 \text{ mm}^2$  section, and they were subjected to a traction test, which yielded the following results:



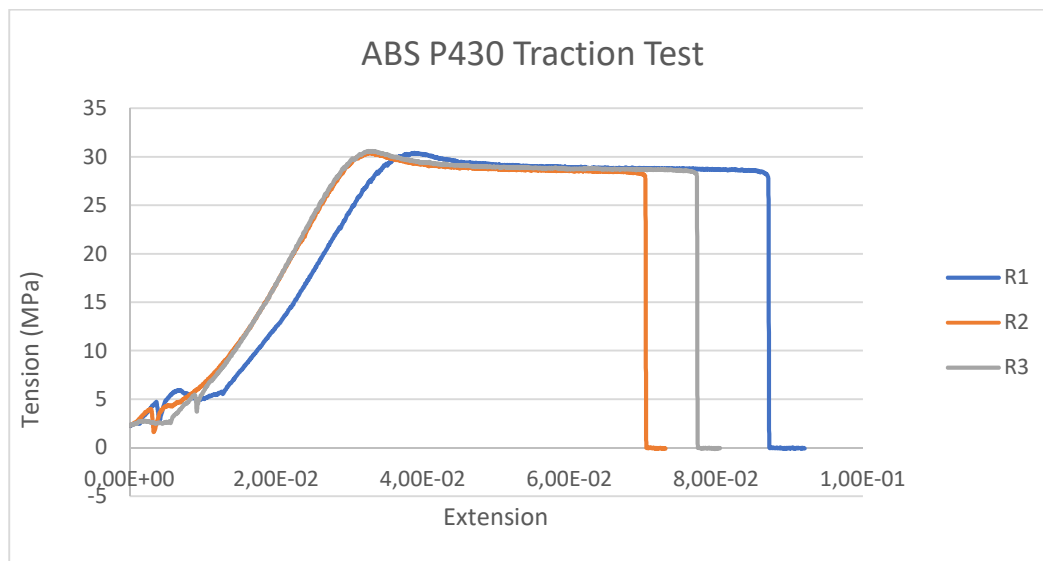


*Figure 11: Traction test for the material used in the 3-D printer.*

Analyzing the results obtained, the approximate values obtained for Young's modulus and the yield strength were respectively:  $E = 0.9\text{GPa}$  and  $\sigma_y = 30\text{MPa}$ . The setup for this test was the same as the one previously used in Figure 9.

## 6. State of the art

For the state of the art of this project, it was decided that three main topics should be addressed. First the rod model used for solving the inverse and forward kinematics of the mechanism is presented. After the theoretical background, since one of the future goals for the prototype would be to perform pick and place operations, an introduction of commercially available pick and place robots, their main characteristics and a list of some of the most important manufacturers is later introduced. Finally, the last subsection inside the state of the art cover what could be the future of both compliant mechanisms, continuum robots and pick and place robots by presenting relevant patents (and also a research paper) on these topics.

## 6.1. Relevant theory on the topic

It is by no means this thesis aim to discuss the different methods that exist for modeling rods or their adequacy for this particular case. If the reader is interested in a more detailed explanation of this topic they should head to (2). It was however deemed appropriate to provide a brief overview of the rod model in which the Matlab programs are based on.

In order to obtain the Cosserat rod model equations one must separately develop the rod kinematics, the equilibrium equations and the constitutive laws and later combine them to obtain the final system of differential equations.

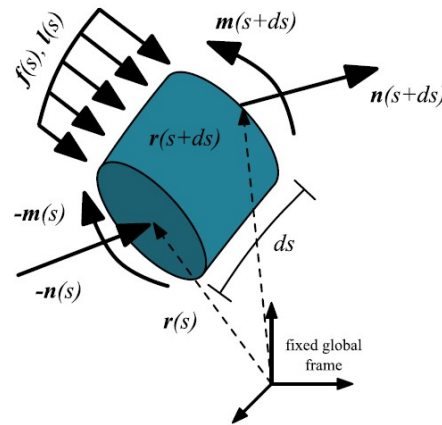


*Figure 12: Rod portion of length  $ds$  subjected to distributed external forces and moments, also showing internal forces and moments.*

- Kinematics:

A rod is characterized by the curve that its centerline describes in space,  $\mathbf{p}(s) \in \mathbb{R}^3$ , and the orthonormal rotation matrix expressing the material orientation,  $R(s) \in SO(3)$ . Both of them are function of a scalar reference length parameter  $s \in [0, L]$ . Thus, a mapping from  $s$  to a homogeneous rigid-body transformation,  $g(s) \in SE(3)$ , describes the whole rod:

$$g(s) = \begin{bmatrix} R(s) & \mathbf{p}(s) \\ 0 & 1 \end{bmatrix} \quad (6.1)$$

SE(3) is the special Euclidean group in three dimensions.

To represent the linear and angular rates of change of  $g(s)$  with respect to  $s$  expressed in coordinates of  $g(s)$  are  $\mathbf{v}(s)$  and  $\mathbf{u}(s)$  respectively. Therefore, the evolution of  $g(s)$  along  $s$  is defined by the relationships:

$$\dot{R}(s) = R(s)\hat{\mathbf{u}}(s) \quad \dot{\mathbf{p}}(s) = R(s)\mathbf{v}(s) \quad (6.2)$$

The dot denotes a derivative with respect to  $s$ . Without going into too much detail, the  $\hat{\cdot}$  symbol represents a transformation such that:

$$\mathbf{u} = [u_x u_y u_z]^T \in \mathbb{R}^3 \rightarrow \hat{\mathbf{u}} = \begin{bmatrix} 0 & -u_z & u_y \\ u_z & 0 & -u_x \\ -u_y & u_x & 0 \end{bmatrix} \quad (6.3)$$

The inverse operation is denoted by the symbol  $^\vee$ .

The undeformed reference configuration of the rod is expressed with  $g^*(s)$ , where the  $z$  axis of  $R^*(s)$  is tangent to the curve  $\mathbf{p}^*(s)$ , and  $x$  and  $y$  should ideally be aligned with the principal axis of the cross section. The reference kinematic variables are calculated as follows:

$$[\mathbf{v}^{*T} \ \mathbf{u}^{*T}]^T = (g^{*-1}(s) \dot{g}^*(s))^\vee \quad (6.4)$$

- Equilibrium equations:

Based on Figure 12: Rod portion of length  $ds$  subjected to distributed external forces and moments, also showing internal forces and moments., the static equilibrium equations are stated for any arbitrary section of rod. By operating and deriving that expression with respect to  $s$  the classic forms of the equilibrium differential equations are obtained:

$$\begin{aligned} \dot{\mathbf{n}}(s) + \mathbf{f}(s) &= \mathbf{0} \\ \dot{\mathbf{m}}(s) + \dot{\mathbf{p}}(s) \times \mathbf{n}(s) + \mathbf{l}(s) &= \mathbf{0} \end{aligned} \quad (6.5)$$

$\mathbf{n}$  and  $\mathbf{m}$  represent the internal force and moment vectors in the global reference frame. The distributed applied force per unit of  $s$  is  $\mathbf{f}$ , and the distributed applied moment per unit of  $s$  is  $\mathbf{l}$ .

- Constitutive equations:

Linear constitutive laws are used to map the kinematic strain variables to the internal forces and moments by taking the elastic material properties into account.

For this formulation it is assumed that the  $x$  and  $y$  axis of  $g^*(s)$  are aligned with the principal axes of the cross section.

The stiffness matrices used:

$$\begin{aligned}
 K_{SE}(s) &= \begin{bmatrix} GA(s) & 0 & 0 \\ 0 & GA(s) & 0 \\ 0 & 0 & EA(s) \end{bmatrix} \\
 K_{BT}(s) &= \begin{bmatrix} EI_{xx}(s) & 0 & 0 \\ 0 & EI_{yy}(s) & 0 \\ 0 & 0 & G(I_{xx}(s) + I_{yy}(s)) \end{bmatrix}
 \end{aligned} \tag{6.6}$$

$K_{SE}$  is the stiffness matrix for shear and extension.  $K_{BT}$  is the stiffness matrix for bending and torsion.  $A(s)$  refers to the area of the cross section,  $E(s)$  is Young's modulus,  $G(s)$  is the shear modulus and  $I_{xx}(s)$  and  $I_{yy}(s)$  are the second moments of inertia about the principal axes.

Thus, the constitutive laws for the rod are:

$$\begin{aligned}
 \mathbf{n}(s) &= R(s)K_{SE}(s)(\mathbf{v}(s) - \mathbf{v}^*(s)) \\
 \mathbf{m}(s) &= R(s)K_{BT}(s)(\mathbf{u}(s) - \mathbf{u}^*(s))
 \end{aligned} \tag{6.7}$$

- Explicit model equations:

To obtain the model equations, (6.5) and (6.7) are expressed in terms of their derivatives and the kinematic relation (6.2). Also, all variables are  $s$ -dependent, except the stiffness matrices, which are considered constant with respect to  $s$ :

$$\begin{aligned}
 \dot{\mathbf{p}} &= R\mathbf{v} \\
 \dot{R} &= R\hat{\mathbf{u}} \\
 \dot{\mathbf{v}} &= \dot{\mathbf{v}}^* - K_{SE}^{-1}(\hat{\mathbf{u}}K_{SE}(\mathbf{v} - \mathbf{v}^*) + R^T\mathbf{f}) \\
 \dot{\mathbf{u}} &= \dot{\mathbf{u}}^* - K_{BT}^{-1}(\hat{\mathbf{u}}K_{BT}(\mathbf{u} - \mathbf{u}^*) + \hat{\mathbf{v}}K_{SE}(\mathbf{v} - \mathbf{v}^*) + R^T\mathbf{l})
 \end{aligned} \tag{6.8}$$

There is an alternate option to express the system of equations, by using  $\mathbf{m}$  and  $\mathbf{n}$  as state variables, instead of  $\mathbf{u}$  and  $\mathbf{v}$ . So called state variables are those that have to be integrated (which would also include  $\mathbf{p}(s)$  and  $R(s)$ ).

$$\begin{aligned}
 \dot{\mathbf{p}} &= R\mathbf{v}, & \mathbf{v} &= K_{SE}^{-1}R^T\mathbf{n} + \mathbf{v}^* \\
 \dot{R} &= R\hat{\mathbf{u}}, & \mathbf{u} &= K_{BT}^{-1}R^T\mathbf{m} + \mathbf{u}^* \\
 \dot{\mathbf{n}} &= -\mathbf{f}
 \end{aligned} \tag{6.9}$$

$$\dot{\mathbf{m}} = -\dot{\mathbf{p}} \times \mathbf{n} - \mathbf{l}$$

- Kirchhoff model:

The Kirchhoff model is a simplification of the Cosserat rod model that has so far been explained. The assumptions made for the Kirchhoff model are that the neutral line of the rod has a constant length and the transverse shear strain is neglected. Thus, this model considers that flexion and torsion stresses alone lead to the deformation of the rod. As the overall length of the bar remains constant, and normally there are no initial deformations,  $\mathbf{v} = \mathbf{v}^* = \mathbf{e}_3$ .

$$\begin{aligned}
 \dot{\mathbf{p}} &= R\mathbf{e}_3 \\
 \dot{R} &= R\hat{\mathbf{u}} \\
 \dot{\mathbf{n}} &= -\mathbf{f}
 \end{aligned} \tag{6.10}$$

$$\dot{\mathbf{u}} = \dot{\mathbf{u}}^* - K_{BT}^{-1}(\hat{\mathbf{u}}K_{BT}(\mathbf{u} - \mathbf{u}^*) + \mathbf{e}_3 R^T \mathbf{n} + R^T \mathbf{l})$$

If the state variables used are  $\mathbf{m}$  and  $\mathbf{s}$  then the only difference with (6.9) is the substitution of  $\mathbf{v}$  by  $\mathbf{e}_3$ .

- Numerical solution methods:

This is not but a brief mention of the resolution of such problems. The systems presented above are systems of non-linear differential equations with boundary conditions. The boundary conditions represent how the ends of the rod are constrained, which is a requirement to be able to obtain its deformed state. Moreover, the nonlinearity of the problem means that the problem needs to be solved numerically. Both in (2) and as part of Diego's research, it was determined that a very efficient way to solve those systems of equations is to use a shooting method, which in essence converts the boundary value problem (BVP) to an initial value problem (IVP), then using standard IVP algorithms to solve the system of equations. The main advantage that this methodology provided for (2) was the possibility of using this method for robot control, as it was fast and accurate enough.

## 6.2. Alternatives in the market already

The use of delta robots for pick and place applications became popular when the need in the industry appeared to quickly handle small objects. This happened during the 1980s in Switzerland, in the chocolate industry. From that origin the delta robots used for industrial pick and place applications have seen their capabilities greatly increase.

Table 1 shows a few examples of robots that are currently available, and it becomes clear how far they have gone when comparing to the previous example. It can be seen that the loads that can be handled range from 0.5 kg up to 12 kg. The robots have from three up to six degrees of freedom, depending on whether they have the ability to change the orientation of the end effector or not. Figure 13 shows an example of one that has that additional mobility. Some attention should also be drawn that except for the smallest FANUC model, which weigh between 20 and 30 kg, most of the other examples are quite heavy, over 100 kg, especially when compared against the payloads that they are capable of handling.

One of the main advantage of these robots is how fast they can move objects. As a showcase of that, Table 2 is included. The motions described consist of three straight trajectories in the following fashion: vertical-up/horizontal/vertical-down. All the robots on the table can perform any of the two trajectories in less than one second. This kind of speed is what our prototype might aim to achieve in the future.

Lastly, the working space for these robots, summing up the different examples on Table 1, is a cylinder of 800 to 1600 mm diameter and a height of approximately 300 mm. The smallest FANUC model was consciously left out, as it shows an exception when compared to the rest of the models. However, that also shows that delta robots can be light and compact too.

The brands whose catalogues were looked into to put Table 1 together include ABB, FANUC, OMRON and YASKAWA.



Figure 13: ABB IRB360 FlexPicker.

Table 1: Collection of commercial pick and place Delta robots.

Brand	Model	Number/Type/Variant	Dof	Working space	Max. Load	Weight	Footprint
ABB	IRB 360 FlexPicker	IRB 360-1/800	4	D = 800 mm ; h1 = 200 mm	1 kg	120/145 kg*	R = 400 mm
		IRB 360-1/1130	3/4	D = 1130 mm ; h1 = 250 mm ; h2 = 50 mm	1 kg	120/145 kg*	R = 565 mm
		IRB 360-3/1130	3/4	D = 1130 mm ; h1 = 250 mm ; h2 = 50 mm	3 kg	120/145 kg*	R = 565 mm
		IRB 360-8/1130	4	D = 1130 mm ; h1 = 250 mm ; h2 = 100 mm	8 kg	120/145 kg*	R = 565 mm
		IRB 360-1/1600	4	D = 1600 mm ; h1 = 300 mm ; h2 = 50 mm	1 kg	120/145 kg*	R = 800 mm
		IRB 360-6/1600	4	D = 1600 mm ; h1 = 305 mm ; h2 = 155 mm	6 kg	120/145 kg*	R = 800 mm
FANUC	M-1iA	M-1iA/0.5A	6	Di=95; De=280; h=100mm	0.5 kg	23 kg	134x370
		M-1iA/0.5AL	6	Di=200; De=420; h=150mm	0.5 kg	26 kg	134x370
		M-1iA/1H	3	Di=94; De=280; h=100 mm	1 kg	18 kg	134x370
	M-2iA	M-2iA/3A	6	Di=566; De=800; h=300 mm	3 kg	140 kg	D = 800 mm
		M-2iA/3AL	6	Di=830; De=1130; h=400 mm	3 kg	140 kg	D = 800 mm
		M-2iA/3SL	4	Di=830; De=1130; h=400 mm	3 kg	120 kg	D = 800 mm
M-3iA	M-3iA/6A	6	Di=900; De=1350; h=500 mm	6 kg	175 kg	D = 860 mm	
	M-3iA/12H	3	Di=900; De=1350; h=500 mm	12 kg	155 kg	D = 860 mm	
OMRON	Hornet 565	3 axes	3	D=1130; h=425 mm	8 kg	52 kg	D = 886 mm
		4 axes	4	D=1130; h=425 mm	3 kg	52 kg	D = 886 mm
	Quattro 650	H	4	D=1300; h=500 mm	6 kg	117 kg	-
		HS	4	D=1300; h=500 mm	6 kg	117 kg	-
Quattro 800	H	4	D=1600; h=500 mm	4 kg	117 kg	-	
YASKAWA	MPP	MPP3H	4	D=1300; h=601	3 kg	115 kg	D = 1040 mm
		MPP3S	4	Di=580; De=800; h=300	3 kg	95 kg	D = 860 mm

*Table 2: Cycle times for ABB IRB 360 FlexPicker.*

Cycle times					
	0.1 kg	1 kg	3 kg	6 kg	8 kg
<b>25/305/25 (mm)</b>					
IRB 360-1/1130	0.30	0.36			
IRB 360-3/1130	0.40	0.40	0.52		
IRB 360-8/1130		0.38	0.42		0.60
IRB 360-1/1600	0.35	0.40			
IRB 360-6/1600		0.43	0.48	0.60	
<b>90/400/90 (mm)</b>					
IRB 360-1/1130	0.44	0.51			
IRB 360-3/1130	0.60	0.60	0.75		
IRB 360-8/1130		0.55	0.65		0.92
IRB 360-1/1600	0.50	0.54			
IRB 360-6/1600		0.57	0.63	0.80	

### 6.3. Patents and relevant research

To conclude the state of the art for the thesis, it seemed appropriate to include a section with mainly patents relevant not only in the field of continuum robots or compliant mechanisms but also for parallel manipulators similar to the one concerning this thesis. Some patents are recent, but there are also some older ones whose inclusion on this list aims to showcase the early stages of continuum robots. There are also two other patents that incorporate a third degree of freedom to a planar mechanism through different alternatives.

- US4765795: Object Manipulator (1988).

One of the first examples of continuum manipulators consisting of links formed by two plates separated by actuated flexible rods that allow it to reach the desired pose. Different actuation methods are presented in the different claims for the actuation of the rods.



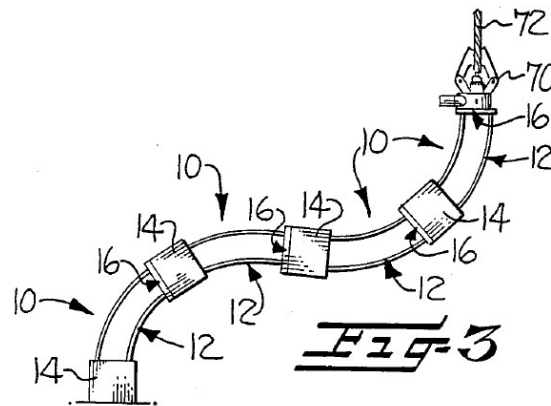


Figure 14: US4765795 drawing of full manipulator.

- US20160016319A1: Continuum mechanisms and their control.
   
 This patent gathers and summarizes all the research carried out in (2). This is a clear example of a recent patent that could yield commercially available products in the future, as it not only introduces the devices themselves but also their control method. The claims comprise the three different types of continuum robots studied during the dissertation. The first two consisting of an elastic structure in which rods slide throughout at least some extension of it. The first of the two having at least one rod defining a strip with an elongated cross-section (Figure 15), the second at least one pre-curved rod (Figure 16). The third type of robot being a two-portion robot with rods extending between both ends and being actuated on one end (Figure 17).

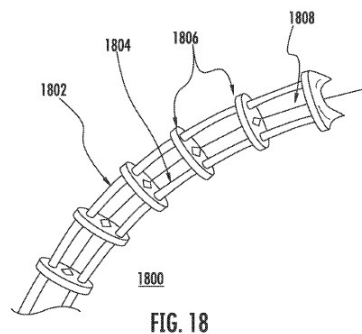


Figure 15: Example of continuum structure using strips.

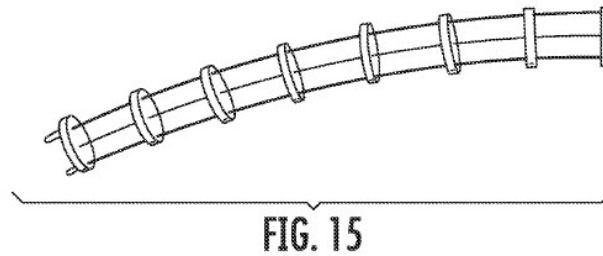


Figure 16: Continuum robot with pre-curved rods.

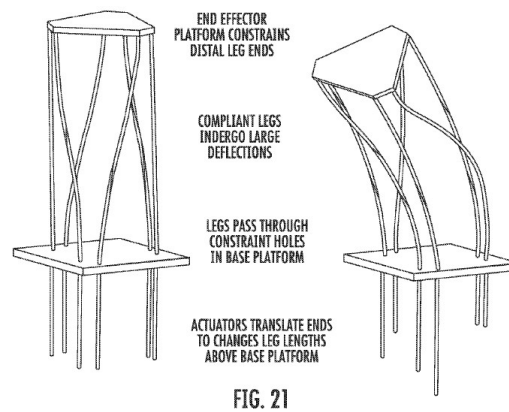


Figure 17: Hexapod example for third device claimed.

- US20080257096A1: Flexible parallel manipulator for nano-, meso-, or macro-positioning with multi-degrees of freedom.

This patent is an example of the potential of flexible parallel manipulators for small-scale applications. The parallel manipulator basically comprises a top platform with a set of flexible legs attached to it, of which at least one is actuated. The different embodiments explore different actuation methods for the legs.

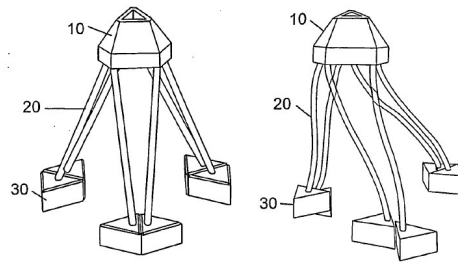


FIG. 1A

FIG. 1B

*Figure 18: Flexible parallel manipulator.*

- US7090458B2: Planar parallel robot mechanism with two translational degrees of freedom.

This patent was included because it explores the possibility of adding a third degree of freedom to a planar pick and place mechanism.

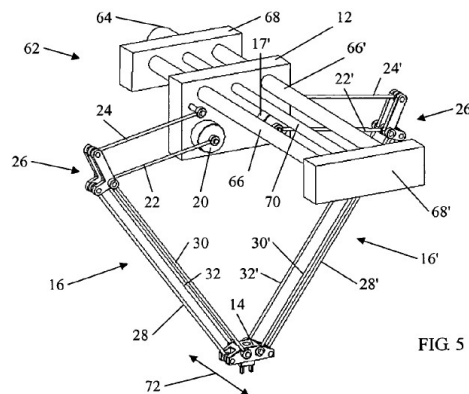
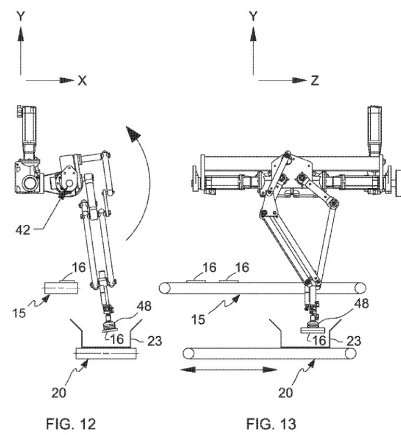


FIG. 5

*Figure 19: Planar parallel robot mechanism on a sliding platform.*

- US7644558B1: Robotic Case Packing System.

Similarly to the previous example, this invention also consists of providing a planar mechanism used for packaging operations with a rocking motion so that the whole working space of the robot is extended beyond the plane containing the two-axis robot. This approach appears to be convenient, as the packaging operation happens between two conveyors carefully placed.



*Figure 20: Robotic case packing system.*

- CN106313034A: Rigid-flexible coupling type flexible mechanical arm.
   
 This Chinese patent shows yet another recent, from 2016, example of using a series of links formed by rigid elements to build a continuum manipulator (Figure 21).

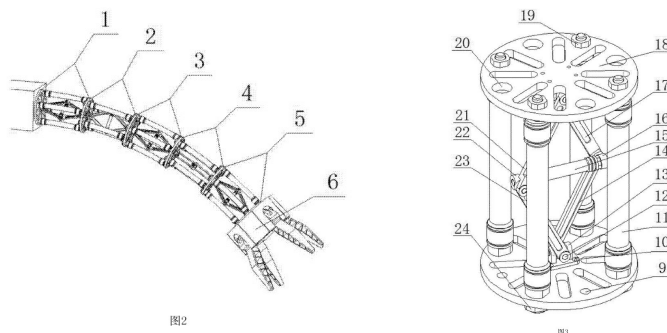


*Figure 21: Rigid-flexible coupling type flexible mechanical arm.*

- Design and Analysis of a Robust, Low-cost, Highly Articulated Manipulator Enabled by Jamming of Granular Media.
   
 Although not a patent, the innovative and completely unexpected approach for designing a continuum manipulator makes this article seem appropriate for this list. The prototype presented in the article addresses some of the disadvantages of hyper-redundant manipulators with a design consisting of an enclosure for the granular material (such as ground coffee) in which they are able to alter its compactness and thus alter the rigidity of the robot.



*Figure 22: Different positions for the manipulator made of ground coffee.*

## 7. Risk Analysis

This section focuses on assessing the severity of potential risk factors that could take place during the development of the project and could hinder its progression to different extents. After briefly describing each factor, they are ranked on a matrix according to their impact and the probability of them taking place.

During the design phase, even if the SolidWorks is great for detecting possible errors in the dimensions of the parts, there could still be some errors that go unnoticed and discovering them in the assembly phase could mean a significant waste of both time and materials, as the affected components would need to be corrected and manufactured again.

The critical machining duties were carried out by the workshop technicians, so the likelihood of defects happening during the machining of the different parts is relatively low. Still, errors during manufacturing is another risk factor that should not be overlooked.

Performing tasks at a workshop, using the machinery, inherently brings the risk of accidents happening, however low their likelihood.

Defective motors, unlikely, since they had already been used, but if the available motors stopped working the progress of the project would be greatly affected. Even if the need for more capable motors was addressed or the same ones were bought, their delivery by

Maxon could take up to eight weeks. An amount of time that could even put some stages of the project in jeopardy, if it were to happen just before the testing.

The small precedent on this kind of mechanisms may result in buying components, or manufacturing them, before knowing if they will be able to function without trouble. If those components ended up not being useful that could even mean going back to the drawing board to change the design, with its subsequent increase in the cost of the project.

During the testing phase, the mechanical failure of components could take place, with various degrees of negative impact, depending if the component could just be replaced with a spare one or would require manufacturing it again.

Potential risk that could hinder the progression of the Project: the ceiling falling upon our heads at the workshop, the already alarming number of leaks on the ceiling, which could be aggravated by the ongoing construction of the new bus station, could cause severe damage on the workshop that could make it unsafe to work there and therefore delaying the whole project to an unknown extent.

After presenting the different risk factor, they are ranked on a matrix according to their risk exposure, which combines the likelihood of each factor with its severity.

*Table 3: Risk exposure matrix.*

		Probability			
		High	Medium high	medium low	Low
Im- pact	High			·The work-shop closing.	·Accidents. ·Defective motors.
	Medium	·Component mechanical failure.	·Wrong selection of materials.	·Design flaws	·Manufacturing flaws.
	Low				

## 8. Design of the prototype

This section is divided into three different parts. Firstly, the design process is described, which includes all the design decisions that were made, an overview of the final design and a description of the individual components, including their manufacturing if relevant. The second part includes a detailed description of the whole assembly process. The third subsection discusses possible modifications or additions that could be performed on the prototype in order to increase its mobility.

As an underlying motive for all the design choices made, the parts had to be as compact as possible (to avoid the waste material when 3D printing), whenever possible.

Most of the parts were not submitted to a FEM test because the loads that we would put on the prototype were not big (not expecting to load it with more than 1 kg any time soon), and nothing about it is critical and something breaking would not be catastrophic. It is not optimized to be the lightest thing possible and lift as much as possible for that weight. Everything is oversized, based on previous experience with 3D printed parts from this same material and printer. For these reasons, getting the parts made was more important than obtaining very precise assessment from some simulations.

In order to keep the document as decluttered as possible, the blueprints with all the dimensions for each part are later attached in the appendix section. In the following description of the parts only some of the most relevant dimensions are mentioned.

### 8.1. Part description

The different functions that the different assemblies inside the mechanism had to fulfill were already explained on Section 5, so this section will mainly focus on breaking down each of the individual parts forming the different assemblies. Figure 23 shows how the different subassemblies are numbered for the following sections.

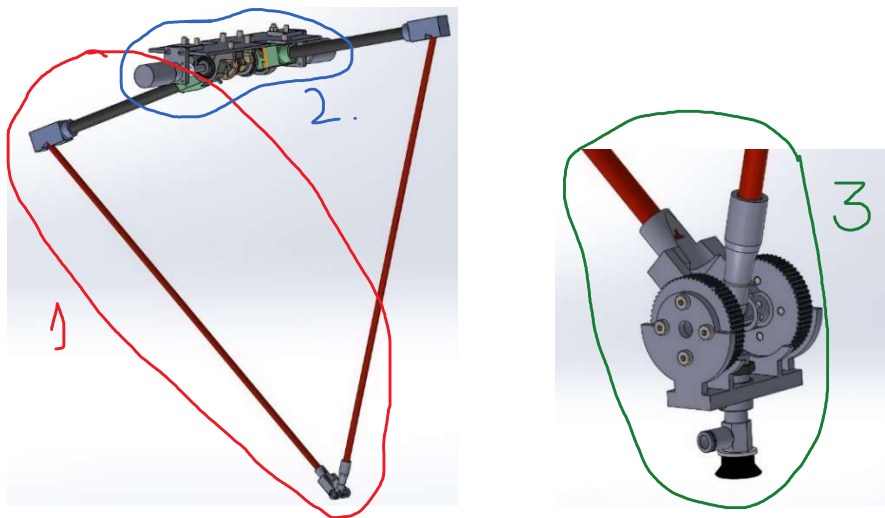


*Figure 23: Subassemblies of the prototype.*

#### 8.1.1. Subassembly 1:

This subassembly comprises four different 3D-printed parts. One to couple the rigid bars to the shaft that transfer the motion generated by the motors, which from now on will be named as the *shaft-bar coupling*, another one to mate the rigid and flexible bars at the required  $115^\circ$  angle, which will be addressed as the *elbow* and the two parts that form the R joint at the end of the two flexible bars.

Here we have to make sure that we stick to the dimensions for the concept, so we first think how the parts that will join the rigid and flexible bars will look, decide some reasonable dimensions for them and at the very end cut the bars to the desired length.

- Shaft-bar coupling:

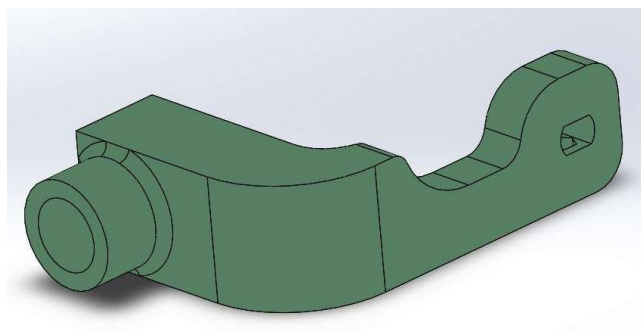


*Figure 24: Shaft-bar coupling.*



This part needed to have an L shape to leave room for the elements in between and simply to make sure that they did not hit each other; no interference.

Where the shaft goes, tried the thickness of the part to be of at least  $1.5 \times D$ ,  $D$  being the diameter of the shaft, so that it had plenty of contact area, and seems to be a design tip when designing that kind of transmission. Only for this particular detail were some finite element method (FEM) simulations carried out, as it was the most sensible point of the mechanism where stresses were concerned. In addition, that part had to be thinner to avoid the part hitting the plate where the motors are mounted, as that would have limited the motion range of the prototype.

This part appeared to be the most critical part, as its function is to transfer the motion from the shaft driven by the motor to the flexible mechanism. The thinness of the arm also raised concerns about how well it would handle the loads, so it was decided that running some FEM simulations was in order.

For the simulation, the part was fixed where the shaft goes, and a remote load was applied at a distance of 0.42 m from the axis where the shaft would be, in the X direction according to the Ansys drawing. The values for the forces applied correspond to one of the points in a trajectory similar to that in Figure 6, for the case when a vertical load of 5 N was applied, simulating carrying a 0.5 kg load. Those values are:  $X = 3.29 \text{ N}$ ;  $Y = 7.78 \text{ N}$ ;  $M_z = 2.41 \text{ Nm}$ .

The test consisted on trying different designs and assessing the effect that the modifications on the design had on the maximum equivalent Von Mises stress and the maximum deformation. The results of the three simulations are summarized on Table 4:

*Table 4: FEM Analysis results*

	Load	Deformation
Case 1	2.90 MPa	0.77 mm
Case 2	1.59 MPa	0.27 mm
Case 3	1.58 MPa	0.17 mm

Case 1 consisted on the part with that basic L shape, without any fins or nerves to act as reinforcements.

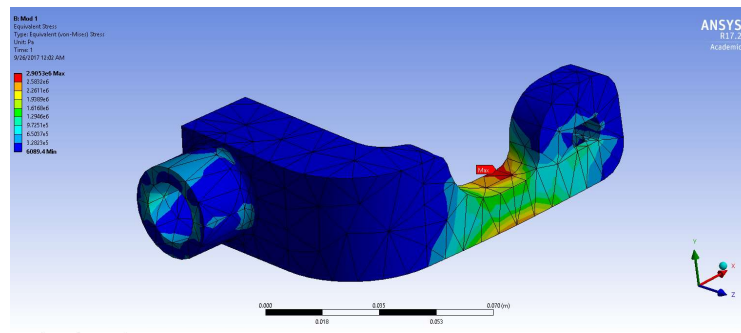


*Figure 25: Case 1 Stress.*

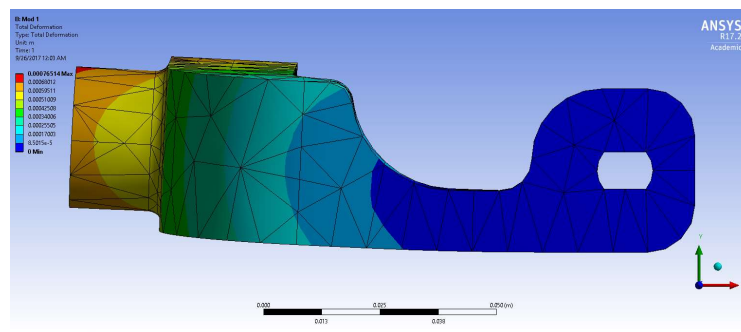


*Figure 26: Case 1 Deformation.*

For case two, some simple design modifications were made to try to minimize the max stress and deformation: two reinforcement fins were added as rein-

enforcement in the inside part of the L and also on the protruding tube-like protrusion where the CF bar is held. After running the simulation, we saw a significant improvement against the first case, the reduction for the maximum stress value was of a 45.2%, and it was 64.9% for the deformation (Figure 27 and Figure 28).

For the third case we wanted to try making the part as bulky as possible but without that interfering with its movement. The result was quite an ugly part and a very minor improvement over case 2 (Figure 29 and Figure 30).

It was therefore decided that the final design for the part would be that of case 2, but without the small fin for the tube-shaped element, as it can be seen from the simulations that its contribution to stress transmission is negligible. The result can be seen (again) in Figure 24.

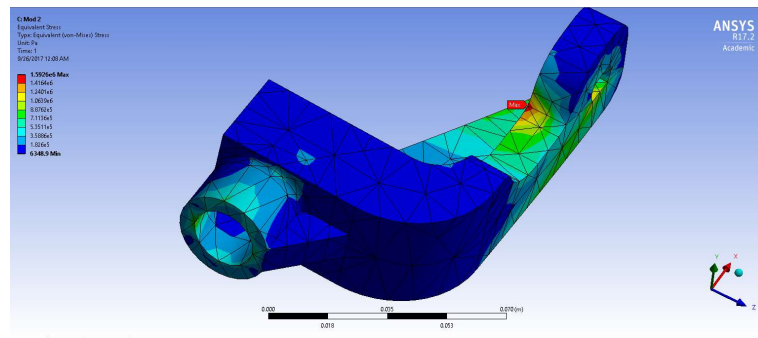


Figure 27: Case 2 Stress.

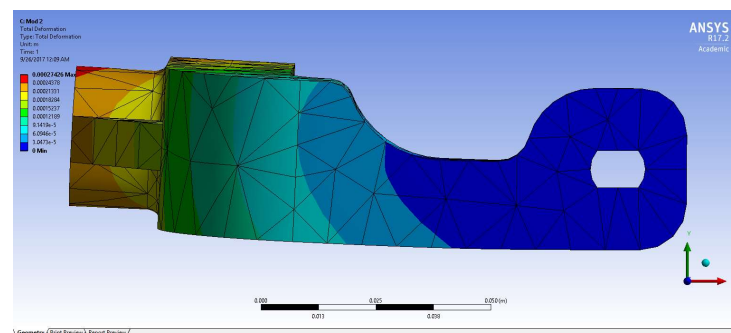


Figure 28: Case 2 Deformation.

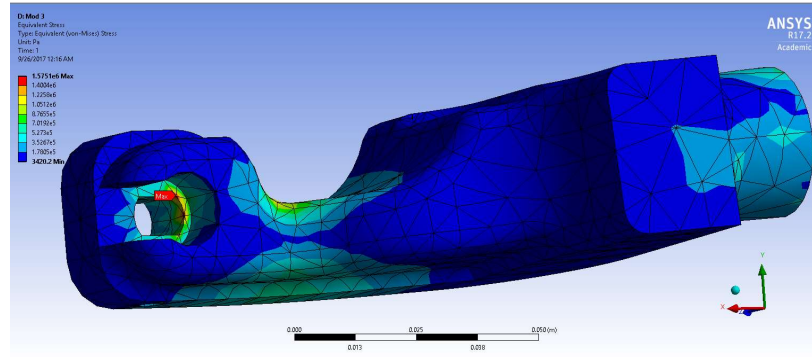


Figure 29: Case 3 Stress.

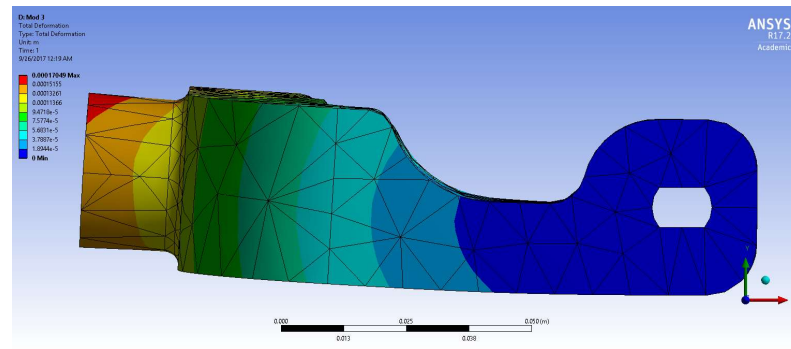


Figure 30: Case 3 Deformation.

Here to ensure the link between the shaft and the 3D-printed part the shaft had two opposing plane faces milled into it, which translates into the shape that this part has over that area. A hole was placed there so that a bolt could be inserted that would tighten the shaft and this part together, by inserting a nut on a cavity inside the contact area between the 3D-printed part and the shaft, and then screwing the bolt to it.

The depth of the cavity for the CF-bar was defined by the diameter of the bar itself, at about twice its diameter, to ensure a sufficient contact patch and the robustness of the union. This reasoning also applies for the bar-holding cavities of the elbows, both for the carbon fiber bar and the nylon one.

The manufacturing of this part consisted only on 3D printing it.

- Elbow:

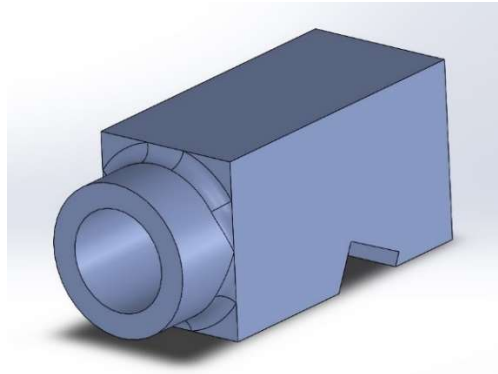


*Figure 31: Elbow.*

Simple shapes proved to be the best for this part. The cavity for the CF-bar same reasoning as before. The one for the nylon bar, however, quite a different story. The nylon bar is simply inserted into the elbow at the right angle. Thanks to this approach we get a flat side for the bottom, assembly again, don't need to worry if the clamping will be strong enough, as the whole part wraps around the bar itself. The boxy shape of the part was chosen to ease the alignment of the parts in the assembly phase.

The manufacturing of this part consisted only on 3D printing it.

- The parts for the R joint: modded a design already existing from another prototype (Mikel made).

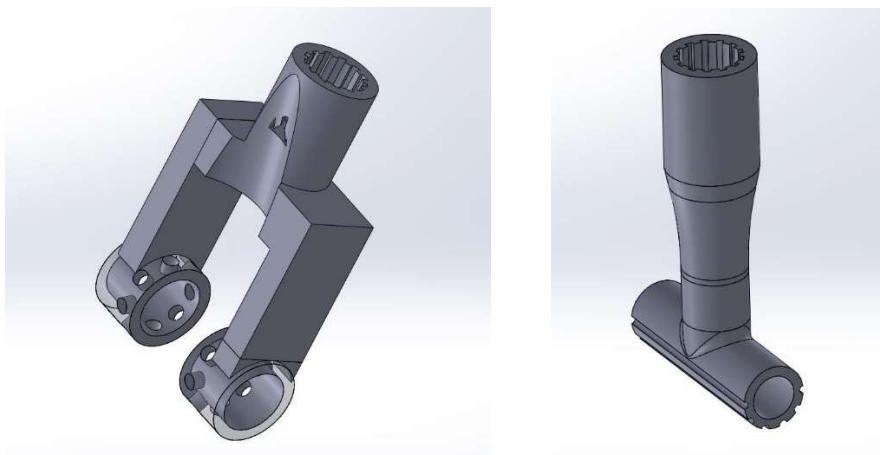


*Figure 32: Parts forming the R joint.*

The part needs to be as compact as possible in the direction of the axis of the joint, as the element used for attaching any element to the end effector wraps around it. The other mod made to the existing design was adding a passing through hole to be able to attach those elements. The diameter chosen for this hole was 8 mm, the same as the center hole of the pulleys chosen. The grooves on the cavity that holds the nylon bars were already present on the original design and worked well, so they were kept in place. That way we could try if gluing the bars was better with or without them. Both cases worked just fine. The other detail already present on the original design is the groove on the U that perfectly fits the T so that their bulk has as small an effect as possible when the bars are closed on a tight angle. It even exposes the tip of the nylon bar on the U side of the joint.

Then the other details have to do with removing the support material after taking the parts right out of the printer. For them in order to form a joint they need to be printed together, as the rings on the U go around the hollow cylinder of the T. Both the tiny holes on the U and the grooves along the length of the T make it easier for the chemical solution that removes the support material to get in the small gab between the two parts, so that they can freely rotate relative to each other.

Manufacturing: just 3D print.

- The bars, and getting to the length of each element:

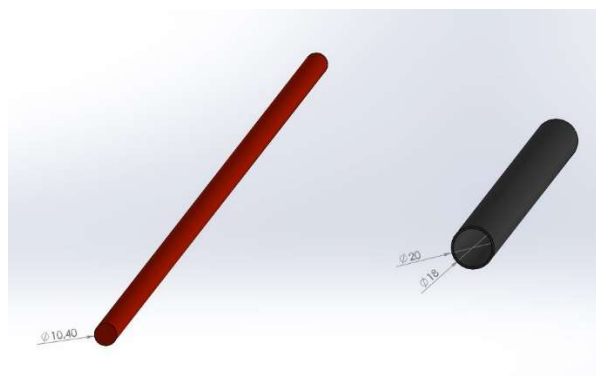


*Figure 33: Bars forming the mechanism.*

Not much mystery here. The bars available already we had. So their final length was calculated from subtracting the overall dimension minus the length of the other 3D-printed elements regarding to where they sit according to the mechanism's imaginary axis of sorts.

The bars were just bought and cut to size. For the carbon fiber used the hand-saw, to avoid cracking the tips of the bars when cutting.

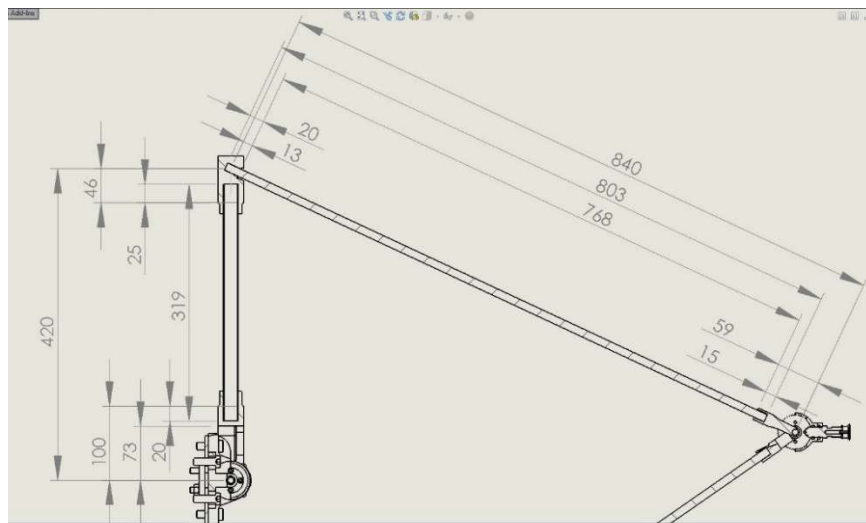


*Figure 34: Detail of how the length of the bars was determined.*

### 8.1.2. Subassembly 2:

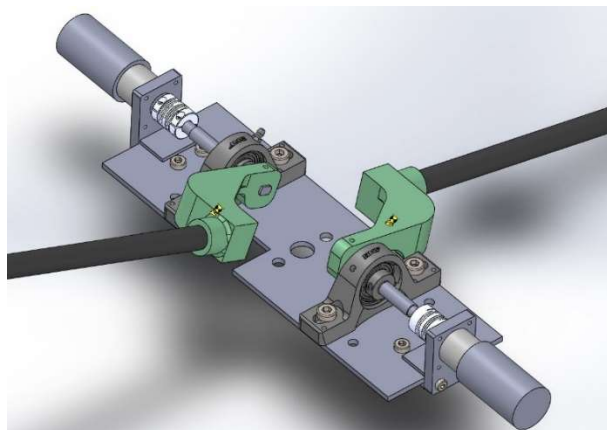


*Figure 35: Detail of the parts on the drivetrain.*

For the second subassembly we have the plate where the elements are mounted and those that act as a support for all the elements of the assembly. On the other hand, we have the elements that generate the motion and transfer it to the bars themselves.

The so-called powertrain consists of the motor+gearhead, the beam coupling, the shaft and the bearing support . All the components bought save the shaft. The function of the rest of the components is to keep everything together: the motor flange, the milled part that joins the motor flange to the plate and the plate itself. The aim was to keep the length of the overall powertrain as compact as possible, but the design was approached with no other considerations in mind.

- The Plate:

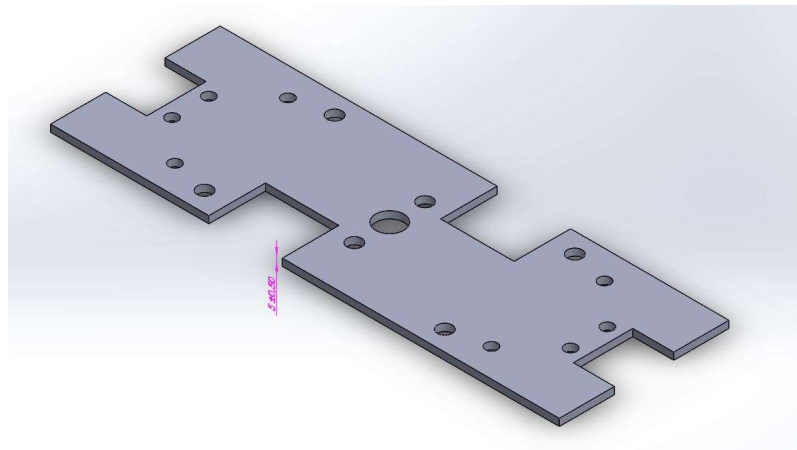


*Figure 36: The support plate.*

Just have enough space for all the elements. Used 5 mm aluminum plate already available in the workshop from another project. It was basically cut to shape using a grinder, and the holes drilled on the milling machine for precision. The cutouts on both ends are for connecting the motors, whilst the ones asymmetrical about the center of the plate are to make rooms for the carbon fiber bars, so that the range of motion is not affected by the plate. The other reason, apart from not working in excess by cutting sections that did not need cutting was to leave some unused area on the plate in case of future modifications to the prototype.



- Motor flange to plate adapter:

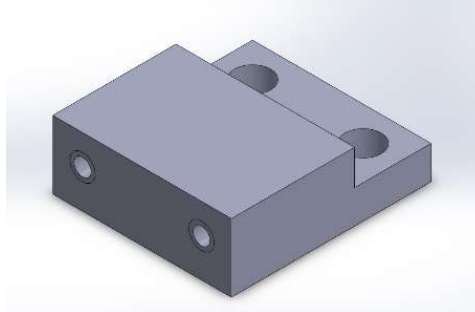


*Figure 37: Motor flange adapter.*

As the name implies, this part is used to attach the motor flange to the plate. It has two threaded holes for the screws on the motor flange, and the vertical ones are used to fix it to the plate using bolts and nuts. This part was machined at the university's workshop out of some scraps from previous projects no longer in use. It already had a thickness of 16 mm, so the operations required were cutting the part to the desired width with the saw, drilling the holes and making the threads for the lateral ones, and milling the flat face where the plate sits.

- Motor flange:



*Figure 38: Motor flange.*

This part was used along with the motors for an old prototype, so when the motors were no longer in use these parts also became available for us to use. It is a commercial part manufactured by Igus, reference: MF-1040-NEMA-17-S (7).

- The bearing and its housing:

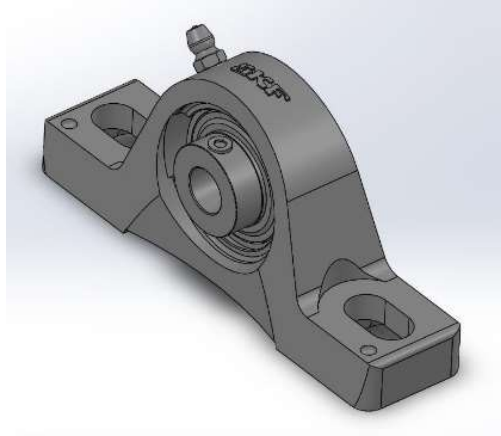


*Figure 39: Bearing in its housing.*

These two parts were also already available at the workshop. They consist of a cast iron housing (SY 503 M) and a 12-mm diameter insert ball bearing (VAR 203/12-2F), both manufactured by SKF. Having this part available determined a couple of very important aspects of the design: the diameter of the shaft and the critical dimension of the motor flange adapter. The diameter of the shaft needs no further explanation, but the height of the bearing's axle on the housing (30,20 mm) determined the 8,20-mm depth of the milling on the motor flange adapter (Figure 40).

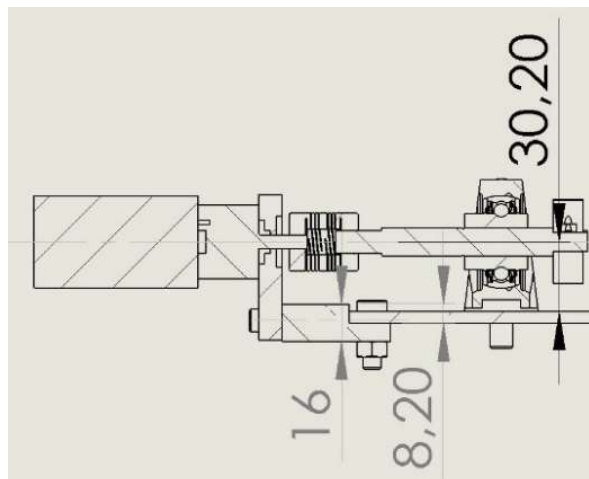


*Figure 40: Detail for the axis height and affected dimensions.*

- The beam coupling:



*Figure 41: Beam coupling.*

This is an aluminum beam coupling by Ruland (MWC25-10-6-A) . It connects the 6-mm shaft on the gearhead to the 10-mm part of the shaft that transmits the motion to the mechanism. Again, those were previously in use already, so by machining a small section of the shaft from 12 to 10 mm we were able to reuse them.

- The shaft:

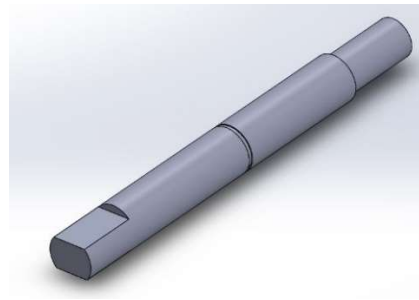


*Figure 42: Shaft.*

As already mentioned, the shaft would need to be 12 mm wide, determined by the bearing. A 12-mm steel rod was used to fabricate it. The operations performed were: cutting it to the right length, milling two flat sides on one end, reducing the diameter by 2 mm on the other end and making a groove for the circlip against which the bearing would sit (Figure 43). This last step is one of the most important ones, as the distance between the circlip and where the shaft-bar coupling sits against the shaft needs to be exactly the same on both shafts to ensure that both bars are on the same plane. A small misalignment here would result in the whole mechanism not being planar. The total length of

the shaft is by no means critical, so a small difference between the two shafts would be irrelevant.

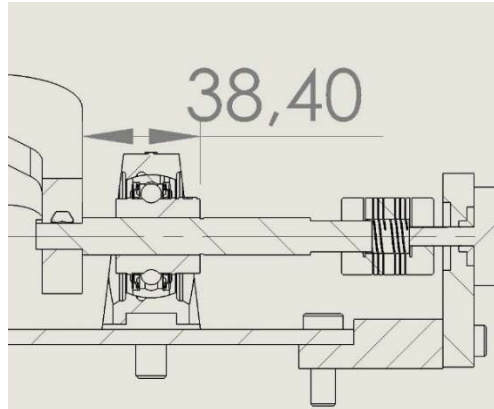


*Figure 43: Critical shaft distance detail.*

- Motor and gearhead (Maxon):



*Figure 44: Motor and gearhead mounted on a previous prototype.*

It should first be mentioned that to this motor and gearhead combination a controller is associated. It had already been in use for previous prototypes, as well as those motors and gearheads. Part numbers as follows:

- Motor: RE 40, 150 W. Part number: 148867.
- Planetary Gearhead: GP 32 A. 1:14 ratio. Part number: 166158.
- Digital positioning controller: EPOS2 50/5. 5 A and 50 V DC. Part number: 347717.

The motor and gearhead combo is mounted on the motor flange using some screws that go around the shaft that outputs the motion. Their full specification list can be found in the appendix.

### 8.1.3. Subassembly 3:

So far, no mention has been made to how end effectors are connected to the prototype, save for the 8-mm hole present at the joint. Two different solutions have been tested so far. It is also important to keep in mind that as a robot for pick and place, the orientation of the gripper must be kept in check. One of the solutions tested was using an action camera 3-axis gimbal, the Feiyu Tech WG (Figure 45), and the other solution consisted of a system with pulleys, belts and rubber bands. In order to attach those solutions to the prototype either an 8-mm bolt or pin were used. If we are using the system with belts and pulleys we would use the pin and use a shaft collar to keep the thing together, but without tightening it, so that the rotation is not impeded. On the other hand, if we re putting something as the gimbal there, that by itself keeps the gripper horizontal we could use a long bolt and tighten it up with a nut.



*Figure 45: FeiyuTech WG 3-axis gimbal.*

As for the second option, a bit more complicated than the gimbal, but it does have some benefits to it: it is lighter and the tension on the rubber bands relieves the mechanism from some of the load generated by its weight.

The procedure followed to decide on the elements: first we chose some pulleys that had a reasonable number of teeth (the more the less that would affect the orientation)

and whose dimensions were compact enough to place two of them so that they don't take too much space in between the shaft-bar couplings on the plate and they could also be separated enough so that there was enough space for the joint where the flexible bars meet. It was very important to balance that out. Once the pulleys were chosen we searched for the belts that meshed and made sure that once we cut them in half they would be long enough and would be no risk of them losing contact with the pulleys.

As for the elastic element that would comply with the length variations to the end effector, regular rubber bands used in clothing were suggested by prof. Altuzarra. A couple of tests were conducted to test its properties and the rubber worked successfully. The first test was to get a rough estimation of the elastic modulus of the bands (which was of about 46N/m). And the other test consisted on hanging some weight from a piece of rubber band and let it hang for a long period of time, the goal of this test was to see if the material would retain its mechanical properties over time. After more than a week no significant permanent deformations were found on the material. The test basically consisted on checking the length of the rubber band for a few days in a row and writing it down, and checking if it changed. It was a 1 kg weight (Figure 46).



*Figure 46: Testing for permanent deformations on the rubber band.*

As everything went well, we then proceeded to buy the required elements and performed some tests to see if the idea worked (Figure 47). It worked relatively well, for the rubber band stretched at various lengths. But it came clear that we had to be really careful with having the same length of rubber on both ends of the belt for it to deform uniformly.

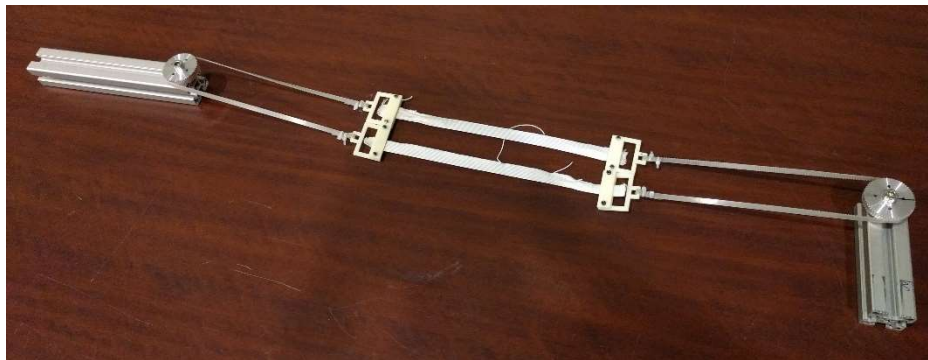


*Figure 47: Testing the system with the belts and pulleys.*

After making sure that it worked we proceeded to make it tidy. The clamps that connected the belt with the rubber bands were slightly redesigned to make them more compact (Figure 48).

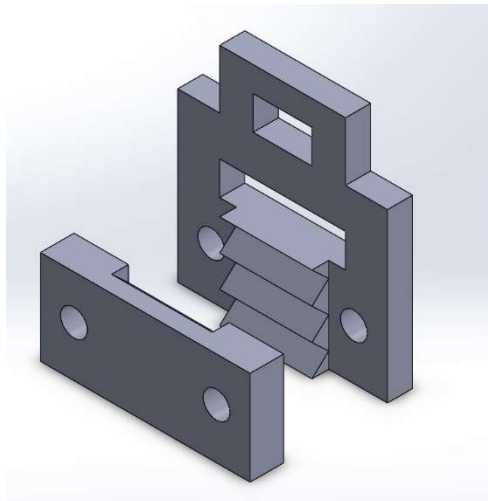


*Figure 48: Clamps for the rubber and the belt.*

To connect them, the belt was wrapped around itself and tied using two zip-ties. The rubber was clamped in the serrated portion of the part using a couple of bolts and nuts.



*Figure 49: Detail of how the clamps work.*

Then we proceeded to design the parts that would house the pulleys both in the plate (Figure 51 - left) and in the end effector (Figure 51 - right). It was very important that the position of the pulleys was correctly considered when designing the parts, making sure that each pair (top and bottom) were located on the same plane. In fact, in order to maximize the space for the end effector, the two pulleys located at the end effector were milled, as shown in (Figure 50).

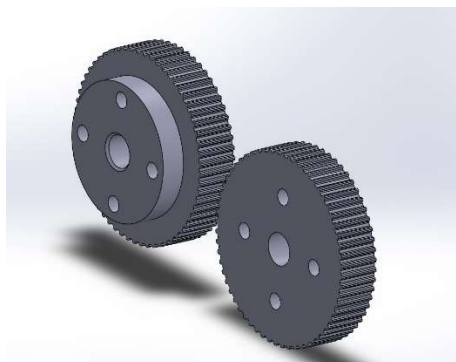


*Figure 50: The two different styles of pulleys.*



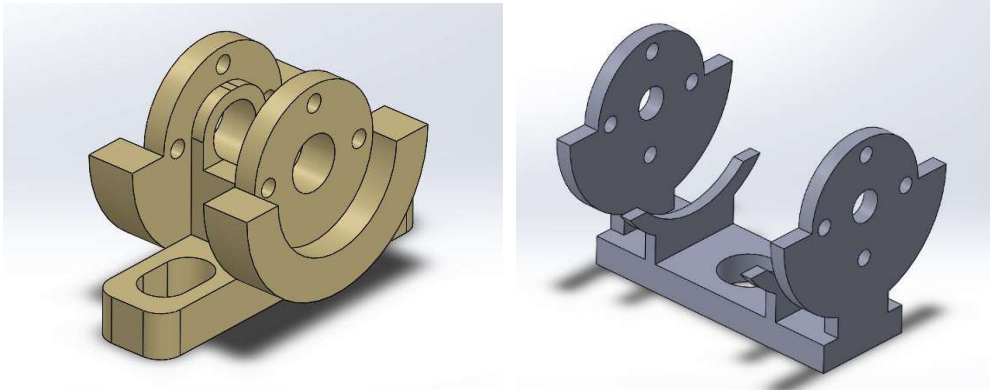


*Figure 51: Parts to house the pulleys.*

Finally, Figure 52 shows two pictures of how each of the end effector solutions look once installed on the prototype.

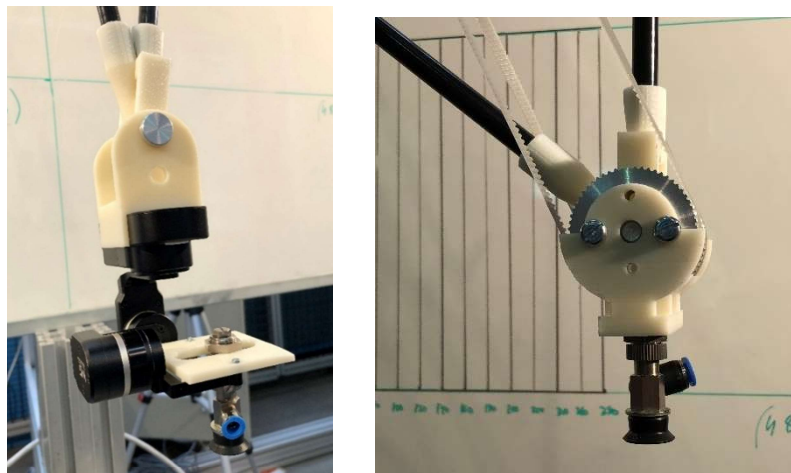


*Figure 52: The two end effector options.*

## 8.2. Assembly process

Once all the components were available, we began with the process of assembling the prototype. Figure 53 shows all the components of the prototype ready for assembly.

The first step of the assembly was gluing the bars into the 3D-printed parts. To ensure a positive outcome, the gluing took place in two steps. First, we separately glued the carbon fiber bars to the shaft-bar coupling and the elbows, and the nylon bars to the two parts forming the R joint at the end effector (Figure 54). Although it would take one more

day due to waiting for the glue to curate, it was deemed necessary in order to correctly align the bars.

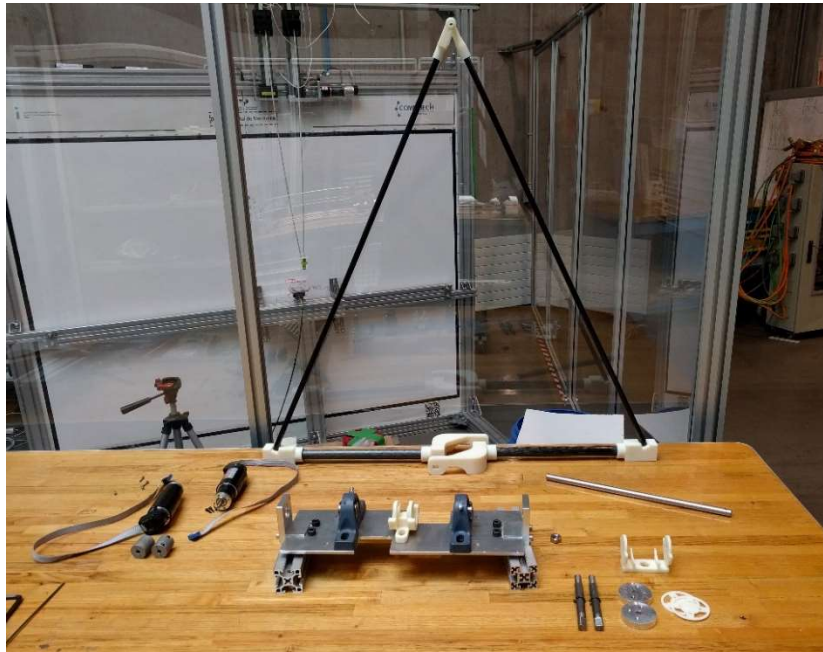


*Figure 53: All the parts.*

The following day we proceeded to glue the flexible bars with the rigid ones, forming the mechanism (Figure 55). Being careful about the alignment of the bars at the time of gluing them together. If this requirement is not met the mechanism will not work as intended.



*Figure 54: Glue bars 1*

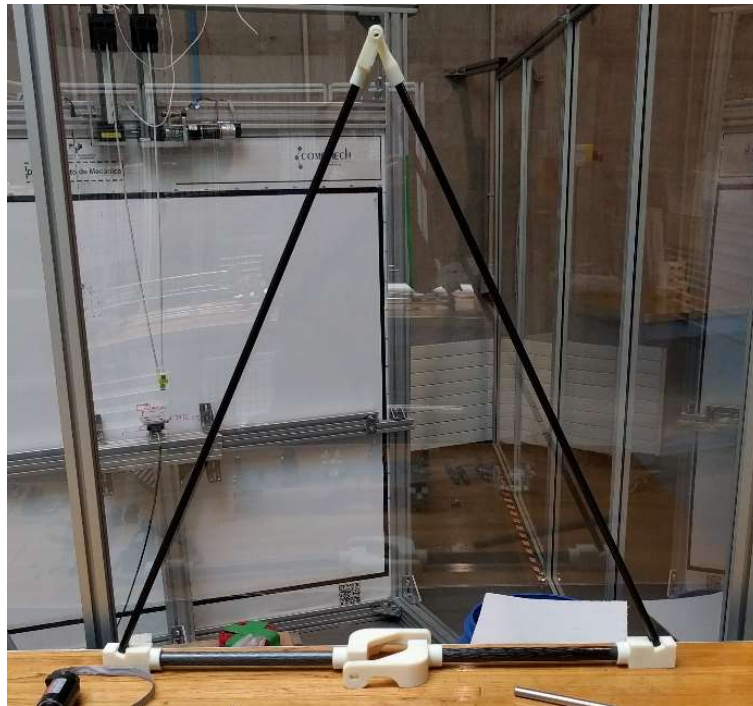


*Figure 55: Glue bars 2*

As the glue on the bars dried, the elements of the powertrain were placed on the plate, carefully checking that all the elements are properly aligned before putting in the bolts (Figure 57).

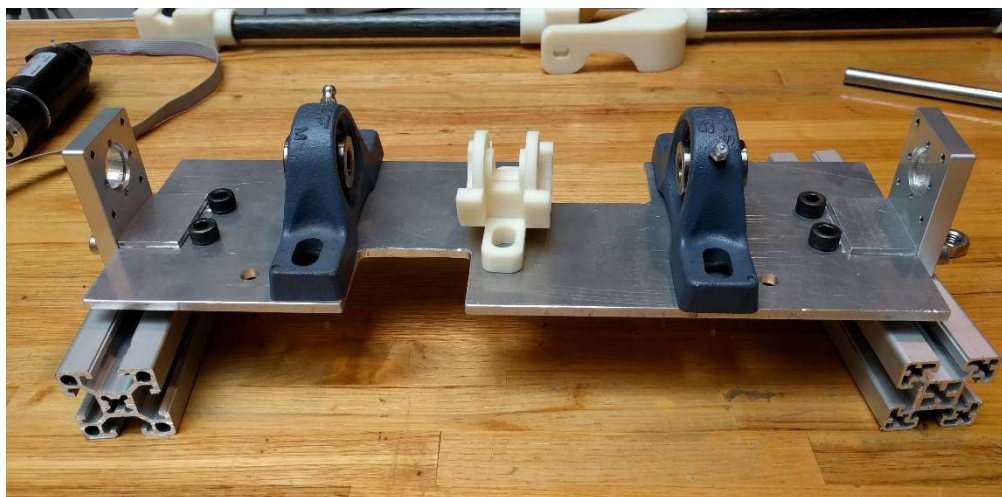


*Figure 56: Powertrain assembly*

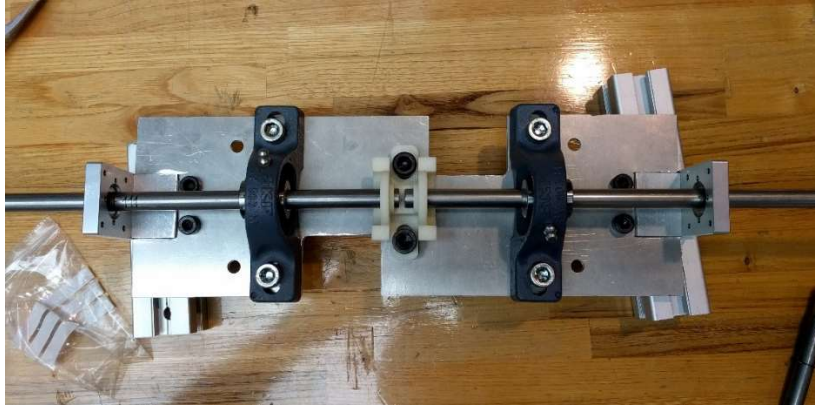


*Figure 57: Powertrain assembly, alignment*

Before mounting everything on the structure, the bars were attached to the shafts to make sure that everything fitted as intended (Figure 58).

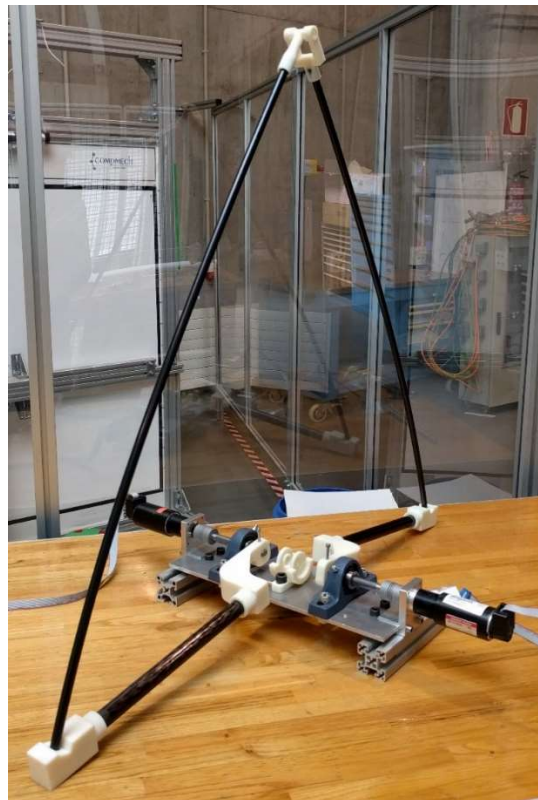


*Figure 58: Preliminary Assembly.*

Once we were sure that everything was in place we proceeded to mount the whole assembly on the aluminium profile structure using the corresponding nuts and bolts and brackets, by using two 40x40 mm profiles acting as separators between the plate and the beam (Figure 59).

As a final note, the footprint of the prototype is approximately a circumference of radius  $R = 437$  mm. That is the distance from the center of the mechanism to the ending of the elbow.



*Figure 59: Mounting of the prototype to the structure.*



*Figure 60: Prototype finally assembled and mounted on its structure.*

### 8.3. Possible future implementations

Should it be decided that it is worth continuing the research on this type of mechanism and investing more time and resources on this prototype, one of the following steps would be to increase its mobility. This concept is not to be developed in detail on this thesis. Nevertheless, two possible options to increase the number of degrees of freedom of the prototype are now presented.

The first option discussed consists on allowing the prototype to perform motions outside the plane that contains the flexible mechanism, thus allowing the prototype to perform pick and place operations in space. This could be achieved by rotating the working space about its centreline, which inevitably would require rotating the whole planar mechanism. A skilful designer could probably come up with a solution to attach the plate that holds the mechanism and the motors to a third motor disposed vertically that could generate the rotation for the whole assembly. The result of this modification to the working space of the prototype can be seen in Figure 61.

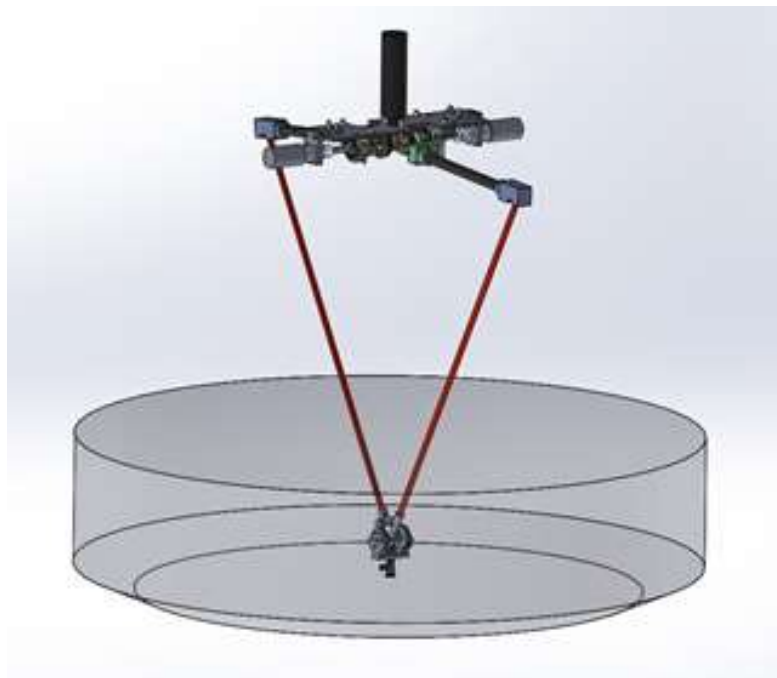


*Figure 61: Example for the working space of the prototype in space.*

The second option is less ambitious than the first one both conceptually and if it were to be implemented. The second option discussed to increase the number of degrees of freedom of the prototype would be to provide it with the possibility of changing the orientation of the terminal element attached to the end effector. There are already pick and place manipulators that opt for this solution, an example of which can be seen with the Omron X-Delta 2+1 (8). In the sketch shown in Figure 62 it can be seen how there is a third actuator vertically oriented and connected to the end effector of the manipulator. The rotation of that motor is what controls the orientation of the end effector, and therefore provides the robot with that +1 degree of freedom.

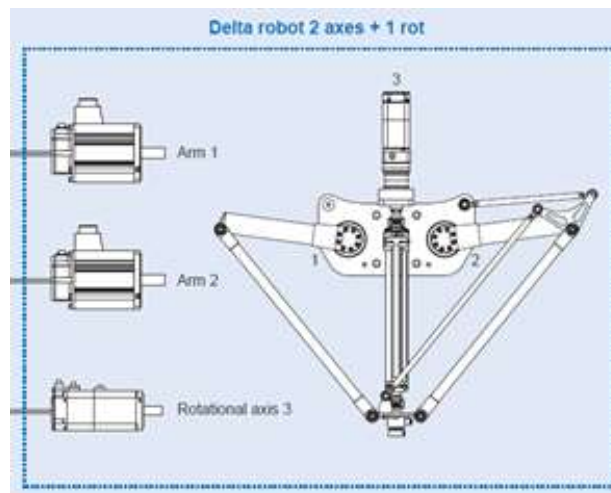


*Figure 62: Omron X-Delta 2+1 variant sketch.*

For our case however, that option could be too complicated to implement and other alternatives should be considered, which luckily there are. The alternative could be to install a rotary actuator between the end effector of the mechanism and the gripper (a suction cup for our case). An example of such device are the Festo semi-rotary drives DVRS (6), which can be found in a wide range of sizes and are actuated using compressed air, which completely removes the need of an additional motor on the prototype (and a mechanical link between it and the end effector). Going back again to our case, with a

clever design it could be possible to have both the gripper and the rotary actuator, which could very much improve the pipe management. An example of such a device can be seen in Figure 63.

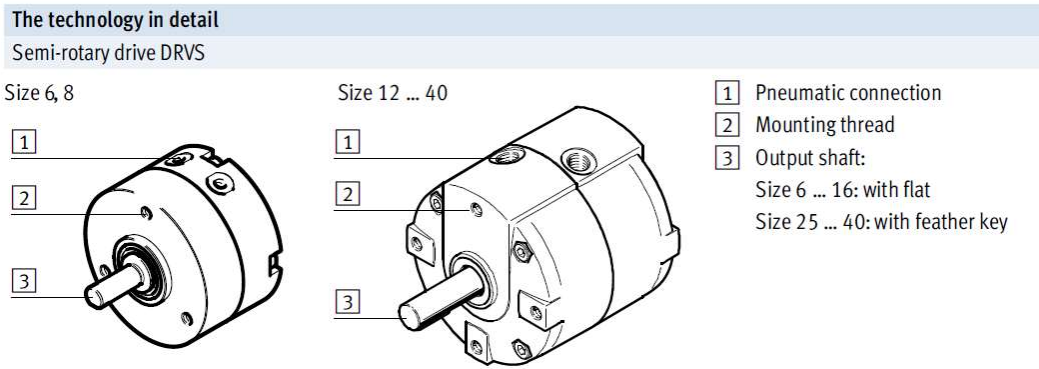


Figure 63: Festo semi-rotary drives DRVS.



## 9. Prototype Testing

So far, the document has focused on explaining the process of making the prototype, from its conception up to its assembly. Now that those very important areas have been covered, it is time to focus on how the prototype performs. It should be noted that some problems, or rather inconveniences, were to be expected during the testing, as it was very likely that the motors used for the prototype's first assembly might not be able to handle the mechanism's own inertia and the forces that would appear on the different tests. Moreover, since the motors and controllers had already been used for previous prototypes that meant that the parameters of the controllers could complicate the initial tests until some more adequate values for the control parameters were found.

To assess the prototype's performance, three different tests were made, based on how far the models were developed at the time of testing. At that point in time, the Matlab models did not take into account the dynamics of the system, so in order to compare the prototype with the static model the first test consisted on describing a vertical path with the end effector and measuring the torque at the motors for the different steps along the trajectory. Those results are to be compared to the results from simulating a vertical trajectory with the same loading conditions (no load) on the Matlab program.

### 9.1. Equipment used



Figure 64: EPOS2 Controllers.

As can be seen in Figure 65, the devices required to fully operate the prototype were a desktop computer, running an old version of windows compatible with the version of the EPOS Studio program required to operate the motors, a more modern laptop and a PXIe-1062Q chassis with the corresponding modules that enable the connection between the laptop running the LabVIEW program and the controllers for the motors (Figure 64). Having that working table there next to the cage containing the prototype proved very helpful, as all those devices take up quite a lot of space. That position also allowed to securely operate the prototype and watch the results.



*Figure 65: Control Center.*

Epos Studio is the software that the motor manufacturer, Maxon, provides for the control of their motors. It lacks the ability to coordinate motions in more than one motor at a time; while moving one of the motors the other possibilities for the other motors is that they are either free to rotate (disabled: no current supplied) or locked in position (enabled: current is supplied to the motor, the amount required to keep the position). The control of the motors is position-based. The units used for the position are quad-counts (qc). For our motors  $2000 \text{ qc} = 1 \text{ revolution}$ . However, since the motors are paired

to a 1:14 gearhead, for the prototype to rotate a bar one complete revolution the motor would need to rotate 28000 qc. When performing a motion, its characteristics can be defined by modifying the profile velocity, acceleration and deceleration, to make it faster or slower and also, more or less sudden. The profile type can also be selected, between a trapezoidal or sinusoidal profile. The interface for actuating a motor can be seen in Figure 66.

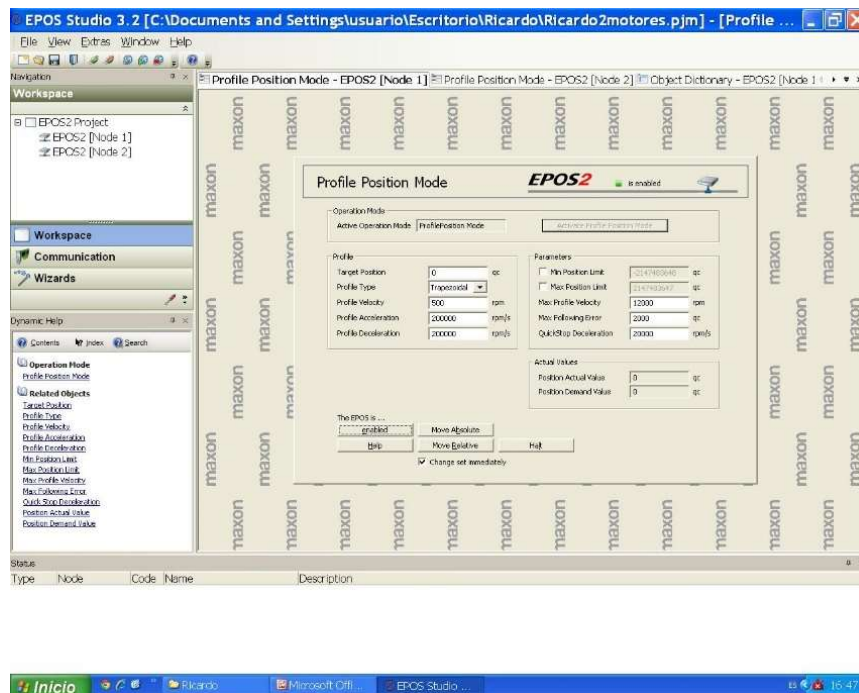


*Figure 66: EPOS Studio. Motor actuation tab.*

This software has many more functions that were not explored during the project. However, the data recording function was widely used, as it is able to plot a wide range of variables, such as current, position or velocity at the selected motor and export the data to a .txt file (Figure 67). Finally, the other aspect of the software used during the project was the Object Dictionary, where the values of the different control parameters can be found and modified at will (Figure 68).

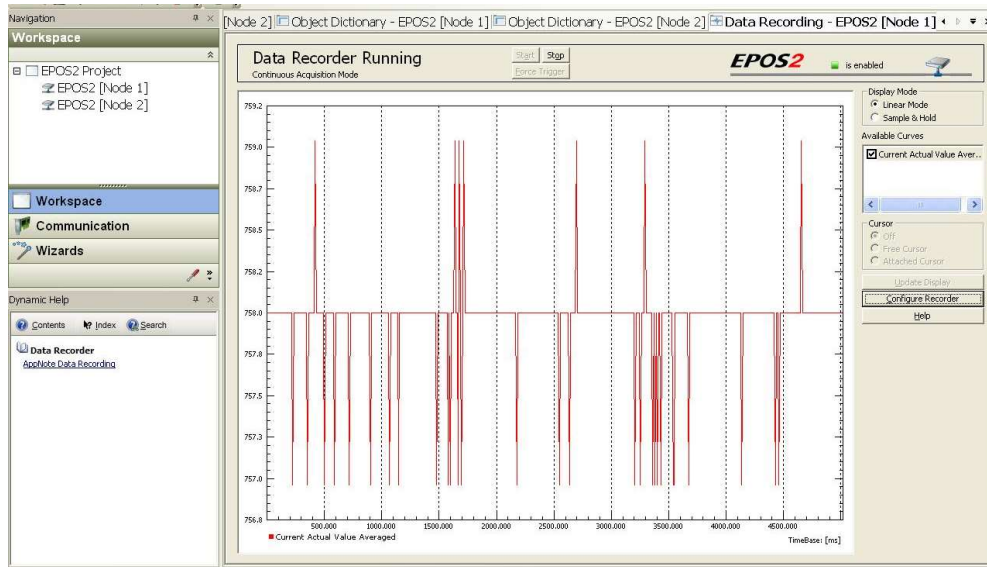
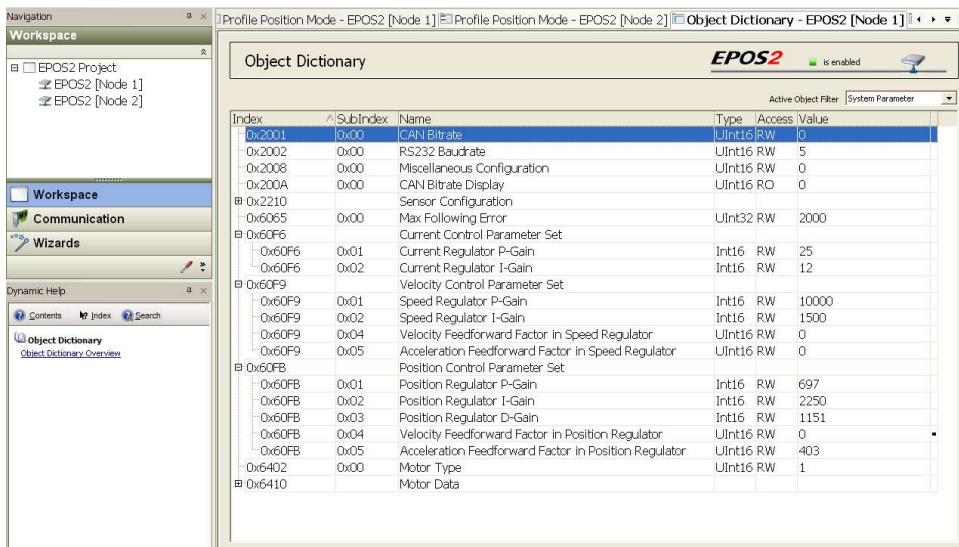


Figure 67: EPOS Studio. Data recorder.



The screenshot shows the 'Object Dictionary' window in EPOS Studio. It displays a table of parameters with columns for Index, SubIndex, Name, Type, Access, and Value. The table is organized into expandable sections for different motor parameters.

Index	SubIndex	Name	Type	Access	Value
0x2001	0x00	CAN Bitrate	UInt16	RW	0
0x2002	0x00	RS232 Baudrate	UInt16	RW	5
0x2008	0x00	Miscellaneous Configuration	UInt16	RW	0
0x200A	0x00	CAN Bitrate Display	UInt16	RO	0
0x2210		Sensor Configuration			
0x6065	0x00	Max Following Error	UInt32	RW	2000
0x60F6		Current Control Parameter Set			
0x60F6	0x01	Current Regulator P-Gain	Int16	RW	25
0x60F6	0x02	Current Regulator I-Gain	Int16	RW	12
0x60F9		Velocity Control Parameter Set			
0x60F9	0x01	Speed Regulator P-Gain	Int16	RW	10000
0x60F9	0x02	Speed Regulator I-Gain	Int16	RW	1500
0x60F9	0x04	Velocity Feedforward Factor in Speed Regulator	UInt16	RW	0
0x60F9	0x05	Acceleration Feedforward Factor in Speed Regulator	UInt16	RW	0
0x60FB		Position Control Parameter Set			
0x60FB	0x01	Position Regulator P-Gain	Int16	RW	697
0x60FB	0x02	Position Regulator I-Gain	Int16	RW	2250
0x60FB	0x03	Position Regulator D-Gain	Int16	RW	1151
0x60FB	0x04	Velocity Feedforward Factor in Position Regulator	UInt16	RW	0
0x60FB	0x05	Acceleration Feedforward Factor in Position Regulator	UInt16	RW	403
0x6402	0x00	Motor Type	UInt16	RW	1
0x6410		Motor Data			

Figure 68: EPOS Studio. Object Dictionary.

Since through the EPOS Studio software the two motors could not be actuated at once the need for the PXI was inevitable. The goal of the PXI was to process all the data regarding the trajectories, sending the instructions of the trajectories from the laptop to

the corresponding controller and also gathering the data of position, velocity and current on the motors along the performed trajectory from the controllers back to the computer (Figure 69).



*Figure 69: The PXI.*

The laptop is used to run a LabVIEW program that enables generating trajectories with the mechanism by actuating both motors at once. The program requires as input a text file with the qc values of the desired position for each motor, a column for the values of each motor. Those positions are relative to the starting position of the motors, so both columns should start from zero and build up the number as the motion progresses. The PXI reads the positions at a fixed refresh rate, so if a faster trajectory is desired, the step between each position should be increased. The LabVIEW program used was developed for a previous prototype with three motors and it had a lot more functionalities than the ones used for this prototype. The only things required for this case were sending the trajectories to the controllers, fetching the data generated on the described trajectory (which happened by default) and learning how to change the relevant control parameters determined through the PXI. Figure 70 shows the user interface of the LabVIEW program used. The small window on the right allowed access to the source code, where the aforementioned parameters can be located and modified.

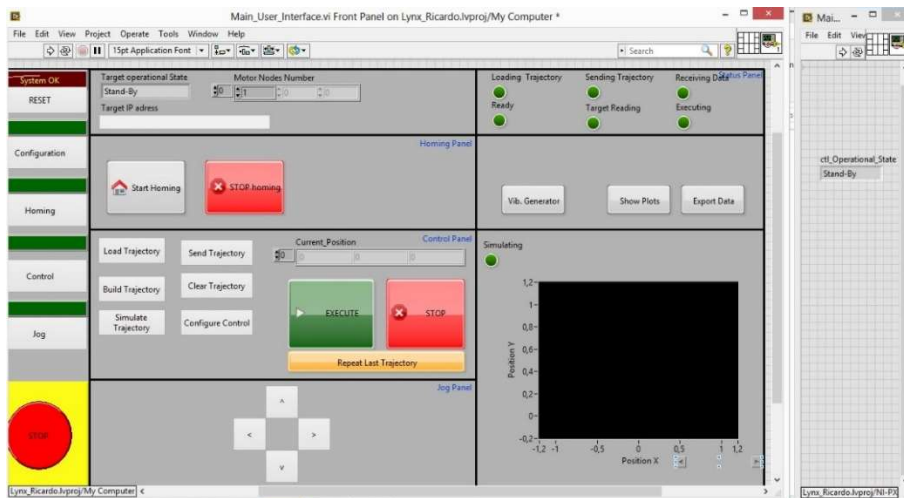


Figure 70: LabVIEW program UI.

## 9.2. Tests performed

Under this section the different tests that have been carried out once the prototype was successfully assembled are described in detail. The tests have two main objectives, the first is to assess the similarities between the results obtained on the Matlab simulations and the real prototype, the second one is to tune in to the best of our ability the parameters that define the gains of the control loops for the variables of the mechanism: position, velocity and current.

### 9.2.1. Test 1: Quasi-static Torque Test.

The main purpose of this particular test is to compare the torque value at the motors obtained on the simulations against the reading obtained directly from the motors. Ultimately, those results provide insight on how the mathematical model compares to the prototype itself and also, by running the simulations multiple times changing the Young's modulus of the flexible bars, we can also see if the possible discrepancy in the results comes from estimating the material properties not accurately enough.

The procedure for performing the test is as follows: Starting at the resting position of the mechanism, the bars are lifted alternatively (first one and then the other) so that the

end effector performs a vertical trajectory. A certain angle is chosen for the steps, and after each step the data for both angles and the torque value at each motor are recorded. The test goes on until the motors are not able to continue moving the end effector upwards.

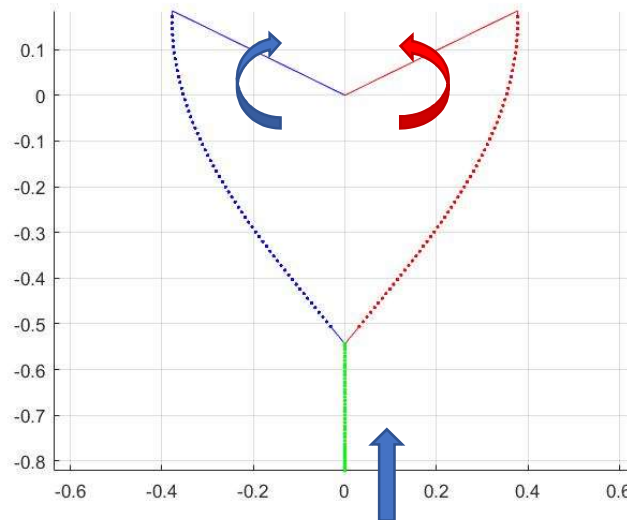


Figure 71: Torque measuring test

For this test the prototype was actuated using the EPOS Studio only. The reason for this was that the angle had to be measured on every step of the vertical trajectory, and also, on the latest iteration of the test the steps were measured directly at the bars, instead of just trusting the reading on the computer. For measuring the angle on the bars, a digital level was used (Figure 72).

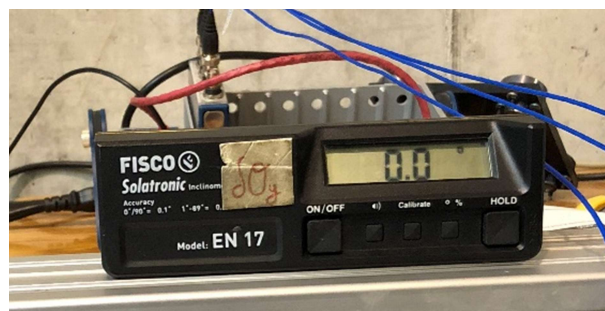
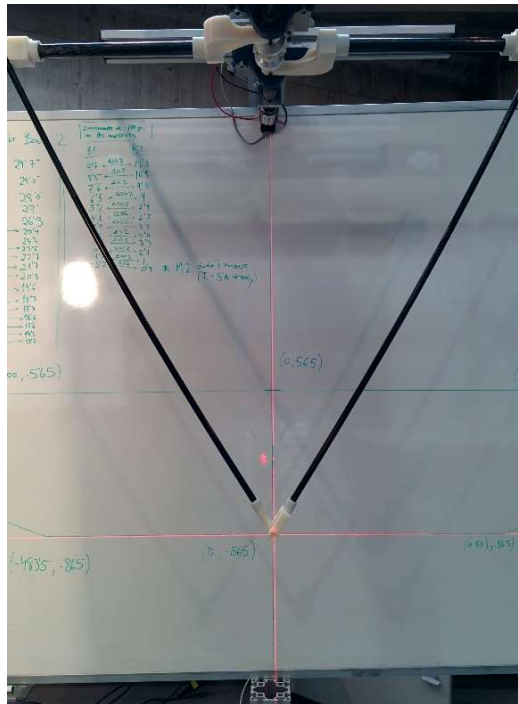


Figure 72: Digital level used.

Every time the two bars were raised, along with recording the value of the angle, the current at the motors was also recorded using the EPOS Studio data recording functionality. The value of the current can easily be converted to torque using the value provided by the manufacturer on the spec sheet (torque constant = 30.2 mNm/A).



*Figure 73: Use of laser level to ensure a vertical trajectory.*

As experiments were being performed, some variations were made to the measurements that were taken. At the beginning instead of measuring the angle on every step, which makes the process much more tedious, only the initial resting position was measured, and the subsequent positions were estimated converting the value of the position on the EPOS Studio from  $q_c$  s to radians. The reason behind that change was that if exactly the same steps were alternatively applied on both bars, bar 2 would end up rising slightly higher than the other one. Figure 74 shows how as one of the experiments progressed the angle bias towards bar 2 became clearer (the angle on the figure is expressed in degrees). The same figure also shows how the motors behaved; the increase on the current was not as progressive as could probably be expected, as the difference between



the torque on M1 and M2 starts to suffer great variations midway through the test and until the end of it. That second trend continued even when the angle of the bars was kept almost identical by measuring it with the digital level. Figure 75 shows how the EPOS Studio was arranged during the testing to have everything in sight.

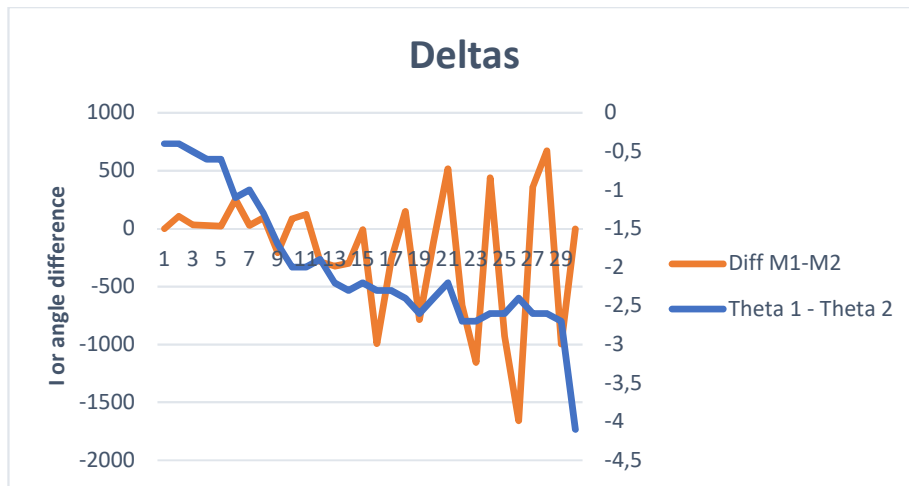


Figure 74: Example of differences in current and angle between M1 and M2.

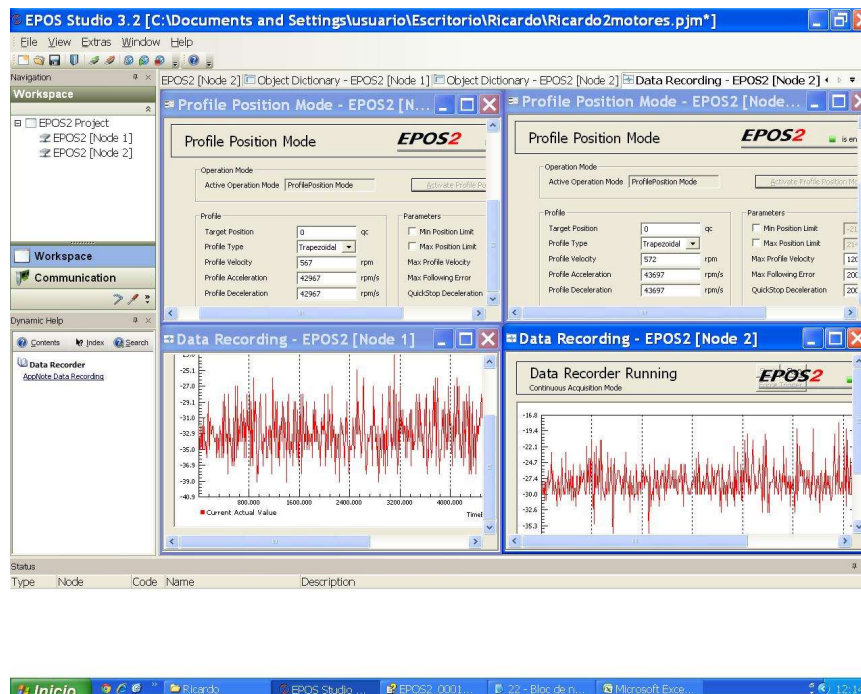


Figure 75: EPOS Software Set Up example

From this test the following conclusions were reached:

- The maximum current at the motors (5000 mA) was reached midway through the tests. The motors not being capable enough prevented us from performing a full vertical trajectory, and as a consequence from comparing the torque value at one of the most critical points on the working space. The top position of the trajectory tested is one of the points where higher torque values are reached.
- The point of zero torque is very different on both model and prototype. Adding to the disparity between the two. Mainly due to the difference in resting position between the two.
- How far up the bars went on the test was highly dependent on the qc steps chosen, the bigger they were the larger the angle both bars were able to cover. However, higher qc steps translated into fewer experimental points from which to gather data. This also translates to not having a maximum vertical position that the prototype can reach for the maximum current during the tests.
- When looking at the results of the different tests and simulations, two different aspects stand out. Except for the test in which the angle at the bars was calculated from the software instead of measured, all of them yield similar results, especially at the beginning of the test. As the tensions on the bars build up the jumps on the current become more drastic, but still the lines follow a similar trend. When looking at the simulations for various values of the Young's modulus on the bars, the plot whose trend looks the most similar to the results obtained is the Reference Simulation, which uses the original value obtained for the 10-mm nylon bars during the testing explained in Section 5 (Figure 76).

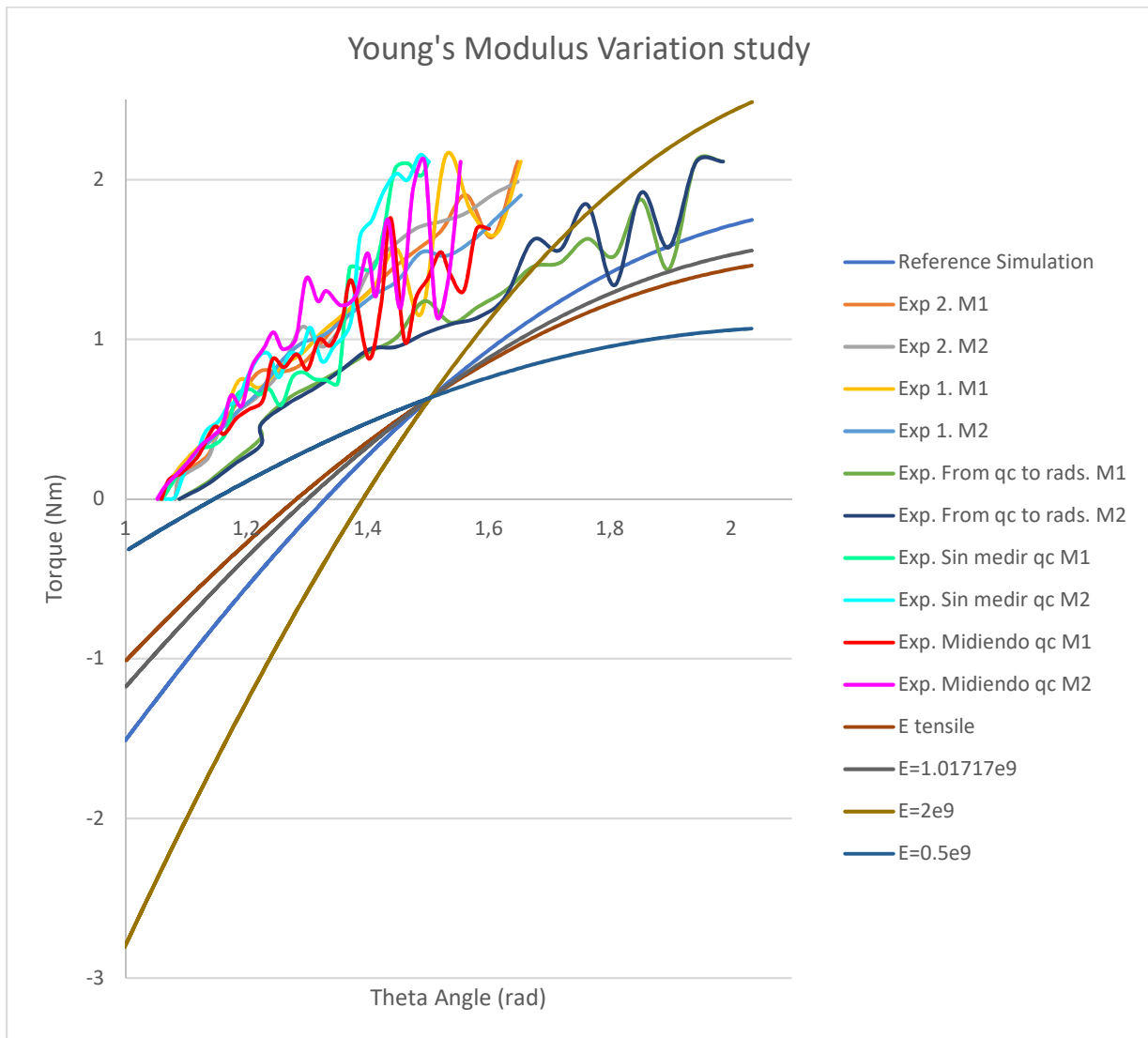
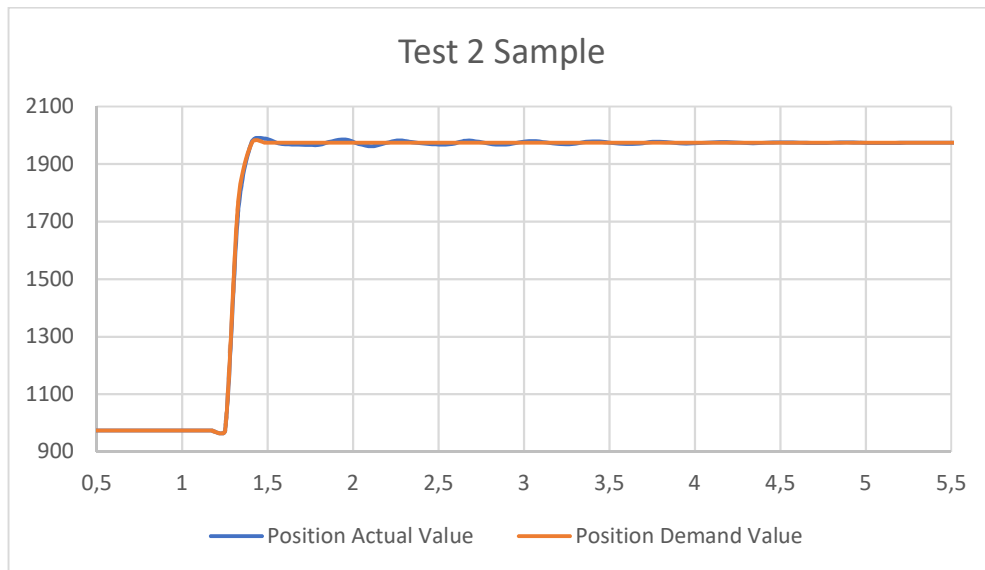


Figure 76: Combined results from the tests and simulations for different values of Young's modulus on the flexible bars.

### 9.2.2. Test 2: EPOS Studio Setup

As mentioned before, there are two ways to actuate the prototype, one of them being through the EPOS software. This software allows the manipulation of one motor at a time.



*Figure 77: Data from EPOS Studio. Plots for Position Actual Value and Position Demand Value.*

The ultimate goal of this test is to select the best set of parameters that govern the position control loop of the motors. Since our goal is to minimize the oscillations on the mechanism each time it performs a motion, those parameters are the ones for which it takes the least amount of time to reach the steady state, which in this case means that the mechanism stops moving. The position parameter is controlled using a PID (proportional integral derivative) control. Those parameters corresponding to each part of the controller are the ones that are tuned through the testing. The other secondary goal of the experiment was to provide a range for those parameters by finding a minimum value that guarantees a lack of error in the steady state or did not make the system unstable and a maximum value from which the actuator saturates and the motor makes unwanted noises.

The procedure followed for the test consisted on checking how long it took the system to stabilize after performing a step on the motor. The time was measured on the software itself, with the data recording tool. The parameters compared were the Position Actual Value and the Position Demand Value (Figure 77). The way in which the time was determined was by measuring the time difference between when the step happened



and when the Position Actual Value reached the Position Demand Value (from now on named as  $t_{ss}$ ). The best set of parameters would be the one that yielded the lowest  $t_{ss}$ .

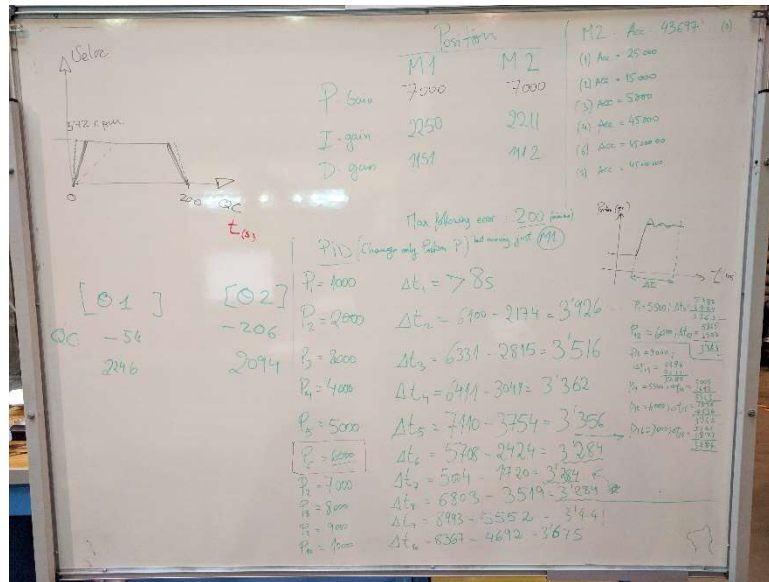


Figure 78: Example of how test 2 developed.

There are two possible ways to operate the prototype with this software, with one or both motors enabled. If only the motor that is actuated is enabled the other motor would sit idle and it wouldn't oppose the motion of the mechanism, thus the more realistic case was to have both motors enabled, as the one that was not actuated would keep in position, offering a resistance to the actuated motor. Apart from this, it was also clear that the  $t_{ss}$  would vary depending on the actual position the mechanism was at, so it was decided to settle for one that was neither the fastest nor the slowest when  $t_{ss}$  was concerned. Such position was when the actuated motor was already at 1000 qc, and the step performed consisted on adding 1000 qc more in the same direction (raising the bar) (Figure 77). As mentioned previously, there were three parameters to tune, all of them being dependent on each other, so an order of preference was settled. First the proportional gain was tuned, leaving the other parameters unchanged from the default values, then the integral gain (keeping the previously selected P value) and finally the derivative gain (keeping previous P and I too). The Order of the tuning was decided based on the relevance of each parameter, according to basic Control Theory. P gain would determine

how fast the response was, I as small as possible (values too big here could increase the instability of the system), but big enough to get rid of the error in the steady state (which happened when we put it to zero) and finally D (helps making the system more stable, but doesn't have a very big effect). Figure 79 shows where to find the parameters that were tuned.

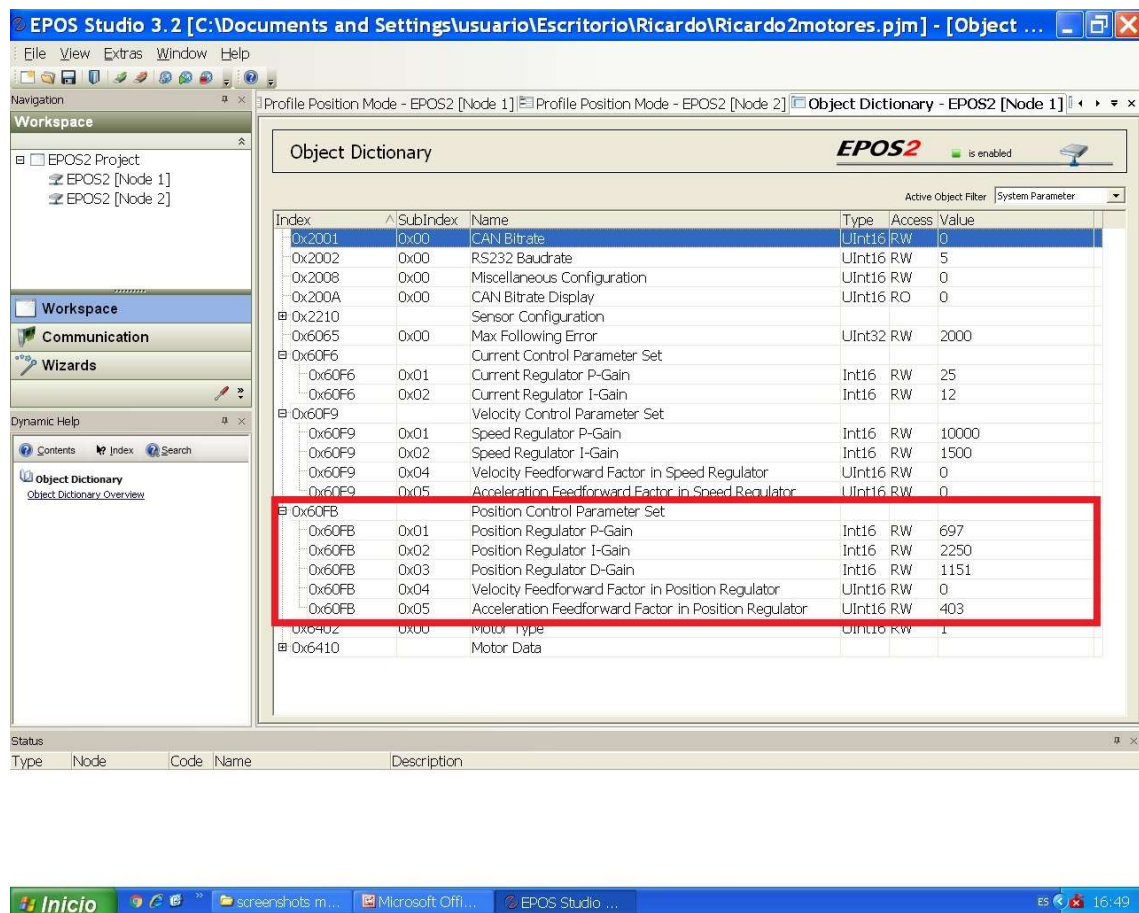


Figure 79: Position Control Parameters

The resulting values from the test are gathered in Table 5. The controllers also allow controlling the velocity and current values on the motors as well. However, when actuating the motors using the EPOS Studio, changing the gains for the current and the velocity yielded no appreciable difference on the results of the test, therefore, they were not included with the results for the test.

*Table 5 : Results from tuning the position PID on the EPOS Studio.*

Position Control Parameter Set:	Value Range		Default Values		Min Value	Max Value	Selected Values
	Min	Max	Motor 1	Motor 2			
<b>Position P-Gain</b>	0	32767	697	679	1000	10000	7000
<b>Position I-Gain</b>	0	32767	2250	2211	1000	32000	1500
<b>Position D-Gain</b>	0	32767	1151	1112	0	5000	2600

Conclusions from the second test:

- After much testing, it became clear that some oscillations would always take place after performing a motion, especially if the motion is fast. On our tests the lowest time until steady-state that we could achieve was approximately 3.3 s.
- At least from the observations on this test, it might be worth sacrificing some speed when performing a motion to minimize the resulting oscillations. However, sacrificing speed does not sound like a very logical option when aiming towards a high-speed application.
- When using the built-in position PID to control the prototype the parameter with the most influence was the proportional gain. The most significant effect was that when setting the integral gain to 0 a small error appeared in the steady state.

### 9.2.3. Tests with the PXI

Once we became familiar with how to operate the prototype with the EPOS Studio, it was time to tackle more advanced matters by starting to generate trajectories for the prototype to describe. As previously mentioned, the PXI and the LabVIEW program are required for that, as well as the other computer running the EPOS Studio. Also, for generating the trajectories, Diego's Matlab programs are used, the same as the ones mentioned previously. Another option for generating the trajectories included making them by hand, just deciding the target positions for each motor and their desired speeds. If the Matlabs were used, the column corresponding to the angle on each bar had to be converted to quadcounts using the conversion:  $2\text{ Pi} = 28000\text{ qc}$ .

The need of two computers for operating on this mode is due to the control being split in two. On one side, the proportional gain of the position control loop (on both motors) is controlled using the Labview program (Figure 80), which overrides values on the EPOS Studio for the position loop. The current and velocity loops however, are determined by the values stated on the System parameter list on the EPOS Studio.

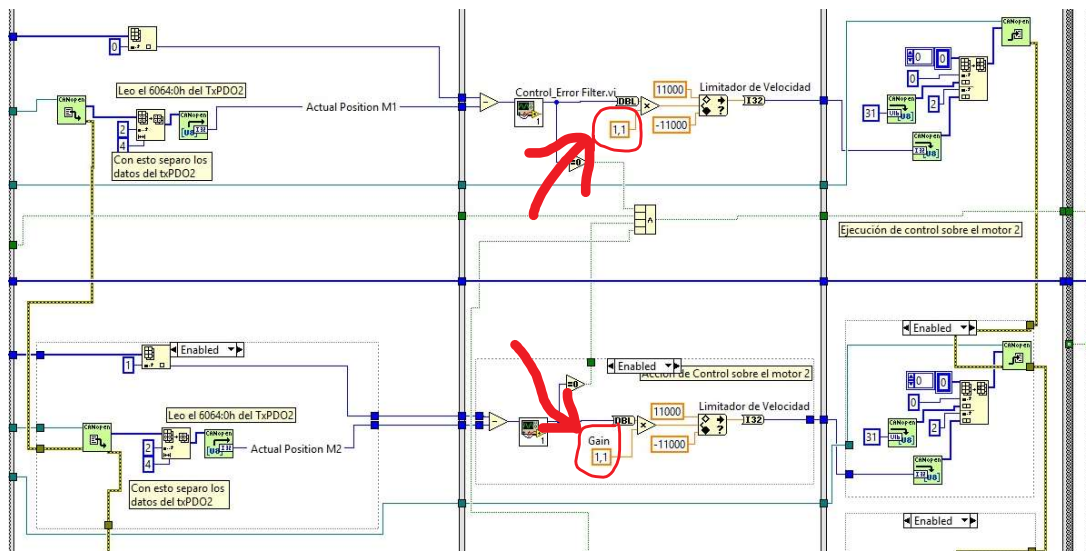


Figure 80: P-gains on the LabVIEW program.

Operating the prototype in this fashion was more complicated in every possible way, so a laid-back approach was taken for the testing. The tests began just by trying to make the mechanism move with the desired trajectory and observe it. Those trajectories were slow at the beginning, to avoid any risks due to the lack of tuning of the gains for the different control loops.

A description of the process is due now. Right after starting up both computers, the parameters on both of them need to be checked, as their values are not saved after the motors are unplugged. Once the values of all parameters are selected correctly the procedure goes as follows: first we select the trajectory that we want to test, then a camera, a mobile phone in this case, is set to record the resulting motion and finally the motion is performed and recorded. Afterwards, the text file containing the results is extracted from the computer and processed using Excel so that we can have a look at the results.



The first major event during this phase happened when during the description of a trajectory the mechanism became so unstable that the bars even started hitting the beam that the prototype is hanging from. The end result was that one of the beam couplings connecting the gearhead to the shaft broke, which can be seen in Figure 84. Figure 81 shows an example of how the motors become unstable with a plot of their position.

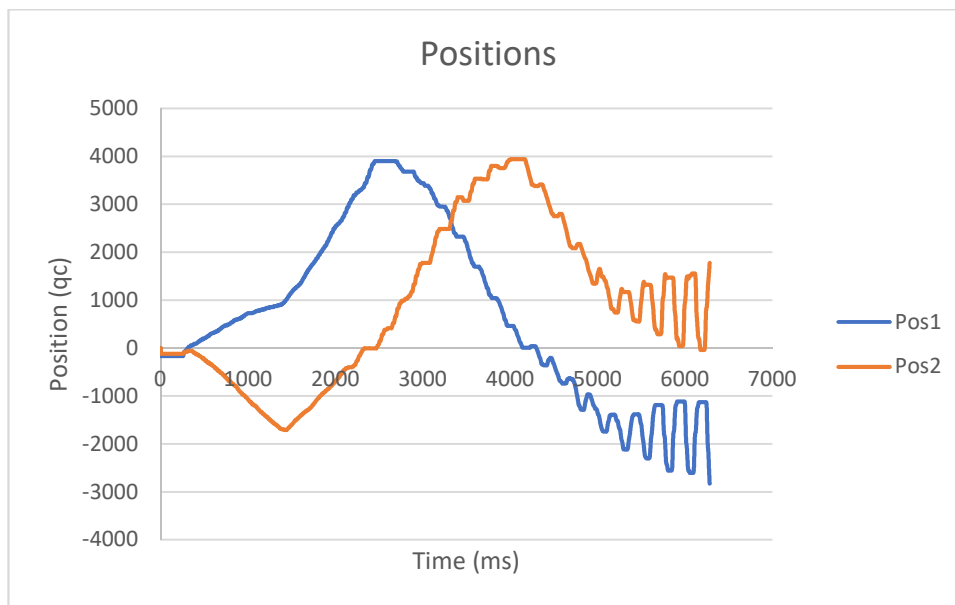


*Figure 81: Example of the motors becoming unstable during a trajectory.*

This event led to changing the cycle period of the control loops. It was set at 5 ms from previous prototypes, but that value seemed to be too low for our application. After changing its value to 10 ms the performance of the prototype greatly improved. Figure 83 shows how after that change the prototype was able to perform feats such as being able to handle steps of about 5000 qc without becoming unstable. This also happened by accident, because of an error while generating the trajectory, but a positive outcome was drawn from it.

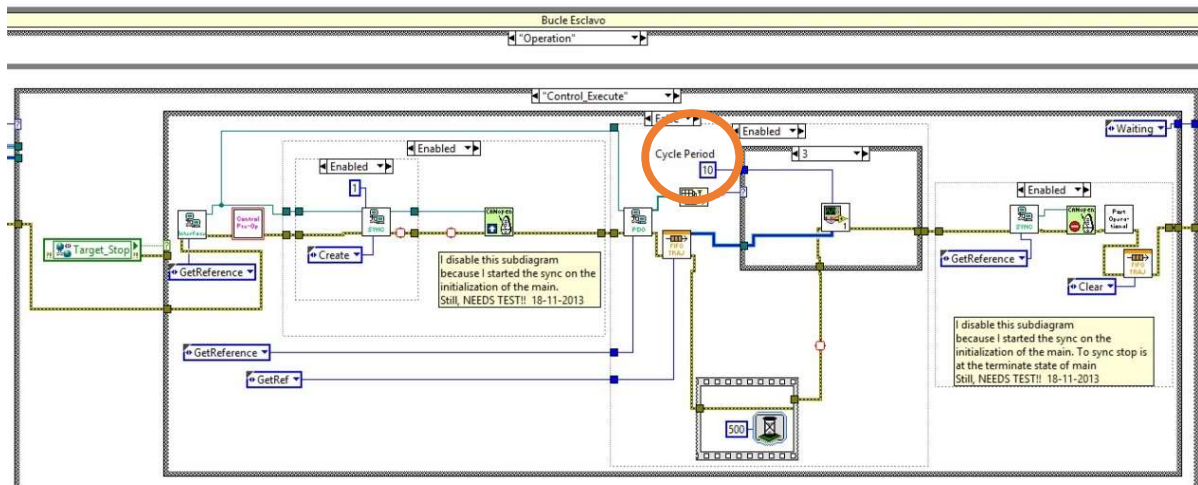


Figure 82: Changing the cycle period inside the LabVIEW program.

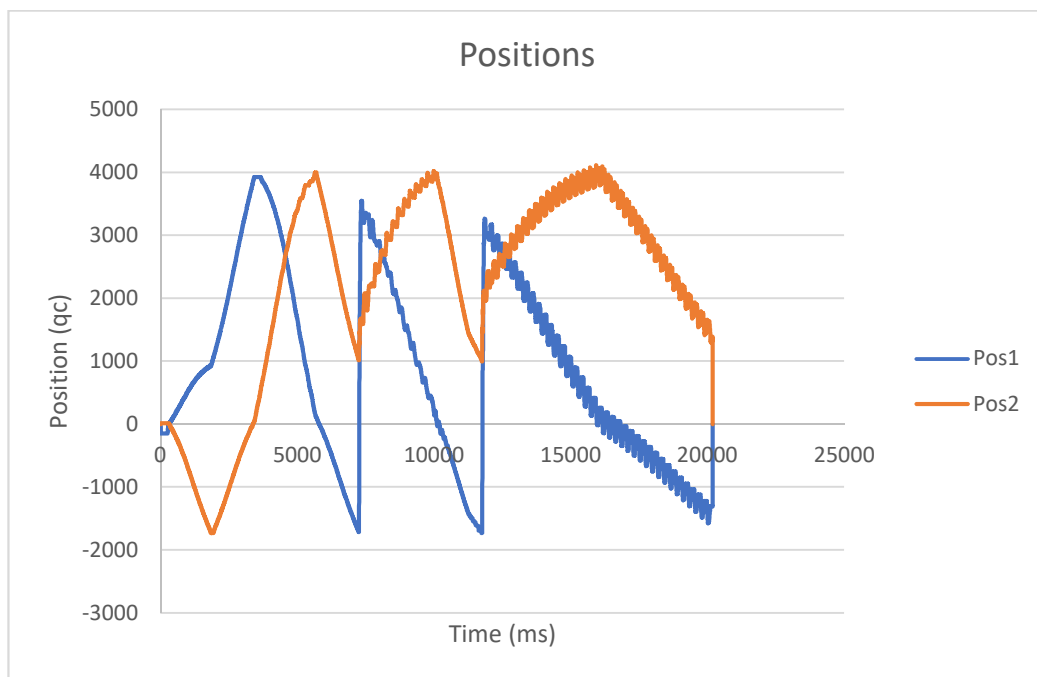
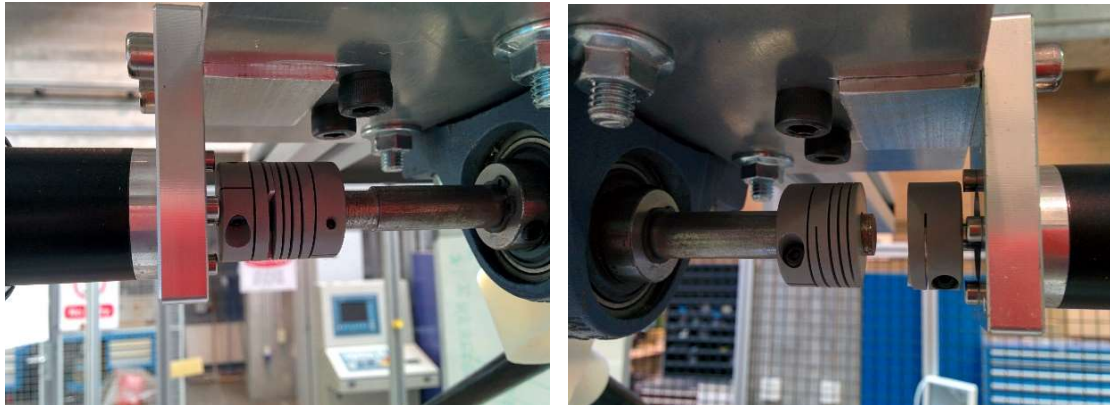


Figure 83: Trajectory with unwanted steps.



*Figure 84: Component critical failure.*

So far, no mention has been made about the gains of the control loops. The values that were finally chosen and which are being used to perform any subsequent tests were obtained from a model of the mechanism developed by prof. Campa, and then fine tuning them on the prototype. The values for each of the controllers of the different variables were:

- Position:  $P = 0.6$ . (PXI)
- Velocity:  $P=10000$ ;  $I = 1500$ . (EPOS)
- Current:  $P = 25$ ;  $I = 12$ . (EPOS)

This set of parameters yielded acceptable results for the trajectories tested, so they were not meddled with. Especially because it was clear that it would not be possible to completely get rid of the oscillations when performing trajectories.

Conclusions from the final testing:

- Big improvements after changing the cycle time from 5 ms to 10 ms. This probably had to do with the fact that the natural frequency of the mechanism is bound to be very low, on under 10 Hz.
- During the testing it became clear that the longer the bars remained flexed during a trajectory the more apparent the oscillations became.
- The peak values of the current when using the PXI reached 10000 mA, instead of the 5000 mA that was obtained from the first test.

- The footage taken was very helpful for analyzing the trajectories performed as many times as required without having to repeat them on the prototype.
- When attaching the gimbal to the prototype the smoothness when performing trajectories suffered. It was probably because attaching the gimbal significantly changed the mass of the mechanism overall, which would render the gains used not so useful any more. This raises the question of how much the load grabbed during a pick and place operation could affect its performance, and maybe would only make the design suitable for handling very light and small objects.

## 10. Task description and project phases

This section includes a description of all the tasks that have taken place during the project. They are organized in tables, inside of which the goals, duration, smaller tasks that the major tasks were divided into and the resources assigned, referring to the working hours, are included.

*Table 6: Task 1.*

<b>Task 1</b>	<b>Documentation collection</b>
<b>Goal</b>	Increase knowledge on the topic and collect relevant documentation.
<b>Duration</b>	2 weeks.
<b>Subtasks</b>	<ol style="list-style-type: none"> <li>1. Research theory behind the Matlab models.</li> <li>2. Research market alternatives.</li> <li>3. Archive the relevant documents found.</li> </ol>
<b>Handouts</b>	Reference compilation.
<b>Resources assigned</b>	50 h junior engineer work. 3 h senior engineer work.

*Table 7: Task 2.*

<b>Task 2</b>	<b>Run Matlab simulations</b>
<b>Goal</b>	Become acquainted with the Matlab programs and estimate the mechanical requirements for the prototype.
<b>Duration</b>	2 weeks.
<b>Subtasks</b>	<ol style="list-style-type: none"> <li>1. Go through the Matlab code.</li> <li>2. Adapt the code to the prototype tuning some of the parameters.</li> <li>3. Run the simulations.</li> <li>4. Analyse the results to obtain the requirements.</li> </ol>
<b>Handouts</b>	Estimation of the mechanical requirements
<b>Resources assigned</b>	50 h junior engineer work. 3 h senior engineer work.

*Table 8: Task 3.*

<b>Task 3</b>	<b>Design of the prototype</b>
<b>Goal</b>	Obtain a final design for the prototype that perfectly defines each of the elements and their function.
<b>Duration</b>	4 weeks.
<b>Subtasks</b>	<ol style="list-style-type: none"> <li>1. Begin with a conceptual design that moves as intended.</li> <li>2. Define a final feasible design.</li> </ol>
<b>Handouts</b>	<ol style="list-style-type: none"> <li>1. Blueprints or CAD files for all the designed parts.</li> <li>2. A list with the components that need to be bought or taken from those available at the workshop.</li> </ol>
<b>Resources assigned</b>	150 h junior engineer work. 6 h senior engineer work.

*Table 9: Task 4.*

<b>Task 4</b>	<b>Manufacture the parts</b>
<b>Goal</b>	Have all the parts ready for assembling.
<b>Duration</b>	2 weeks.
<b>Subtasks</b>	<ol style="list-style-type: none"> <li>1. 3D print parts.</li> <li>2. Machine parts.</li> <li>3. Make sure that the remaining parts are available by the time the manufacturing ends.</li> </ol>
<b>Handouts</b>	All the parts ready for assembly.
<b>Resources assigned</b>	15 h junior engineer. 20 h workshop technician.

*Table 10: Task 5.*

<b>Task 5</b>	<b>Assembly of the prototype</b>
<b>Goal</b>	Put the prototype together and mount it on the structure in the workshop.
<b>Duration</b>	1 week.
<b>Subtasks</b>	<ol style="list-style-type: none"> <li>1. Mount the structure that will hold the prototype.</li> <li>2. Cut the bars to length and glue them to the 3D-printed parts.</li> <li>3. Bolt the powertrain elements to the plate.</li> <li>4. Attach the compliant mechanism to the shafts.</li> <li>5. Hang the prototype from the structure.</li> </ol>
<b>Handouts</b>	The prototype mounted correctly on the aluminium profile structure.
<b>Resources assigned</b>	35 h junior engineer work. 1 h senior engineer work.

*Table 11: Task 6.*

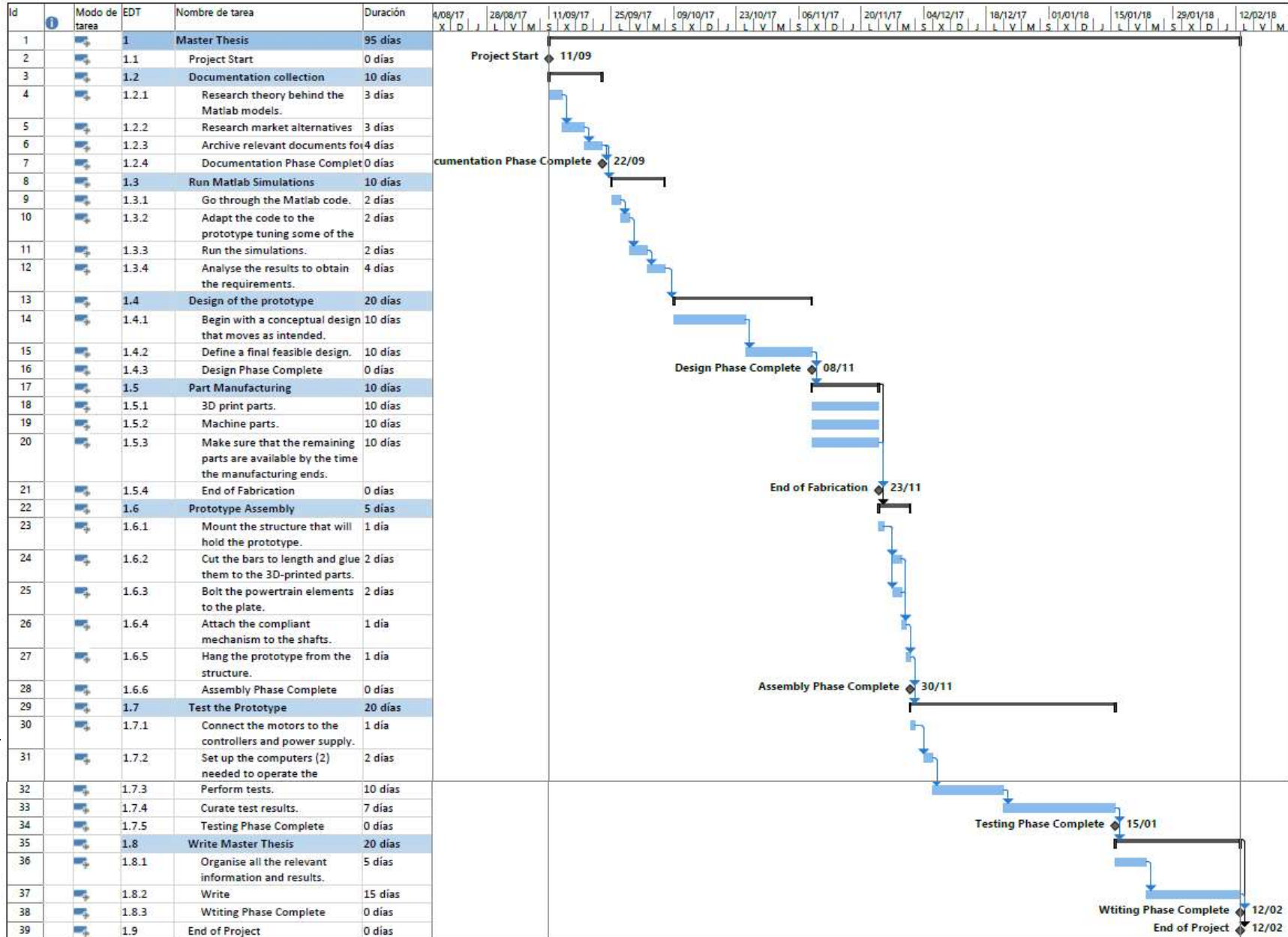
<b>Task 6</b>	<b>Perform the tests on the prototype</b>
<b>Goal</b>	Get the prototype ready for the scheduled and any future testing that may be required.
<b>Duration</b>	4 weeks.
<b>Subtasks</b>	<ol style="list-style-type: none"> <li>1. Connect the motors to the controllers and power supply.</li> <li>2. Set up the computers (2) needed to operate the prototype.</li> <li>3. Perform tests.</li> <li>4. Curate test results.</li> </ol>
<b>Handouts</b>	<ol style="list-style-type: none"> <li>1. The prototype ready to work.</li> <li>2. Test results.</li> </ol>
<b>Resources assigned</b>	150 h junior engineer work. 24 h senior engineer work.

*Table 12: Task 7.*

<b>Task 7</b>	<b>Write the master thesis</b>
<b>Goal</b>	Collect all the knowledge gathered throughout the process on a single document.
<b>Duration</b>	4 weeks
<b>Subtasks</b>	<ol style="list-style-type: none"> <li>1. Organise all the relevant information and results.</li> <li>2. Proceed with the writing.</li> </ol>
<b>Handouts</b>	The final document for the Master Thesis.
<b>Resources assigned</b>	150 h junior engineer work. 20 h senior engineer work.



# 11. Planning: Gantt diagram





## 12. Overall Project Expenses

This section presents the cost of the whole project broken down into the labour, the amortizations and the expenses. The overall cost of the project was 31.182,67.

Table 13: Labour costs.

Labour	Per hour cost	Total hours	Cost
Junior Engineer	35 €/h	600 h	€ 21,000.00
Senior Engineer	85 €/h	57 h	€ 4,845.00
Workshop Technician	45 €/h	20 h	€ 900.00
<b>Total:</b>			<b>€ 26,745.00</b>

Table 14: Amortizations costs.

Amortizations	Units	Per hour cost	Total hours	Cost
Matlab License	1	0.35 €/h	125 h	€ 43.75
SolidWorks License	1	3.33 €/h	150 h	€ 499.50
LabVIEW License	1	2.22 €/h	75 h	€ 166.50
ANSYS License	1	4.41 €/h	5 h	€ 22.05
Laptop	1	0.08 €/h	150 h	€ 11.67
Workstation PC	1	0.12 €/h	600 h	€ 73.33
PXI Control Unit	1	0.56 €/h	75 h	€ 41.67
<b>Total:</b>				<b>€ 858.47</b>

Table 15: Cost of the expenses.

Expenses	Per unit cost	Amount	Cost
3D - printing material	ABS-P430	198,1 €/kg	0,55 kg € 108,96
Nuts and bolts		0,25 €/u	32 u € 8,00
Nylon bars		11,74 €/set	1 set € 11,74
Carbon fiber bars		32,67 €/u	2 u € 65,34
Elastic strip		2,2 €/m	2 m € 4,40
Pulleys		10,77 €/u	4 u € 43,08
Belts		20,28 €/u	3 u € 60,84
DC Motor	148867	347,74 €/u	2 u € 695,48
Planetary Gearhead	166158	137,55 €/u	2 u € 275,10
Controller	347717	545,18 €/u	2 u € 1.090,36
Igus Motor flange	MF-1040-NEMA17-S	66,76 €/u	2 u € 133,52
Aluminium Profiles	80 x 80	30 €/m	14 m € 420,00
Brackets	40 x 80	3,64 €/u	14 u € 50,96
<b>Total:</b>			<b>€ 2.967,78</b>

*Table 16: Overall expenses*

<b>Overall Expenses:</b>		
<b>Labour</b>	€	26.745,00
<b>Expenses</b>	€	858,47
<b>Amortizations</b>	€	2.967,78
<b>Subtotal</b>	€	30.571,24
<b>Indirect Costs (2%)</b>	€	611,42
<b>Grand Total:</b>	€	<b>31.182,67</b>

### 13. Conclusions and Future Outlines:

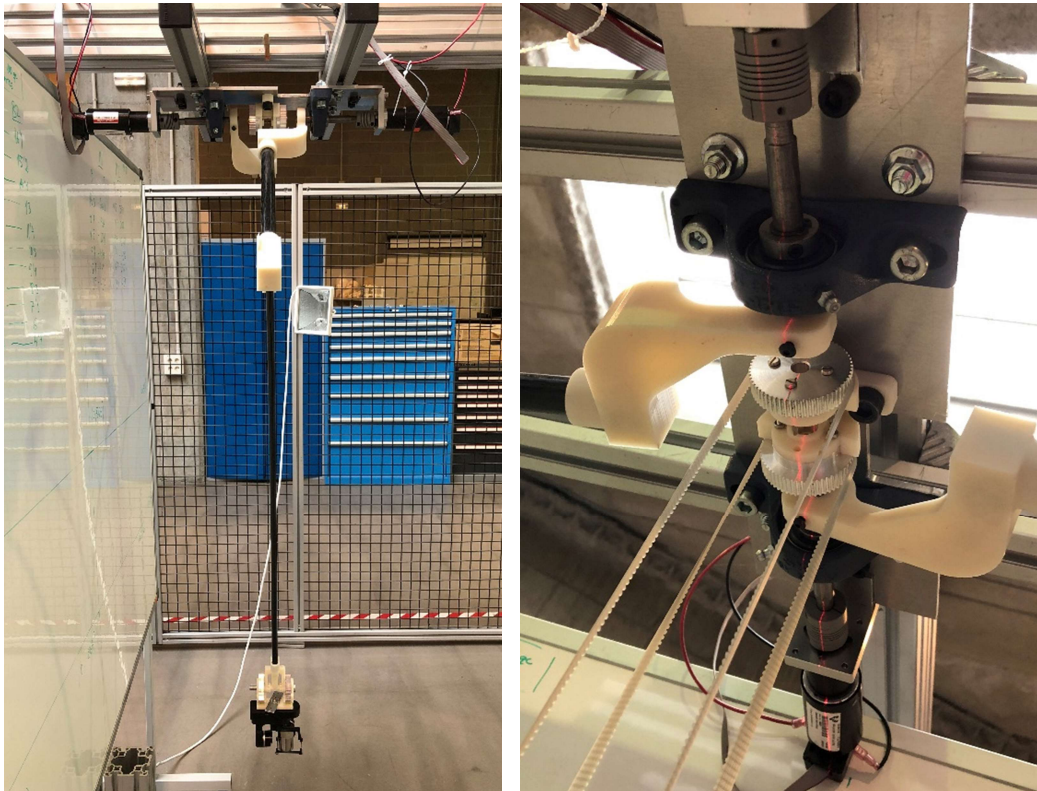


*Figure 85: Showing the correct alignment of the mechanism.*

What originally started as an idea for a parallel robot has successfully been built into a functioning prototype. Only minor setbacks took place during the design

and assembly phases, and they did not have barely any impact on the final prototype.

During the design the future need to replace the motors loomed over the whole process, so as a result, changing the motors for some new ones would only require swapping the motor flange with another one compatible with the new motor and also compatible with the part that attaches the flange to the support plate. And the flexible coupling between the gearhead and the shaft would also require replacing.

Once the assembly was complete the motors were connected to their corresponding controllers and at the same time these were connected to the computers that would enable us to perform motions with the prototype.

When it came to the tests the results were not the most satisfactory. On the test that compared the torque at the motors between the simulations and the prototype the results did not match as expected. They were indeed in the same order of magnitude and the evolution of the torque with the angle was relatively similar, but overall not close enough to deem the test as successful. In this test it already became apparent that more capable motors would be required: from a standstill position the bars of the prototype were barely able to go horizontal, when the uppermost point in the trajectory requires them to go as high as  $30^\circ$  more.

The following test consisted on tuning the gains of the PID control of the position loop on the EPOS Studio. Each time the motors/controllers are plugged in all the gains default to some values. These values were not adequate at all, they clearly made the system unstable, as the oscillations after performing a single position change in one motor would increase instead of dampen and eventually stop moving. After much tuning we did arrive to a set of values that greatly improved the behaviour of the prototype towards oscillating. It is however impossible to completely get rid of it, due to the low rigidity of the flexible bars that form the mechanism. The consequences of the low rigidity of the bars are discussed later.

The tests with the PXI required adjusting the gains for velocity and current on the EPOS Studio, as well as the P-gain for the position on the LabVIEW program. The initial tests with the PXI were conducted using the default values, which ended up causing some problems. The control was very unstable and on one of the attempts one of the beam couplings broke due to the impacts of the mechanism against the beam where it is hanging. After that event, it was decided to increase the cycle time from 5 ms to 10 ms, which clearly improved the performance of the prototype. As for the relevant gains of the velocity, position and current parameters they were obtained thanks to the model prof. Campa developed. The new set of parameters also contributed to the prototype performing the trajectories better.

The overall outcomes of the project were quite positive, but some potential issues that could make future testing more difficult became apparent too. These issues should be addressed in future ramifications of the project.

Finally, a list of the possible future modifications or things that should be looked into about the prototype are stated:

- In order to mitigate the oscillations of the mechanism when describing trajectories, it could be useful to find a way to increase its rigidity. Possible ways to tackle this could be to modify its design, maybe by adding two sets of flexible bars on each side, instead of just one, or making a thorough research to find a different material to replace the nylon bars that performs better.
- The motors currently on the prototype struggle with the stresses generated during operation and should be replaced with more capable ones. This task should be relatively easy to perform; thanks to the design the only additional part that should need replacing is the motor flanges.
- The control strategy used was imposed by the lack of time to develop a new one from scratch. However, it is possible that the PID control strategies used are not the most appropriate and other forms of control or actuation for the prototype should be considered. Maybe using a control

strategy based on the torque at the motors, instead of the position, velocity and/or current, could yield better results. Since the mechanism has two flexible bars, when they move the stresses that take place translate to some strain energy stored in the bars, which influences the loads the motors have to deal with. Therefore, a control strategy that took that into consideration could be more successful at handling the oscillations generating on the mechanism during trajectories. On the other hand, since the behaviour of the mechanism is difficult to predict or too complex for a regular PID, maybe a more straightforward control/actuation strategy could be useful, such as a bang-bang control strategy paired with an external braking system from the motors to stop the bars if needed.

- The development of the dynamic models of rods could also greatly help come up with a successful control strategy, as we would be able to better predict the behaviour of the prototype when performing a certain trajectory at a certain speed.

## 14. References

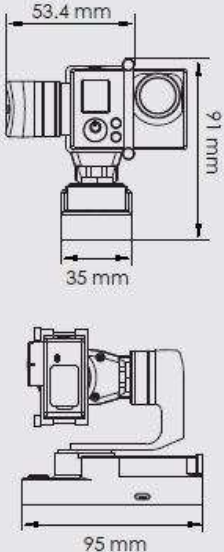
1. Howell, Larry L., Magleby, Spence P. y Olsen, Brian M. Handbook of Compliant Mechanisms. s.l. : John Wiley & Sons, 2013.
2. Rucker, Daniel Caleb. The Mechanics of Continuum Robots: Model-Based Sensing and Control. Nashville : PhD Disertation, 2011.
3. Development of a slender continuum robotic system for on-wing inspection/repair of gas turbine engines. Dong, X., y otros. Robotics and Computer-Integrated Manufacturing, s.l. : Elsevier, 2016, Vol. 44.
4. Compmech Research Group. Compmech Research Group. [En línea] <http://www.ehu.eus/compmech/>.
5. Ruiz, Antonio, y otros. Dynamic Model of a Compliant 3PRS Parallel Mechanism for Micromilling. Microactuators and Micromechanisms. s.l. : Springer, 2017.
6. ABB. IRB 360 FlexPicker. [En línea] <http://new.abb.com/products/robotics/industrial-robots/irb-360>.
7. Igus. drylin ZLW-NEMA motor flange. [En línea] [Citado el: 5 de 3 de 2018.] [https://www.igus.com/wpck/7784/ZLW\\_Motorflansch](https://www.igus.com/wpck/7784/ZLW_Motorflansch).
8. Omron Industrial Automation. Omron X-Delta 2+1. [En línea] <https://industrial.omron.eu/en/products/x-delta>.
9. Festo. Festo Products, Semi-rotary drives with rotary vane. [En línea] [https://www.festo.com/cat/en\\_gb/products\\_010501](https://www.festo.com/cat/en_gb/products_010501).
10. Zhu, Zhenqi, Cui, Hongliang y Pochiraju, Kishore. Flexible Parallel Manipulator for Nano-, Meso- or Macro-positioning with Multi-degrees of Freedom. 20080257096A1 US, 23 de October de 2008.
11. Yao, Jiantao, y otros. Rigid-flexible Coupling Type Flexible Mechanical Arm. 106313034 (A) CN, 11 de 01 de 2017.

12. Efficient Computation of Multiple Coupled Cosserat Rod Models for Real-Time Simulation and Control of Parallel Continuum Manipulators. Till, John, y otros. International Conference on Robotics and Automation, Seattle : IEEE, 2015.
13. Ramirez, Andria A., Rucker, Caleb Daniel y Webster, Robert James. Continuum Devices and Control Thereof. 2016/0016319A1 US, 21 de January de 2016.
14. Rebman, Jack. Object Manipulator. 4765795 US, 23 de August de 1988.
15. Procter, Margaret. University of Toronto, Writing. [En línea] 2015. [Citado el: 17 de 4 de 2015.] <http://www.writing.utoronto.ca/images/stories/Documents/abstract.pdf>.
16. Huang, Tian, y otros. Planar Parallel Robot MEchanism with Two Translational Degrees of Freedom. 7090458B2 US, 15 de August de 2006.
17. Fallas, David M. Robotic Case Packing System. 7644558 B1 US, 12 de January de 2010.
18. Design and Analysis of a Robust, Low-cost, Highly Articulated Manipulator Enabled by Jamming of Granular Media. Cheng, Nadia G., y otros. In Pp. 4328-4333, s.l. : IEEE, 2012.
19. Caballero, Diego. Nonlinear Flexure Analysis of Mechanisms. Bilbao : DPI2015-64450-R Project Report, 2018.
20. TraceParts. [www.tracepartsonline.net](http://www.tracepartsonline.net). [En línea] [https://www.tracepartsonline.net/\(S\(pfeyui04izyufprujyx1ivea\)\)/content.aspx](https://www.tracepartsonline.net/(S(pfeyui04izyufprujyx1ivea))/content.aspx).
21. Feiyu Tech. Feiyu Tech Downloads. [En línea] <http://www.feiyu-tech.com/Product/download/p/8>.


## 15. Appendix

### 15.1. FeiyuTech WG specsheet:

Parameters



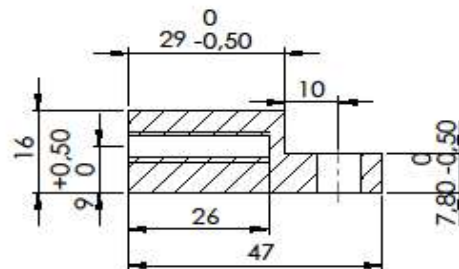
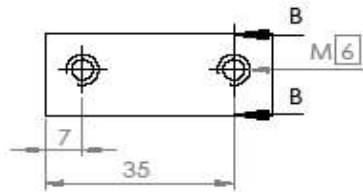
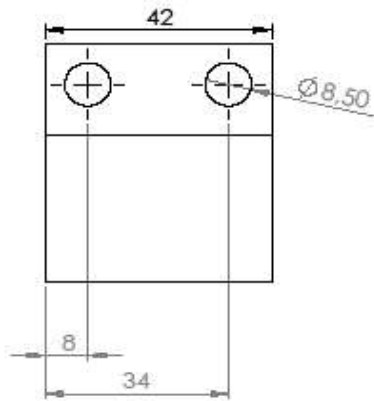
Working Voltage	6.0 V ~ 9 V
Vertical Tilting Angle	320°
Rolls Angle	100°
Horizontal Panning Angle	320°
Tilting Increments	2° /S ~ 75° /S
Panning Increments	3° /S ~ 150° /S
Static Attitude Tracking Accuracy	0.01 ~ 0.05 (Working Voltage)
Motion Attitude Tracking Accuracy	0.1 ~ 0.5 (Motor Overload<2G)
Overload Current Protection	800 mA
Weight	188 g (Without Batteries & Camera)
Usage Time	3 ~ 4 Hours
Camera Maximum Height	43.6 mm ( Replaceable mounting bracket )
Camera Maximum Thickness	31.7 mm ( Replaceable mounting bracket )
Camera Maximum Weight	150 g



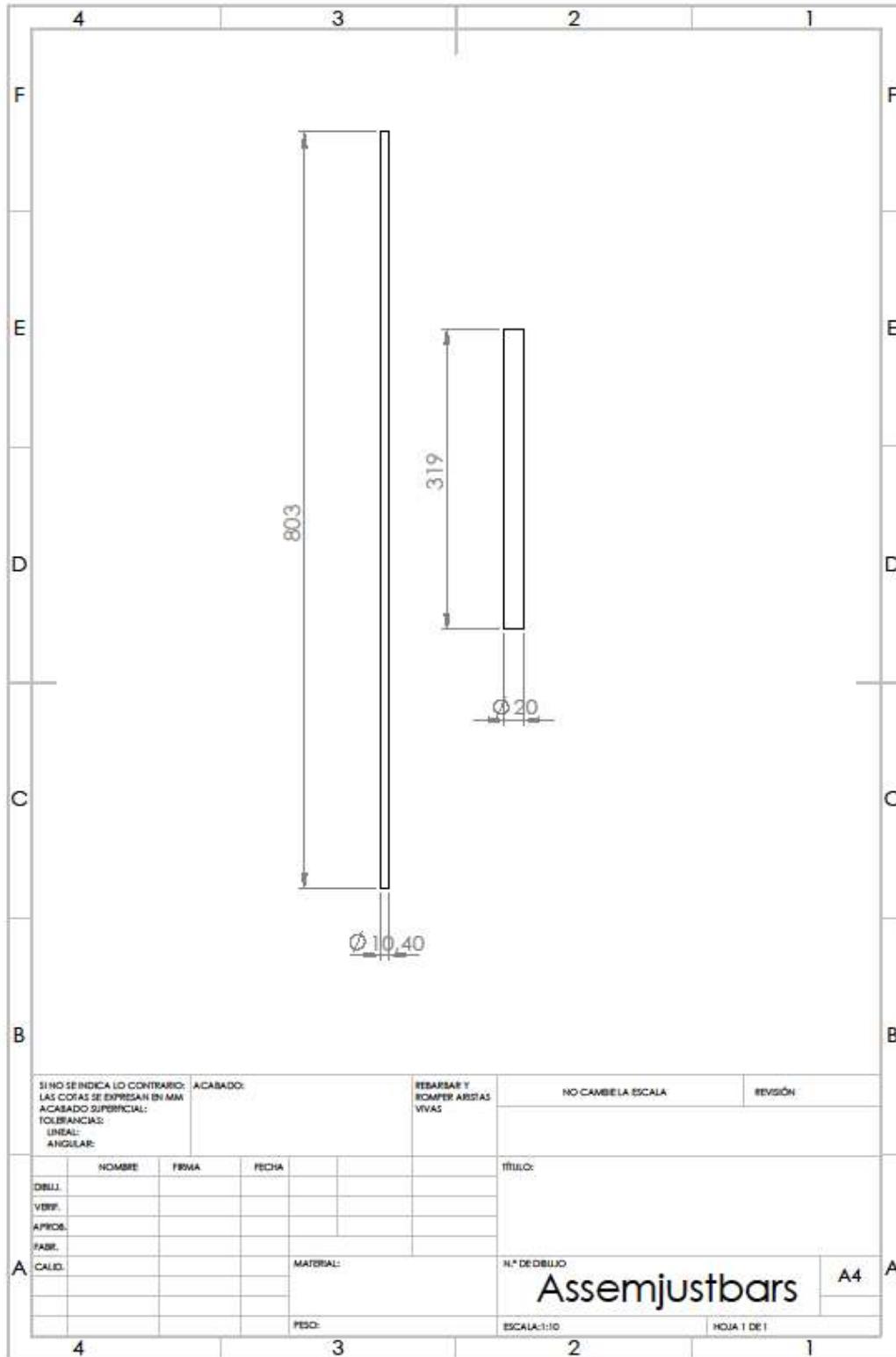


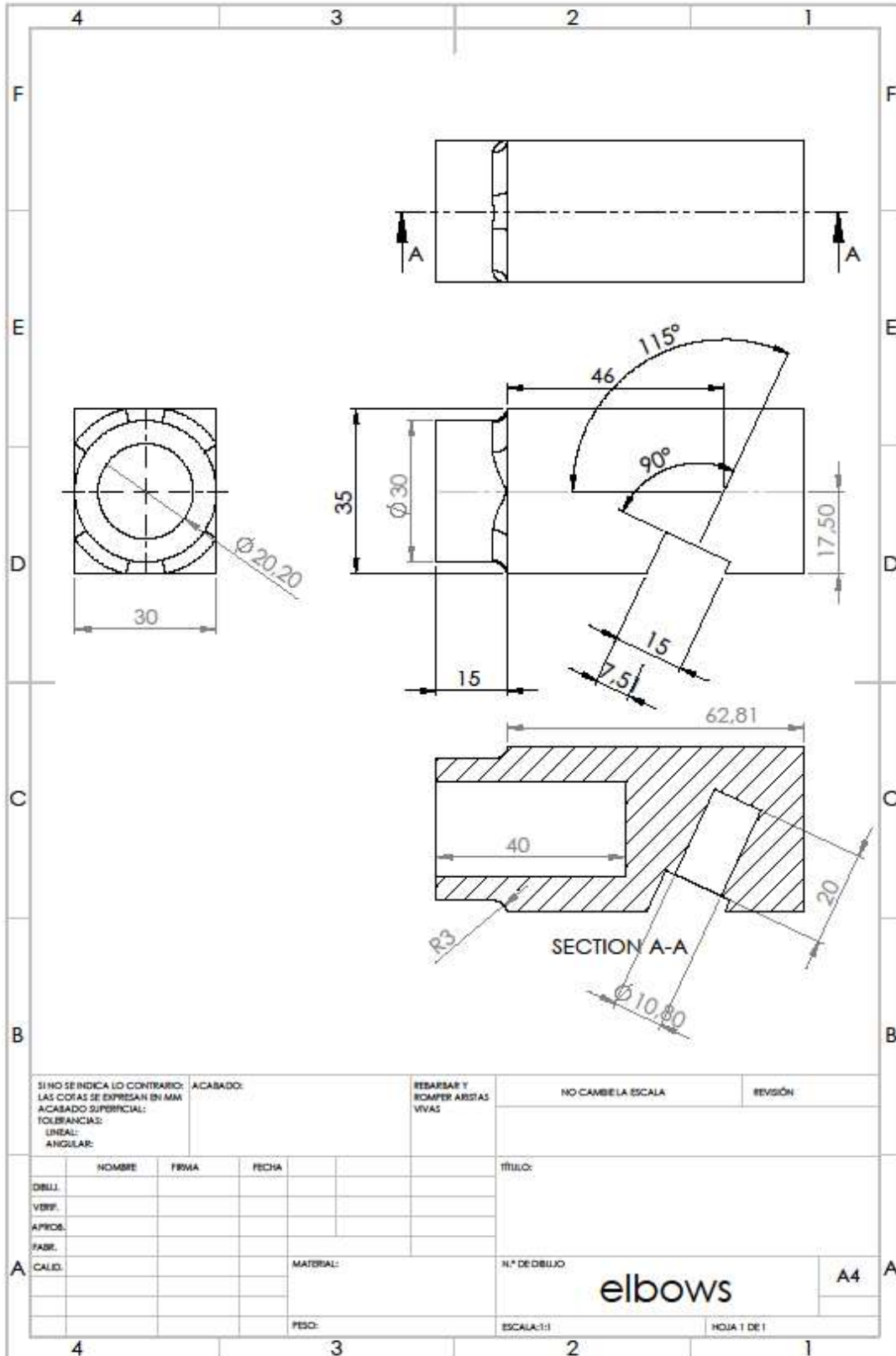


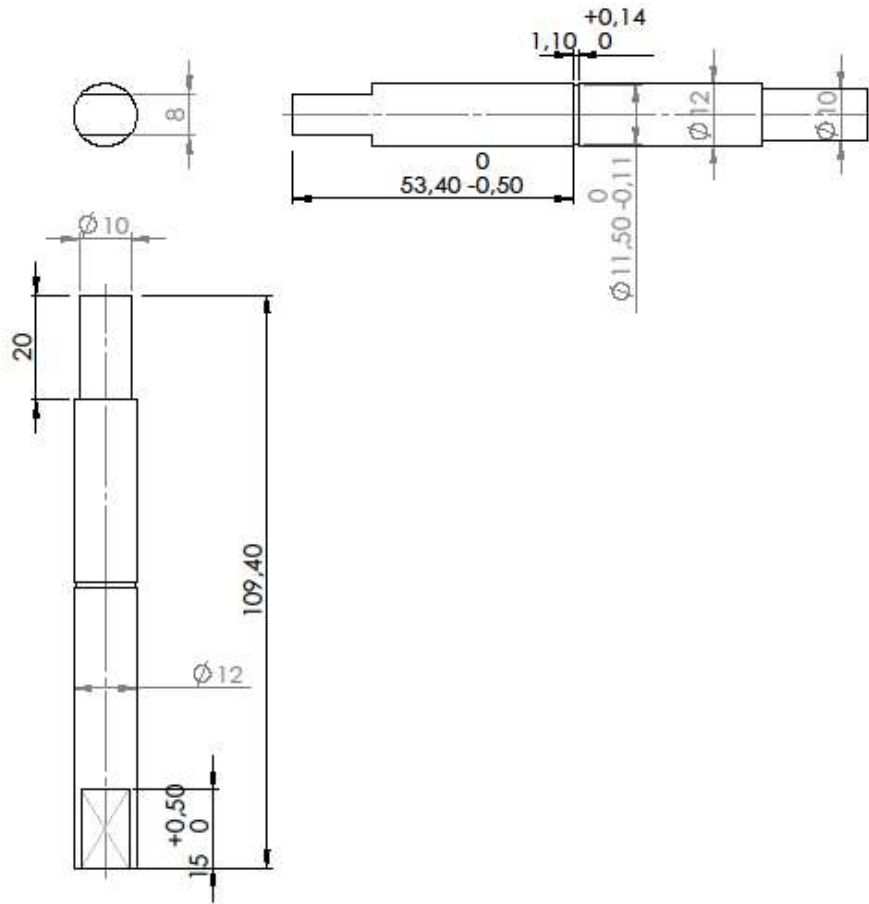
15.2. Blueprints:

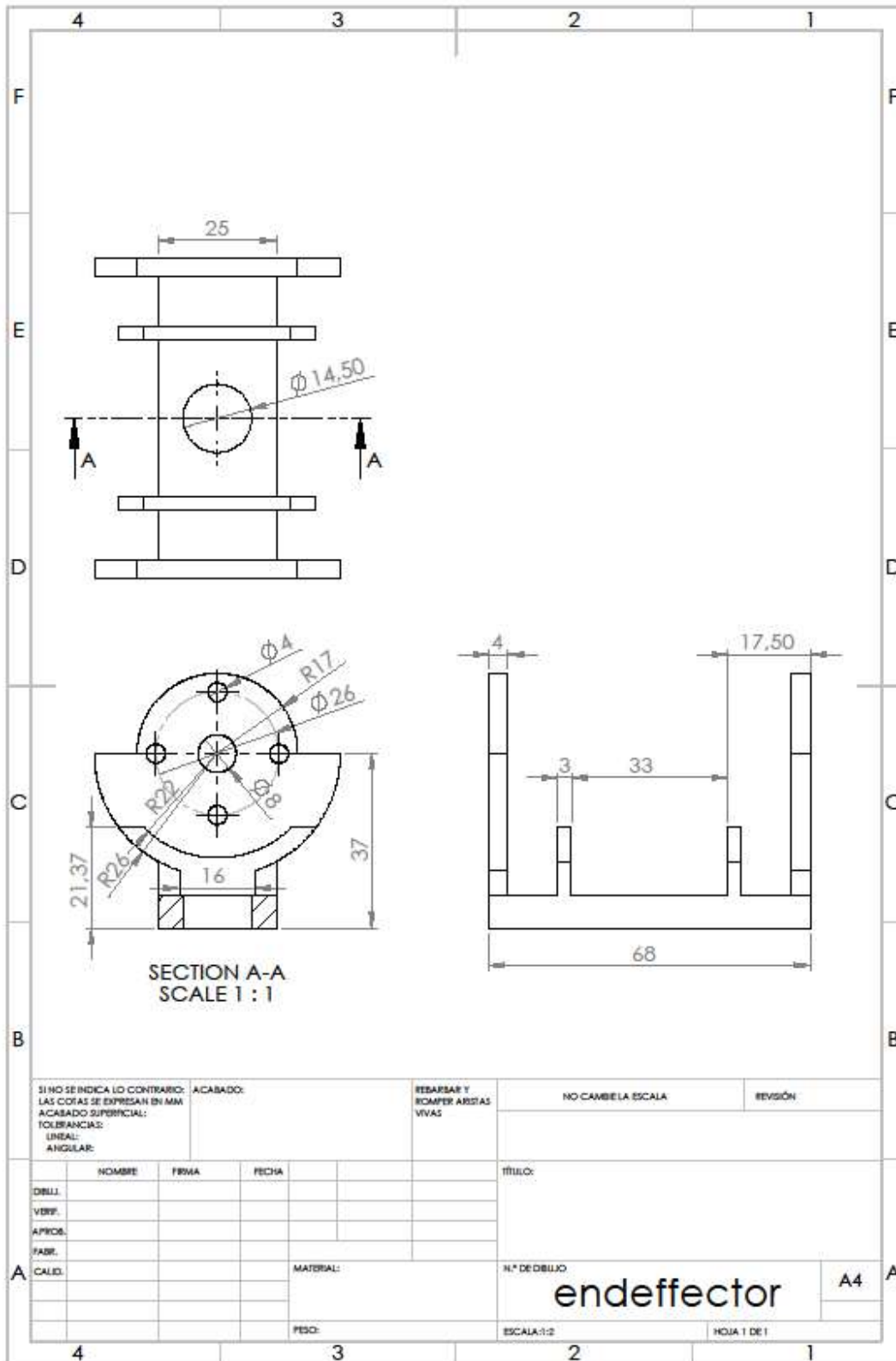


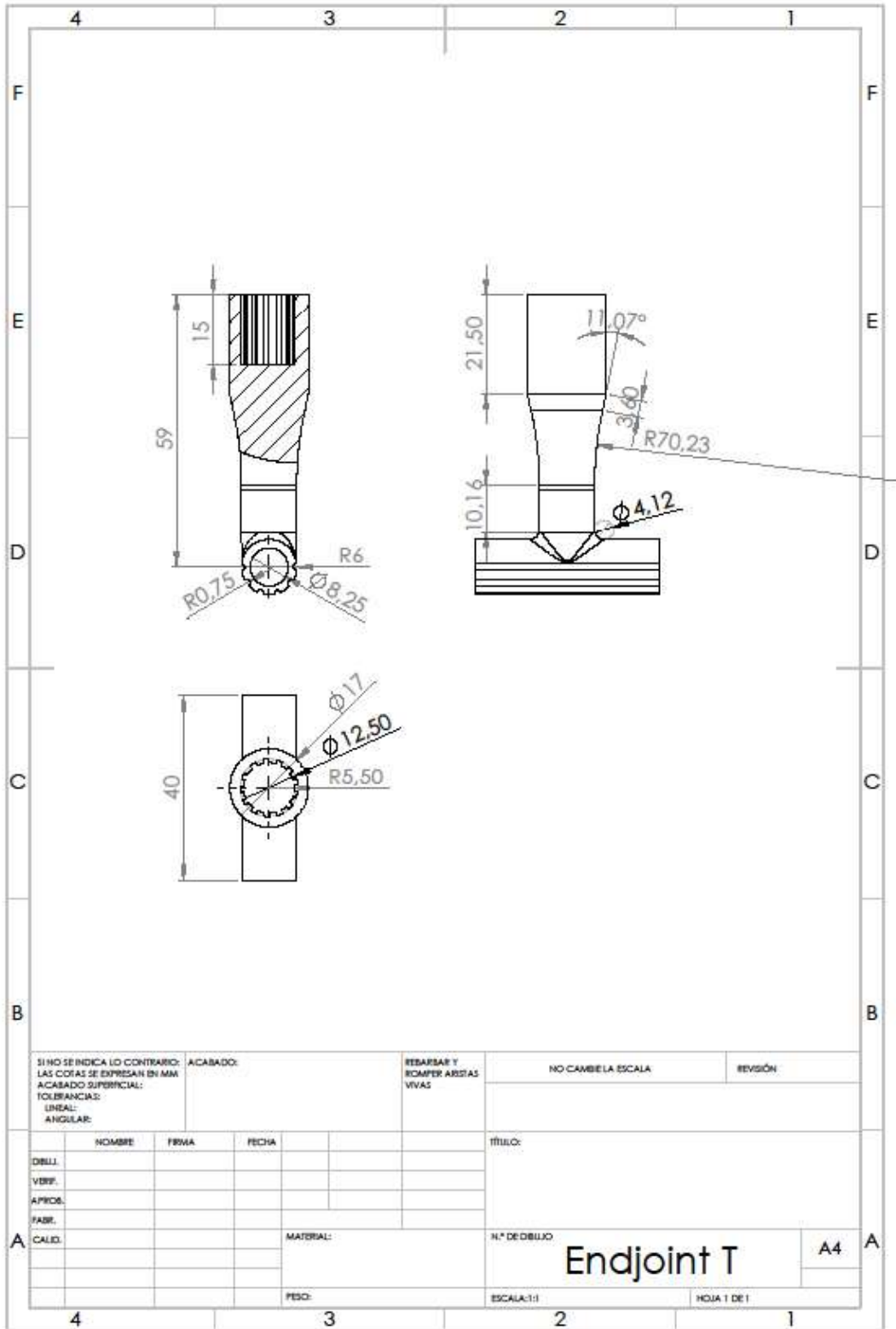
SECTION B-B



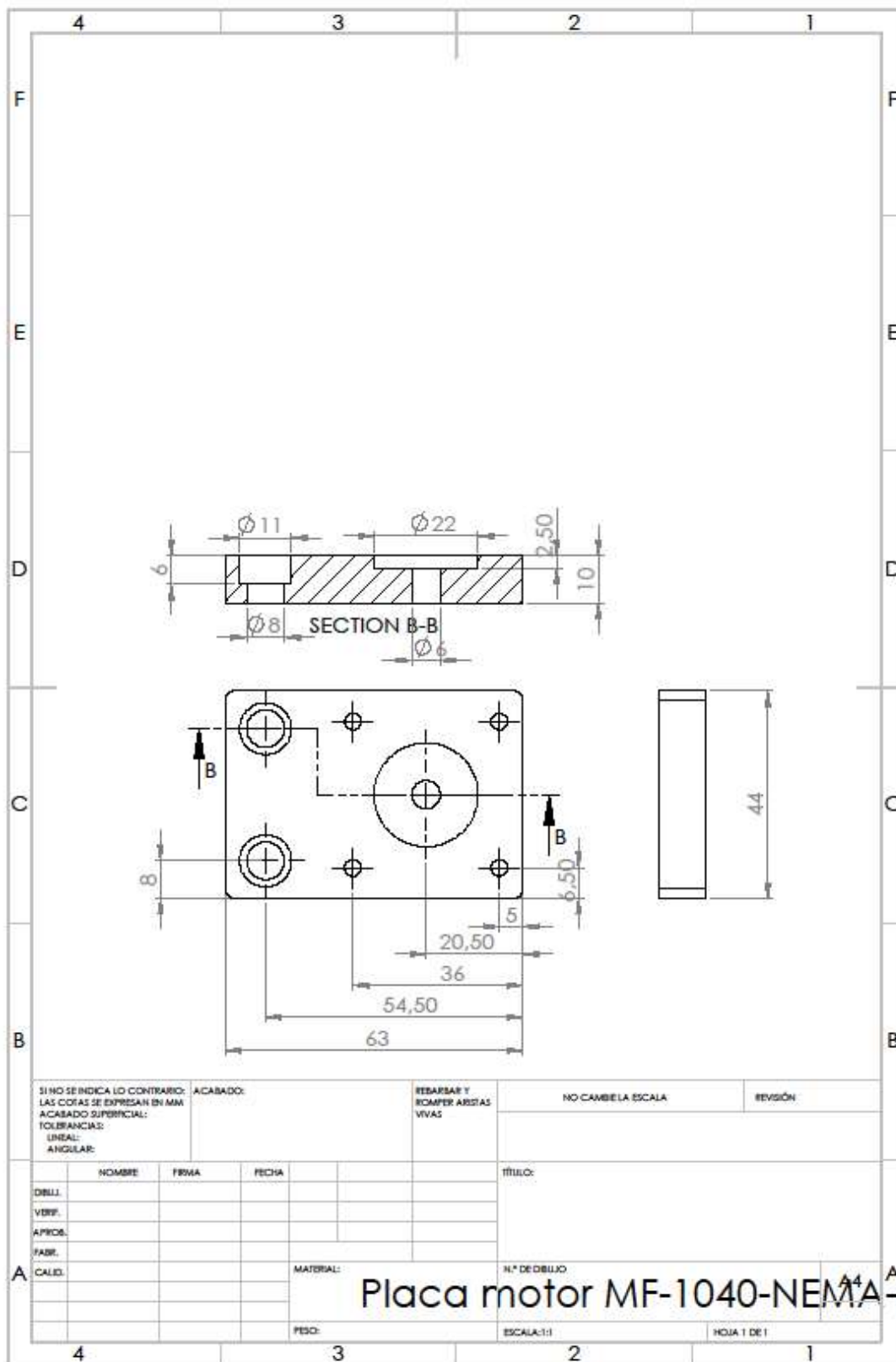






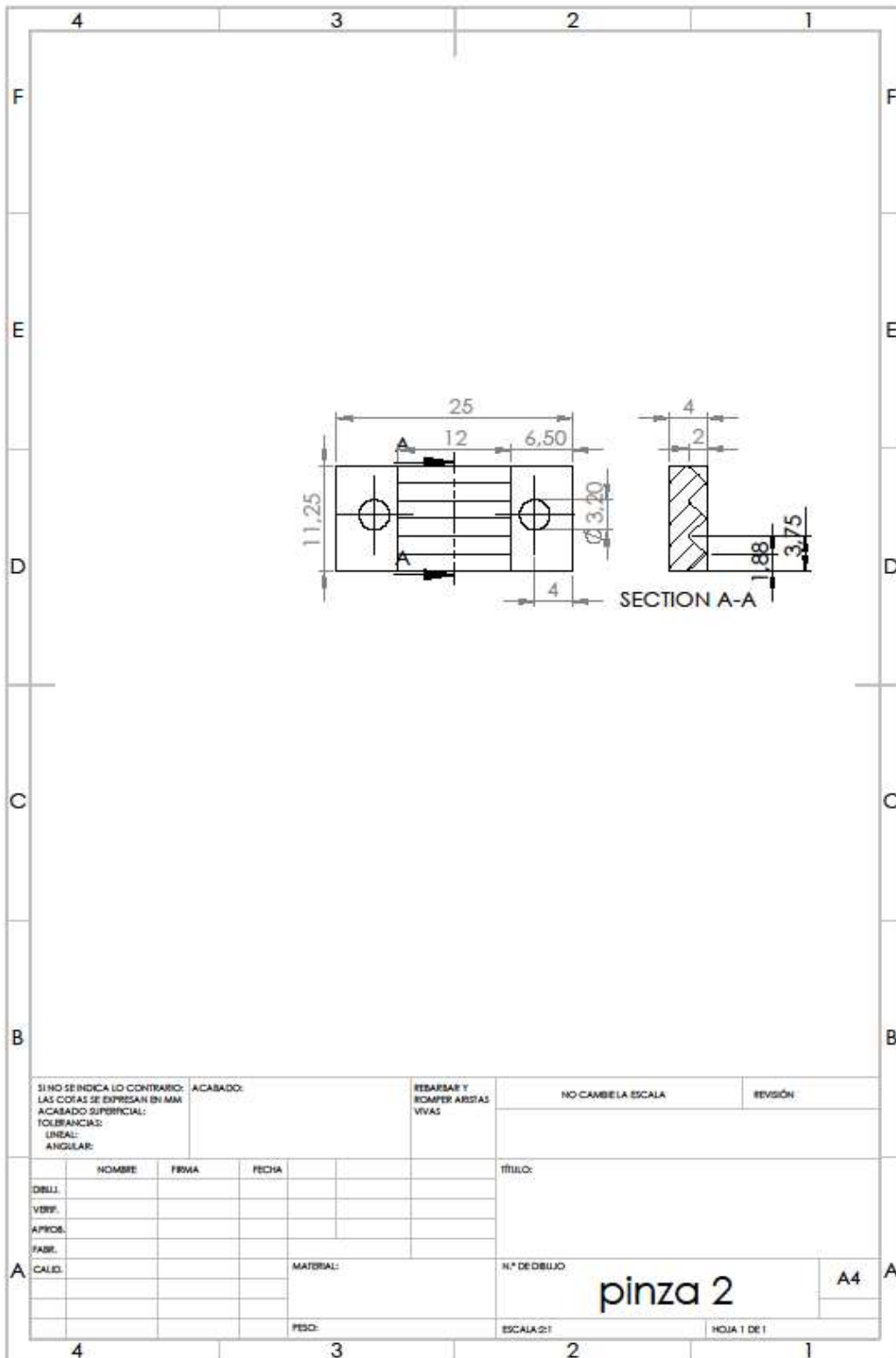


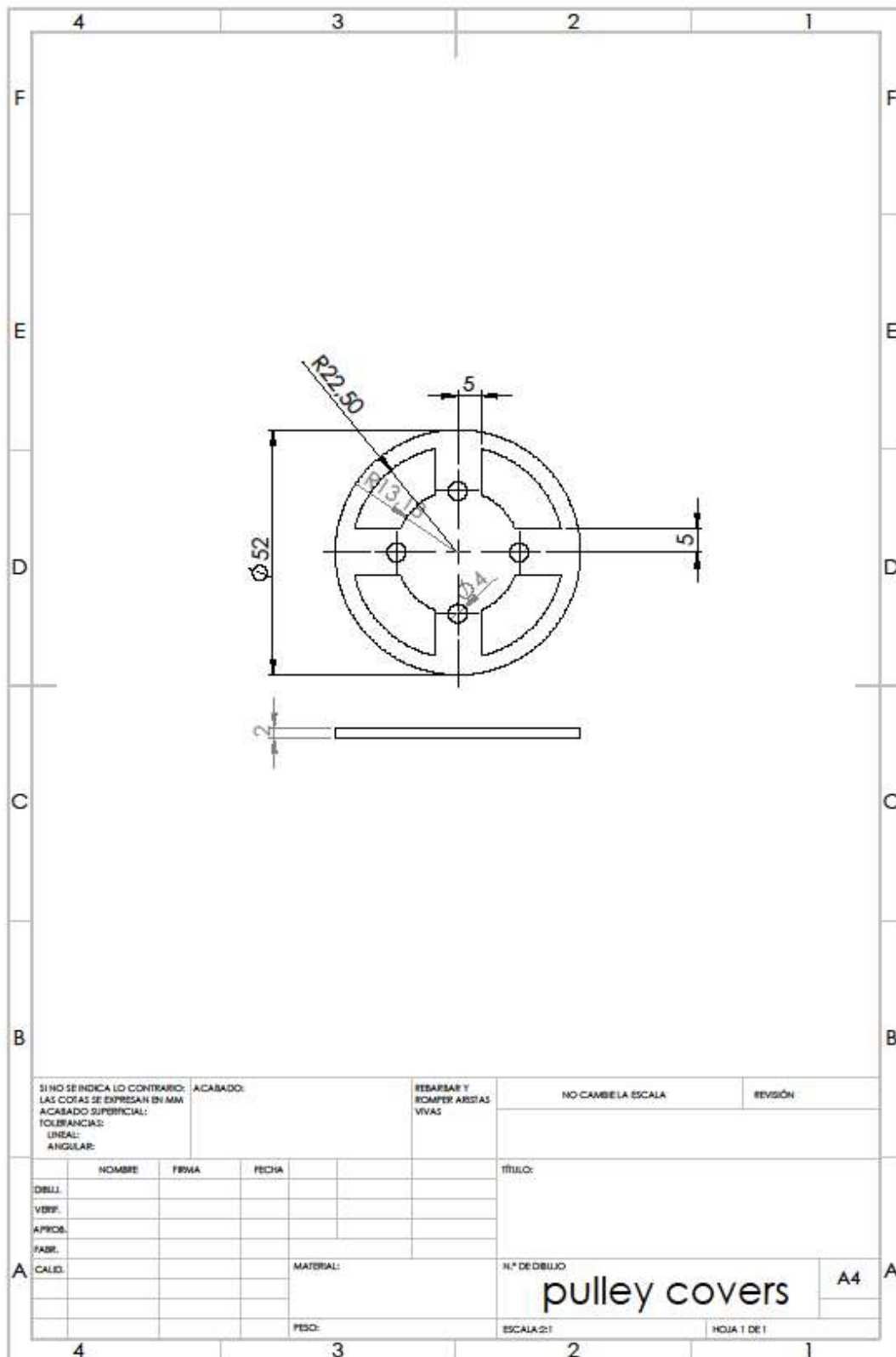


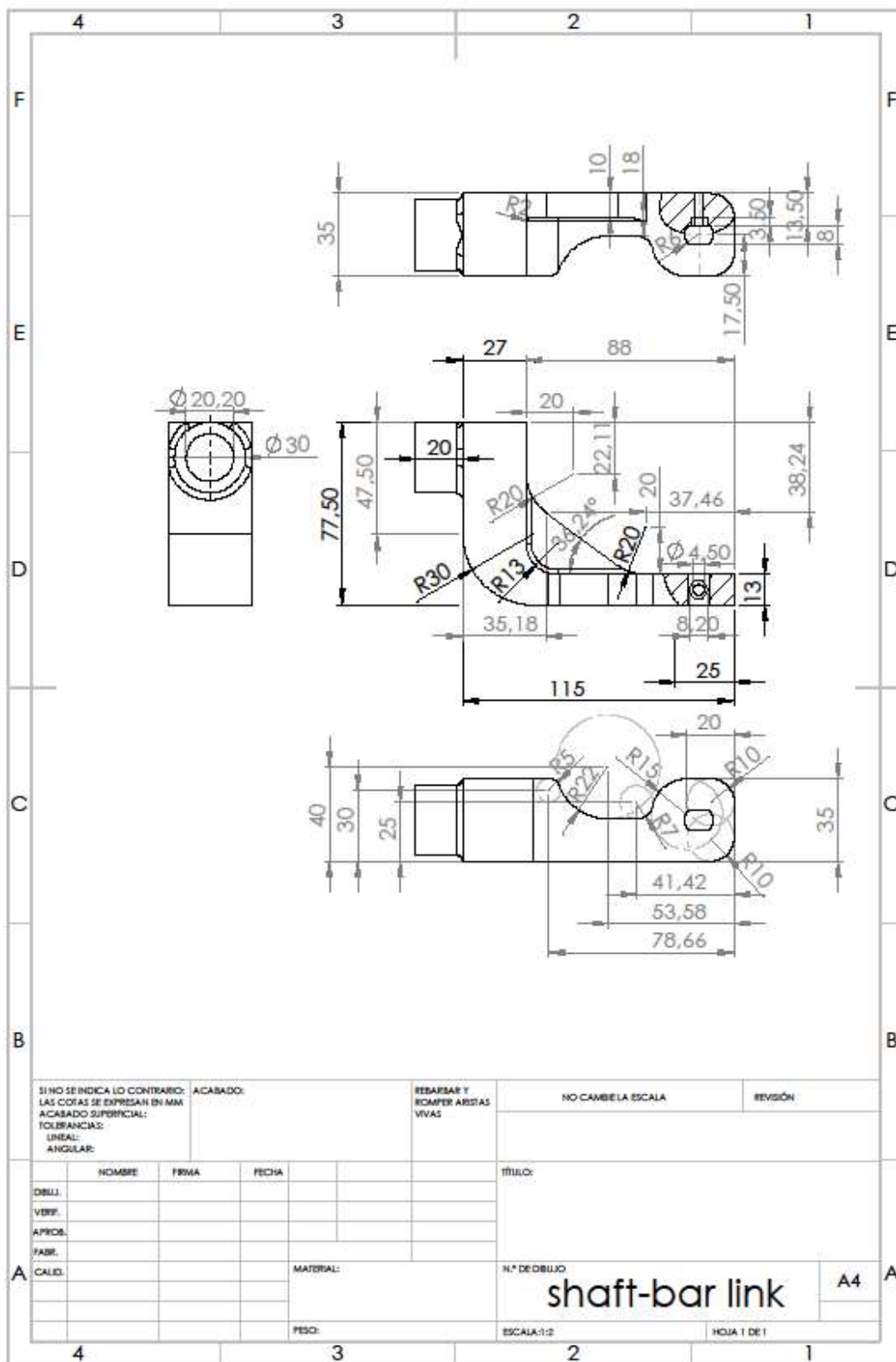


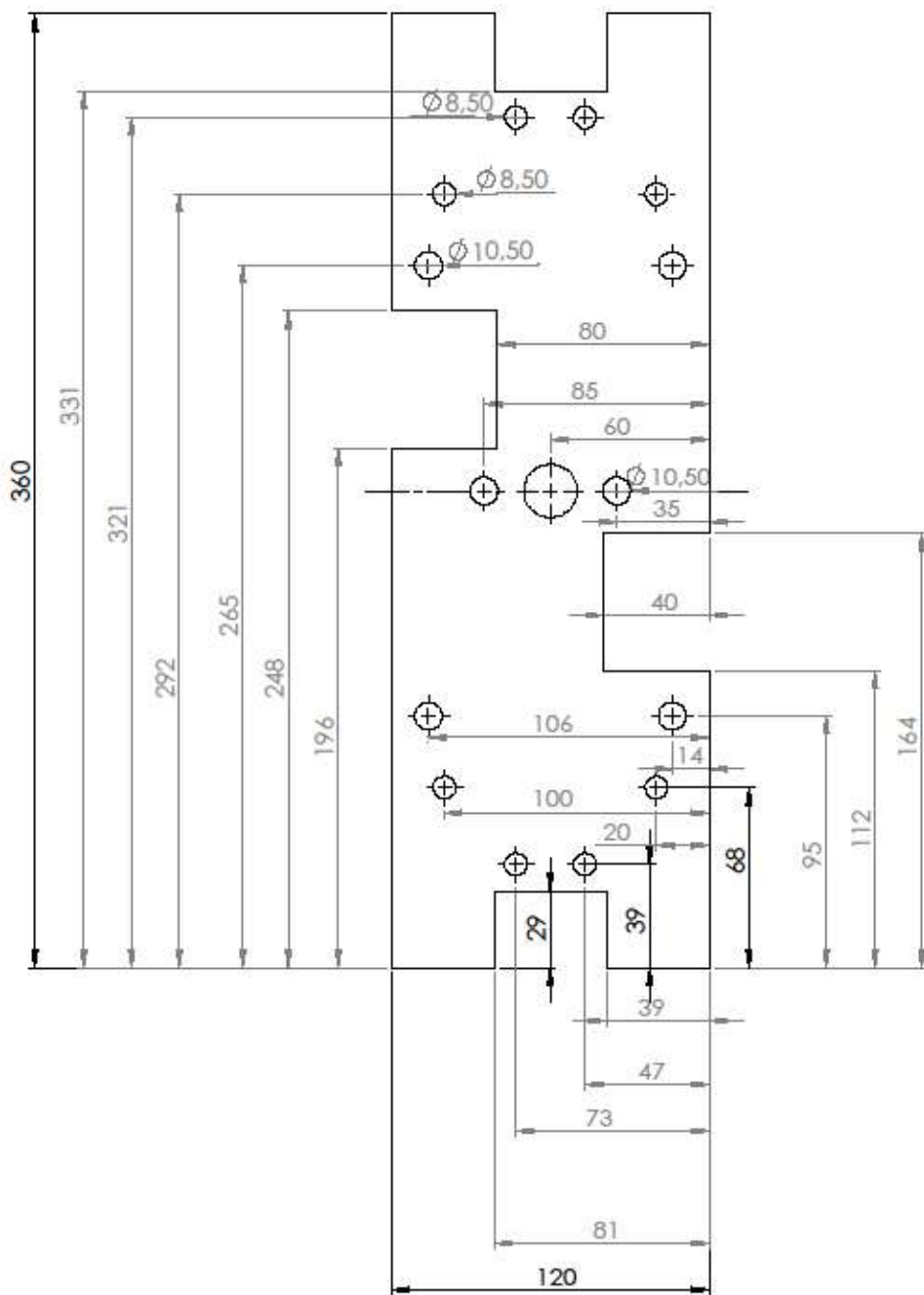


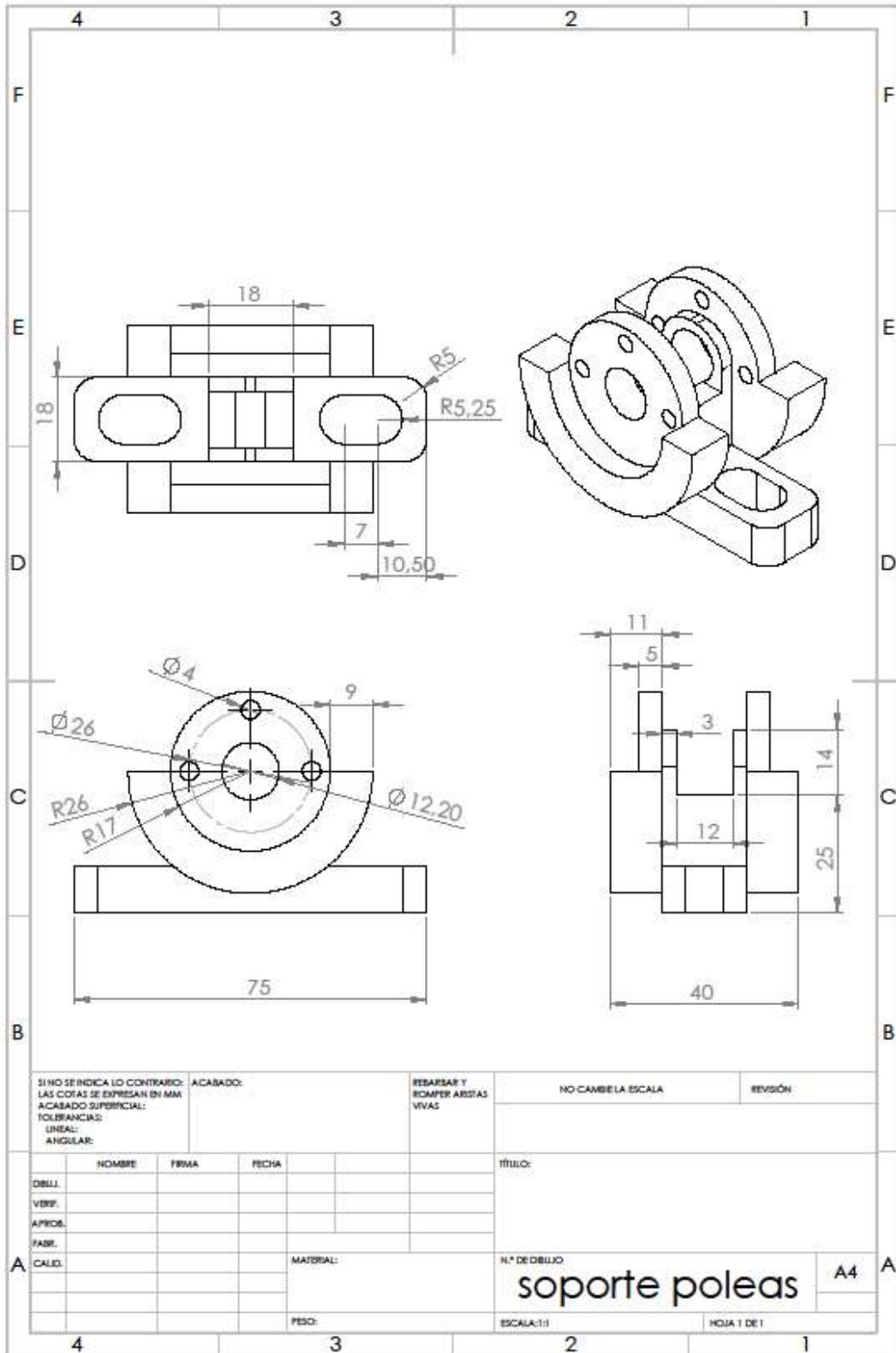












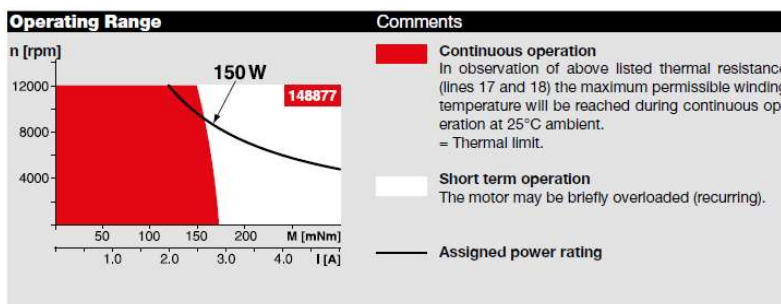


15.3. Motor:

RE 40, Graphite brushes, 150 W.

Part number: **148867**

Motor Data			
<b>Values at nominal voltage</b>			
1	Nominal voltage	V	24
2	No load speed	rpm	7580
3	No load current	mA	137
4	Nominal speed	rpm	6940
5	Nominal torque (max. continuous torque)	mNm	177
6	Nominal current (max. continuous current)	A	6
7	Stall torque	mNm	2420
8	Stall current	A	80.2
9	Max. efficiency	%	91
<b>Characteristics</b>			
10	Terminal resistance	$\Omega$	0.299
11	Terminal inductance	mH	0.082
12	Torque constant	mNm/A	30.2
13	Speed constant	rpm/V	317
14	Speed / torque gradient	rpm/mNm	3.14
15	Mechanical time constant	ms	4.67
16	Rotor inertia	gcm <sup>2</sup>	142



Specifications		
<b>Thermal data</b>		
17	Thermal resistance housing-ambient	4.7 K/W
18	Thermal resistance winding-housing	1.9 K/W
19	Thermal time constant winding	41.5 s
20	Thermal time constant motor	809 s
21	Ambient temperature	-30...+100°C
22	Max. winding temperature	+155°C
<b>Mechanical data (ball bearings)</b>		
23	Max. speed	12000 rpm
24	Axial play	0.05 - 0.15 mm
25	Radial play	0.025 mm
26	Max. axial load (dynamic)	5.6 N
27	Max. force for press fits (static) (static, shaft supported)	110 N
28	Max. radial load, 5 mm from flange	28 N
<b>Other specifications</b>		
29	Number of pole pairs	1
30	Number of commutator segments	13
31	Weight of motor	480 g

Values listed in the table are nominal.  
Explanation of the figures on page 64.



15.4. Gearhead:

GP 32 A, planetary gearhead, 0.75 4.5 Nm

Part number: **166158**

<b>Gearhead Data</b>		
1 Reduction		14:1
2 Absolute reduction		$\frac{676}{49}$
3 Max. motor shaft diameter	mm	6
4 Number of stages		2
5 Max. continuous torque	Nm	2.25
6 Max. intermittent torque at gear output	Nm	3.4
7 Max. efficiency	%	75
8 Weight	g	162
9 Average backlash no load	°	0.8
10 Mass inertia	$\text{gcm}^2$	0.8
11 Gearhead length L1	mm	36.4

<b>Technical Data</b>	
Planetary Gearhead	straight teeth
Output shaft	stainless steel
Shaft diameter as option	8 mm
Bearing at output	ball bearing
Radial play, 5 mm from flange	max. 0.14 mm
Axial play	max. 0.4 mm
Max. axial load (dynamic)	120 N
Max. force for press fits	120 N
Direction of rotation, drive to output	=
Max. continuous input speed	6000 rpm
Recommended temperature range	-40...+100°C
Number of stages	1 2 3 4 5
Max. radial load, 10 mm from flange	90 N 140 N 200 N 220 N 220 N





15.5. Results test 1: steps of 100 qc.

Position M1	Measured Angle M1	Absolute Angle M1	Delta theta 1	qc to rad (M1)	Theta 1 - Theta 2	Position M2	Measured	Absolute Angle M2	Delta theta 2	qc to rad (M2)	Current M1	Current M2	Torque M1	Torque M2	Diff M1-M2
0	29.3	1.059414856		29.30	-0.4	0	29.7	1.052433539		29.70	-1	-1	-0.000423	-0.000423	0
100	28.6	1.071632161	0.7	28.01	-0.4	100	29	1.064650844	0.7	28.41	285	179	0.120498	0.0756812	106
200	27.5	1.090830782	1.1	26.73	-0.5	200	28	1.082104136	1	27.13	374	341	0.158127	0.1441748	33
300	26.4	1.110029404	1.1	25.44	-0.6	300	27	1.099557429	1	25.84	535	507	0.226198	0.2143596	28
400	25.7	1.122246709	0.7	24.16	-0.6	400	26.3	1.111774734	0.7	24.56	668	647	0.28243	0.2735516	21
500	24.3	1.146681319	1.4	22.87	-1.1	500	25.4	1.127482697	0.9	23.27	1069	817	0.451973	0.3454276	252
600	23.4	1.162389282	0.9	21.59	-1	600	24.4	1.144935989	1	21.99	963	937	0.407156	0.3961636	26
700	22.2	1.183333233	1.2	20.30	-1.3	700	23.5	1.160643953	0.9	20.70	1196	1103	0.505669	0.4663484	93
800	21	1.204277184	1.2	19.01	-1.7	800	22.7	1.174606587	0.8	19.41	1329	1537	0.561901	0.6498436	-208
900	19.7	1.226966464	1.3	17.73	-2	900	21.7	1.192059879	1	18.13	1466	1381	0.619825	0.5838868	85
1000	18.8	1.242674427	0.9	16.44	-2	1000	20.8	1.207767842	0.9	16.84	2069	1944	0.874773	0.8219232	125
1100	17.7	1.261873049	1.1	15.16	-1.9	1100	19.6	1.228711793	1.2	15.56	1953	2237	0.825728	0.9458036	-284
1200	16.5	1.282817	1.2	13.87	-2.2	1200	18.7	1.244419757	0.9	14.27	2145	2470	0.906906	1.044316	-325
1300	15.5	1.300270293	1	12.59	-2.3	1300	17.8	1.26012772	0.9	12.99	1921	2220	0.812199	0.938616	-299
1400	14.4	1.319468915	1.1	11.30	-2.2	1400	16.6	1.281071671	1.2	11.70	2362	2372	0.998654	1.0028816	-10
1500	13.3	1.338667536	1.1	10.01	-2.3	1500	15.6	1.298524963	1	10.41	2277	3271	0.962716	1.3829788	-994
1600	12.2	1.357866158	1.1	8.73	-2.3	1600	14.5	1.317723585	1.1	9.13	2665	2932	1.126762	1.2396496	-267
1700	11.3	1.373574121	0.9	7.44	-2.4	1700	13.7	1.331686219	0.8	7.84	3232	3084	1.36649	1.3039152	148
1800	9.7	1.401499389	1.6	6.16	-2.6	1800	12.3	1.356120829	1.4	6.56	2081	2868	0.879847	1.2125904	-787
1900	8.5	1.42244334	1.2	4.87	-2.4	1900	10.9	1.380555438	1.4	5.27	2909	3022	1.229925	1.2777016	-113
2000	7.6	1.438151304	0.9	3.59	-2.2	2000	9.8	1.39975406	1.1	3.99	4159	3642	1.758425	1.5398376	517
2100	6.3	1.460840584	1.3	2.30	-2.7	2100	9	1.413716694	0.8	2.70	2346	3007	0.991889	1.2713596	-661
2200	5.2	1.480039206	1.1	1.01	-2.7	2200	7.9	1.432915316	1.1	1.41	2989	4144	1.263749	1.7520832	-1155
2300	4.1	1.499237827	1.1	-0.27	-2.6	2300	6.7	1.453859267	1.2	0.13	3269	2829	1.382133	1.1961012	440
2400	2.9	1.520181778	1.2	-1.56	-2.6	2400	5.5	1.474803218	1.2	-1.16	3658	4588	1.546602	1.9398064	-930
2500	2	1.535889742	0.9	-2.84	-2.4	2500	4.4	1.49400184	1.1	-2.44	3337	4996	1.410884	2.1123088	-1659
2600	0.7	1.558579022	1.3	-4.13	-2.6	2600	3.3	1.513200461	1.1	-3.73	3088	2730	1.305606	1.154244	358
2700	-0.5	1.579522973	1.2	-5.41	-2.6	2700	2.1	1.534144413	1.2	-5.01	3999	3326	1.690777	1.4062328	673
2800	-1.7	1.600466924	1.2	-6.70	-2.7	2800	1	1.553343034	1.1	-6.30	4002	4998	1.692046	2.1131544	-996
2900	-3.2	1.626646863	1.5	-7.99	-4.1	2800	0.9	1.555088364	0.1	-6.30	4998	5000	2.113154	2.114	-2



Position M1	Measured Angle M1	Absolute Angle M1	Delta theta 1	qc to degrees (M1)	Theta 1 - Theta 2	Position M2	Measured Angle M2	Absolute Angle M2	Delta theta 2	qc to degrees (M2)	Current M1	Current M2	Torque M1	Torque M2	Diff M1-M2
-245	29.2	1.061160185		32.35	0.3	45	28.9	1.066396173		28.32142857	0	0	0	0	0
194	28.4	1.075122819	0.8	26.71	0.4	-96	28	1.082104136	0.9	30.13428571	204	34	0.0862512	0.0143752	170
294	27.1	1.0978121	1.3	25.42	0.1	4	27	1.099557429	1	28.84857143	492	443	0.2080176	0.1873004	49
394	26.3	1.111774734	0.8	24.13	0.3	104	26	1.117010721	1	27.56285714	595	663	0.251566	0.2803164	-68
494	25.5	1.125737368	0.8	22.85	0.4	204	25.1	1.132718685	0.9	26.27714286	749	1002	0.3166772	0.4236456	-253
594	24.4	1.144935989	1.1	21.56	0.5	354	23.9	1.153662636	1.2	24.34857143	795	1150	0.336126	0.48622	-355
694	23.2	1.16587994	1.2	20.28	0.2	454	23	1.169370599	0.9	23.06285714	981	1375	0.4147668	0.58135	-394
794	22.2	1.183333233	1	18.99	0.2	554	22	1.186823891	1	21.77714286	1526	1485	0.6451928	0.627858	41
894	21	1.204277184	1.2	17.71	-0.2	654	21.2	1.200786525	0.8	20.49142857	1628	1799	0.6883184	0.7606172	-171
994	20	1.221730476	1	16.42	0	754	20	1.221730476	1.2	19.20571429	1549	2126	0.6549172	0.8988728	-577
1094	19.1	1.23743844	0.9	15.13	0	854	19.1	1.23743844	0.9	17.92	1631	2142	0.6895868	0.9056376	-511
1194	18	1.256637061	1.1	13.85	-0.2	954	18.2	1.253146403	0.9	16.63428571	1388	1803	0.5868464	0.7623084	-415
1294	16.9	1.275835683	1.1	12.56	-0.3	1054	17.2	1.270599695	1	15.34857143	1806	2149	0.7635768	0.9085972	-343
1394	15.9	1.293288976	1	11.28	-0.2	1154	16.1	1.289798317	1.1	14.06285714	1879	2165	0.7944412	0.915362	-286
1494	14.8	1.312487597	1.1	9.99	-0.4	1254	15.2	1.30550628	0.9	12.77714286	1776	2539	0.7508928	1.0734892	-763
1594	13.7	1.331686219	1.1	8.71	-0.4	1354	14.1	1.324704902	1.1	11.49142857	1764	2038	0.7458192	0.8616664	-274
1694	12.6	1.350884841	1.1	7.42	-0.4	1454	13	1.343903524	1.1	10.20571429	1724	2256	0.7289072	0.9538368	-532
1794	11.5	1.370083463	1.1	6.13	0.1	1554	11.4	1.371828792	1.6	8.92	3415	2616	1.443862	1.1060448	799
1794	10.5	1.387536755	1	6.13	0	1604	10.5	1.387536755	0.9	8.277142857	3415	3891	1.443862	1.6451148	-476
1894	9.2	1.410226036	1.3	4.85	-0.2	1704	9.4	1.406735377	1.1	6.991428571	3428	4127	1.4493584	1.7448956	-699
1994	8.3	1.425933999	0.9	3.56	0	1804	8.3	1.425933999	1.1	5.705714286	3963	4550	1.6755564	1.92374	-587
2094	7.2	1.445132621	1.1	2.28	0.1	1904	7.1	1.44687795	1.2	4.42	4888	4819	2.0666464	2.0374732	69
2194	6	1.466076572	1.2	0.99	0	2004	6	1.466076572	1.1	3.134285714	4973	4729	2.1025844	1.9994212	244
2294	4.8	1.487020523	1.2	-0.29	-0.1	2104	4.9	1.485275193	1.1	1.848571429	4788	5090	2.0243664	2.152052	-302
2394	4	1.500983157	0.8	-1.58	0	2204	4	1.500983157	0.9	0.562857143	4998	4998	2.1131544	2.1131544	0
		1.570796327	4	29.20	0			1.570796327	4	28.9					



15.6. EPOS Studio System Parameters:

Parameters:	Value Range		Default Values		Min Value	Max Value	Selected Values	Units
	Min	Max	Motor 1	Motor 2				
<b>Profile:</b>								
Profile Velocity	0	12000	567	572				rpm
Profile Acceleration	0	4.29E+09	42967	43697				rpm/s
Profile Deceleration	0	4.29E+09	42967	43697				rpm/s
<b>Object Dictionary</b>								
Current Control Parameter Set:								
Current P Gain	0	32767	234	191			25	-
Current I Gain	0	32767	91	134			12	-
Velocity Control Parameter Set:								
Speed P-Gain	0	32767	3069	2965		12000	10000	-
Speed I-Gain	0	32767	465	453		1500	1500	-
Position Control Parameter Set:								
Position P-Gain	0	32767	697	679	1000	10000	7000	-
Position I-Gain	0	32767	2250	2211	1000	32000	1500	-
Position D-Gain	0	32767	1151	1112	0	5000	2600	-

The values on the yellow box were the ones used during test 2 to tune the position P/I/D gains.

Those on the blue box were the ones that were deemed adequate when working with the PXI.